Supporting Information for

How to Control the Rate of Heterogeneous Electron Transfer Across the Rim of M_6L_{12} and $M_{12}L_{24}$ Nanospheres

Riccardo Zaffaroni,[†] Eduard.O.Bobylev,[†] Raoul Plessius,[†] Jarl Ivar van der Vlugt,[†] and Joost N. H. Reek*,[†]

[†] van 't Hoff Institute for Molecular Sciences, University of Amsterdam, Science Park 904, 1098 XH Amsterdam, the Netherlands.

Table of Contents

Materials and methods S3
Ligands synthesis and characterization S5
Synthesis of 4-(trimethylsilanylethynyl)pyridine hydrochloride S5
Synthesis and characterization of FcBB **A** S7
Synthesis and characterization of TTFBB **B** S11
Synthesis and characterization of twisted TTFBB **C** S15
Synthesis and characterization of BBH **E** S20
Synthesis and characterization of ferrocenyl sulfonate tetrabutylammonium S21
Cages synthesis and characterization S22
Cages containing FcBB **A** S22
Cage $[Pd_{12}\mathbf{A}_{24}]^{24+}$ S22
Cage $[Pd_{12}\mathbf{E}_{23}\mathbf{A}_{1}]^{24+}$ S29
Cage $[Pt_{6}\mathbf{A}_{12}]^{12+}$ S36
Cage $[Pt_{6}\mathbf{E}_{11}\mathbf{A}_{1}]^{12+}$ S41
Cages containing TTFBB **B** S46
Cage $[Pt_{6}\mathbf{E}_{11}\mathbf{B}_{1}]^{12+}$ S46
Cage $[Pt_{6}\mathbf{E}_{10}\mathbf{B}_{2}]^{12+}$ S54
Cage containing twistedTTFBB **C** S61
Cage $[Pt_{6}\mathbf{E}_{11}\mathbf{C}_{1}]^{12+}$ S61
Cage containing guanidinium building block **D** S67
Cage $[Pd_{12}\mathbf{D}_{24}]^{48+}$ S67

Electrochemistry S82
FcBB **A** and FcBB **A** containing cages S82
FcBB **A** S82
Cage $(Pd_{12}\mathbf{A}_{24})^{24+}$ S83
Cage $(Pd_{12}\mathbf{E}_{23}\mathbf{A}_{1})^{24+}$ S85
Cage $(Pt_{6}\mathbf{A}_{12})^{12+}$ S87
Cage $(Pt_{6}\mathbf{E}_{11}\mathbf{A}_{1})^{12+}$ S89
TTFBB **B** and TTFBB **B** containing cages S91
TTFBB **B** S91
Cage $(Pt_{6}\mathbf{E}_{11}\mathbf{B}_{1})^{12+}$ S94
Cage $(Pt_{6}\mathbf{E}_{10}\mathbf{B}_{2})^{12+}$ S98
twistedTTFBB **C** and TTFBB **C** containing cage S102
twistedTTFBB **C** S102
Cage $(Pt_{6}\mathbf{E}_{11}\mathbf{C}_{1})^{12+}$ S105
Guanidinium building block **D** containing cage S108
UV-VIS and Spectroelectrochemistry S110
Molecular mechanics modeling S112
DFT orbital computations S113
EPR S115
References S116

Materials and methods

General procedures: all synthetic procedures were carried out under an argon or nitrogen atmosphere using standard Schlenk techniques. All commercially available chemicals were used as received without further purification. Solvents used for synthesis were dried, distilled and degassed with the most suitable method. Column chromatography was performed open to air using solvents as received.

Electrochemistry: Cyclic voltammetry was performed on 1 mM solution of analyte (unless otherwise stated) using 0.1 M tetrabutylammonium hexafluorophosphate as supporting electrolyte. The voltammograms were recorded using a PG-STAT302N potentiostat at glassy carbon disk electrode (2 mm diameter). A platinum coil was used as auxiliary electrode and a leak free silver electrode (inner compartment 3 M KCl/Ag) as reference electrode. For all ferrocene building block **A** containing systems a 1 to 1 mixture of MeCN and DCM was used, otherwise the experiments were performed in pure MeCN.

Spectroelectrochemistry was performed in an optically transparent thin layer OTTLE cell with platinum working electrode, platinum auxiliary electrode and silver wire as reference electrode, using 0.2 M tetrabutylammonium hexafluorophosphate as supporting electrolyte.

Bulk electrolysis was carried out in a two-compartment cell using Duocel® reticulated vitreous carbon foam as working electrode (used as received from ERG Aerospace Corporation) and a leak free silver electrode (inner compartment 3 M KCl/Ag). The platinum auxiliary electrode was separated from the main solution by a P4 glass frit. Both compartments contained 0.5 M solution of tetrabutylammonium hexafluorophosphate supporting electrolyte.

Mass analysis: high resolution mass spectra for all compounds were collected on an AccuTOF GC v 4g, JMS-T100G-CV mass spectrometer (JEOL, Japan).

Cryospray-ionization MS (CSI-MS): Mass spectra were collected on a HR-ToF Bruker Daltonik GmbH (Bremen, Germany) Impact II, an ESI-ToF MS capable of resolution of at least 40000 FWHM, which was coupled to a Bruker cryo-spray unit. Detection was in positive-ion mode and the source voltage was between 4 and 6 kV. The sample was introduced with a syringe pump at a flow rate of 18 μL/hr. The drying gas (N_2) was held at -35 °C and the spray gas was held at – 40 °C. The machine was calibrated prior to every experiment via direct infusion of a TFA-Na solution, which provided a *m*/*z* range of singly charged peaks up to 3500 Da in both ion modes.

Software acquisition Compass 2.0 for Otof series Software processing m-mass (spectra with* were baseline corrected and averaged).

EPR spectroscopy: Experimental X-band EPR spectra were recorded on a Bruker EMX spectrometer (Bruker BioSpin Rheinstetten), on an ELEXSYS 680 spectrometer and using an in-house developed setup based on the resonator ER4116X-MD-5-W1. All oxidation reactions were carried out electrochemically in acetonitrile solution containing 0.5 M tetrabutylammonium hexafluorophosphate. After electrolysis was completed, samples were transferred, under inert

conditions, to a melting point glass capillary that was then placed inside a standard EPR tube at room temperature.

DFT calculations: Gas phase geometry optimizations were computed with the program ORCA at RI-DFT/BP86 level with def2-SVP basis set. Frontier orbitals were computed using a single point calculation at DFT/B3LYP level with def2-TZVP basis set.

X-ray Crystal Structure Determination: X-ray intensities were measured on a Bruker D8 Quest Eco diffractometer equipped with a Triumph monochromator (λ = 0.71073 Å) and a CMOS Photon 50 detector at a temperature of 150(2) K. Intensity data were integrated with the Bruker APEX2 software.[1] Absorption correction and scaling was performed with SADABS.[2] The structures were solved using intrinsic phasing with the program SHELXT.[1] Least-squares refinement was performed with SHELXL-2013[3] against F^2 of all reflections. Non-hydrogen atoms were refined with anisotropic displacement parameters. The H atoms were placed at calculated positions using the instructions AFIX 13, AFIX 43 or AFIX 137 with isotropic displacement parameters having values 1.2 or 1.5 times *U*eq of the attached C atoms.

Ligands synthesis and characterization

Synthesis of 4-(trimethylsilanylethynyl)pyridine hydrochloride

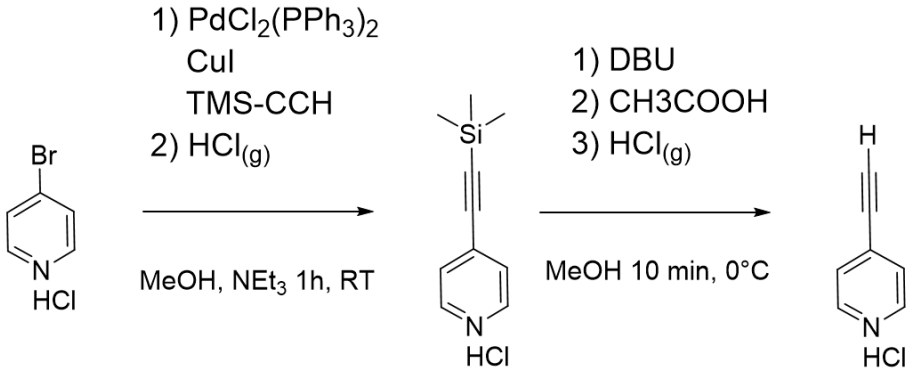

Scheme S1. Synthetic route for large scale preparation of 4-ethynyl pyridine hydrochloride.

Synthesis of 4-(trimethylsilanylethynyl)pyridine hydrochloride: this compound was prepared according to a modified literature procedure.[4] The modifications enable the reaction to be performed on a scale of several grams, with significantly easier workup that avoid column chromatography whilst giving comparable yield as the original procedure. A 500 mL roundbottom three-neck flask equipped with a mechanical stirrer was charged with 15 g of finely ground *p*-bromopyridine hydrochloride (1 equiv, 77.14 mmol). The flask was purged with argon before the addition of 40 mL of degassed methanol. The suspension was stirred at room temperature for 10 minutes, followed by the addition of 230 mL of degassed triethylamine. Subsequently, 0.270 g of [$PdCl_2(PPh_3)_2$] (0.5 mol%) and 0.105 g of [CuI] (0.7 mol%) were added as solids against a positive pressure of argon. After stirring the suspension for approx. 5 minutes, degassed (trimethylsilyl)acetylene (1.5 equiv, 16.4 mL, 115.71 mmol) was added by syringe. The reaction mixture, which immediately turned dark, was stirred at room temperature and monitored by TLC (eluent ethylacetate:hexanes 2:1). The reaction went to completion in approx. 1 hour. The formed suspension was filtered through a glass frit and the solids washed with diethyl ether. All the volatiles were removed at the rotary evaporator, being careful to fully remove triethylamine, to afford a dark oil. To this residue, 500 mL of diethyl ether were added and the resulting suspension filtered through Celite. Hydrochloric acid, generated by addition of concentrated H_2SO_4 to solid NaCl, was bubbled into the dark, clear ether solution obtained after filtration for 15 minutes, causing the formation of an off-white precipitate. This solid material was filtered and washed with diethyl ether before being subjected to overnight drying under vacuum to afford 15.8 g of the title compound (97% yield). **^{1}H NMR (CD_3OD, ppm)** δ 8.86 (m, 4H), δ 8.09 (m, 4H), δ 0.34 (s, 9H) (spectral data in agreement with literature).

Synthesis of 4-ethynyl pyridine hydrochloride: A 500 mL roundbottom flask was charged with 5 g of 4-(trimethylsilanylethynyl)pyridine hydrochloride (1 equiv, 23.6 mmol) and 10 mL of methanol. The flask was purged with argon and cooled with an ice/salt bath before 17.5 mL DBU (5 equiv, 118 mmol) and 425µL of water (1 equiv, 23.6 mmol) were added to the flask.

The solution was stirred for 10 minutes before 6.75 mL of acetic acid (5 equiv, 118 mmol) followed by 400 mL of diethyl ether were added to the flask. The resulting suspension was stirred at room temperature for 10 minutes, dried with magnesium sulfate and filtered through a plug of Celite. Hydrochloric acid, generated by addition of concentrated H_2SO_4 to solid NaCl, was bubbled into the ether solution obtained after filtration for 15 minutes, causing the formation of an off-white precipitate. This suspension was filtered, the solids washed with diethyl ether and hexane and then dried under vacuum overnight to afford 3.13 g of the title compound in 95% yield. **^{1}H NMR (CD_3OD, ppm)** δ 8.91 (m, 4H), δ 8.17 (m, 4H), δ 4.84 (s, 1H).

Synthesis and characterization of FcBB A

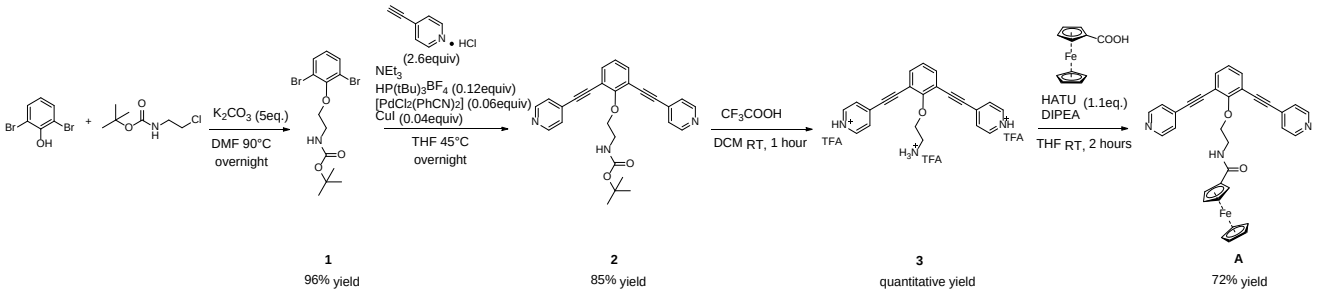

Scheme S2. Synthetic route for the preparation of FcBB **A.**

Synthesis of compound 1: A roundbottom Schlenk flask was charged with 2.5 g of 2,6-dibromophenol (1 equiv, 9.92 mmol) and 6.86 g of K_2CO_3 (5 equiv, 49.6 mmol). Next, 50 mL of dry and degassed DMF were added followed by slow addition of 1.78 g of *N*-(*tert*-butoxycarbonyl)-2-chloroethylamine (1 equiv, 9.92 mmol) prepared according to literature procedure. The mixture was stirred overnight at 90 °C, then cooled to room temperature and the volatiles subsequently removed under reduced pressure. To the residue was added 100 mL of water and the suspension extracted with dichloromethane (4×50 mL), dried over $MgSO_4$ and the volatiles removed under vacuum. The residue was purified by silica column chromatography with diethyl ether:triethylamine 9:1 to afford a white solid 3.76 g, 96%. **^{1}H NMR (CD_2Cl_2, ppm)** 7.57 (d, *J* = 8.0 Hz, 2H), 6.94 (t, *J* = 8.0 Hz, 1H), 5.24 (br s, 1H), 4.12 (t, *J* = 5.1 Hz, 2H), 3.57 (q, *J* = 5.1 Hz, 2H), 1.48 (s, 9H).

Synthesis of compound 2: A roundbottom Schlenk flask was charged with 1.9 g of **1** (1 equiv, 4.82 mmol), 1.74 g of 4-ethynylpyridine hydrochloride (2.6 equiv, 12.5 mmol) and 36.6 mg of CuI (0.05 mmol). The flask was flushed with argon before a degassed mixture of 40 mL of THF and 20 mL of triethylamine was added. A separate Schlenk flask was charged with 110.67 mg of $[Pd(PhCN)_2Cl_2]$ (6 mol%) and 167.4 mg of $P(tBu)_3{\cdot}HBF_4$ (12 mol%). To this mixture, 5 mL of triethylamine and 10 mL of THF were added. The mixture was stirred for five minutes before it was transferred to the first flask by syringe. The mixture was stirred at 45 °C overnight, then cooled to room temperature, quenched with water and extracted with ethyl acetate (4×50 mL). The organics were washed with water (2×50 mL) and brine (2×50 mL) then dried over $MgSO_4$ and the volatiles removed under vacuum. The residue was purified by silica column chromatography with dichloromethane:methanol 96:4 to afford a white solid 1.79 g, 85% yield. **^{1}H NMR (CD_2Cl_2, ppm)** δ 8.66 (m, 4H), 7.63 (d, *J* = 7.7 Hz, 2H), 7.46 (m, 4H), 7.21 (t, *J* = 7.7 Hz, 1H), 4.48 (t, *J* = 5.1 Hz, 2H), 3.60 (q, *J* = 5.1 Hz, 2H), 1.39 (s, 9H).

Synthesis of compound 3: A roundbottom flask was charged with **2**, 1.79 g (1 equiv, 4.07 mmol) dissolved in 20 mL of dichloromethane. 15 mL of trifluoroacetic acid were slowly added and the solution was stirred at room temperature for 1 h. The volatiles were removed under vacuum to afford a light brown solid which was thoroughly washed with dichloromethane and isolated in quantitative yield. **^{1}H NMR (CD_3CN, ppm)** δ 8.80 (m, 4H), 8.00 (m, 4H), 7.83 (d, *J* = 7.7 Hz, 2H), 7.38 (t, *J* = 7.7 Hz, 1H), 7.05 (br s, 3H), 4.62 (t, *J* = 5.2 Hz, 2H) 3.52 (br m 2H).

Synthesis of FcBB, A: A roundbottom Schlenk flask was charged with 260 mg of ferrocene carboxylic acid (1 equiv, 1.13 mmol) and 473 mg of HATU (1.1 equiv, 1.24 mmol). The flask was flushed with argon before a degassed mixture of 30 mL of dry THF and 0.64 mL of DIPEA (2.5 equiv, 2.83 mmol) was added. This mixture was stirred for 1 hour. A separate Schlenk flask was charged with 770 mg of compound **3**, (1 equiv, 1.13 mmol). After dissolving the compound in 10 mL of dry THF, 2.5 mL of DIPEA (10 equiv, 11.30 mmol) were added and the mixture stirred for few minutes before it was transferred to the first flask. The reaction mixture was stirred for additional 2 hours at room temperature then quenched with water and extracted with ethyl acetate (4×50 mL). The organics were washed with water (2×50 mL) then saturated $NaHCO_3$ solution (2×50 mL). 1 M HCl was added causing the product to go into the water phase. The aqueous phase was then washed with ethyl acetate (2×50 mL) before 5 M NaOH was added and the product extracted back into the organic phase which was washed with brine (2×50 mL) then dried over $MgSO_4$ and the volatiles removed under vacuum. The residue was recrystallized from dichloromethane and hexane to afford a light yellow solid, 473 mg, 72% yield. **^{1}H NMR (CD_3CN, ppm)** δ 8.61 (m, 4H), 7.62 (d, *J* = 7.8 Hz, 2H), 7.48 (m, 4H), 7.21 (t, *J* = 7.7 Hz, 1H), 6.72 (br s, 1H), 4.61 (q, *J* = 2.2 Hz, 2H), 4.52 (t, *J* = 5.6 Hz, 2H), 4.28 (q, *J* = 2.2 Hz, 2H), 4.09 (s, 5H), 3.83 (q, *J* = 5.7 Hz, 2H). **^{13}C NMR (CD_2Cl_2, ppm)** δ 169.88, 149.95, 134.92, 130.51, 125.32, 123.98, 116.45, 91.61, 89.17, 76.01, 74.23, 70.38, 69.62, 68.02, 40.07. **HR FDMS** (m/z) found 551.1291 expected 551.1297, $C_{33}H_{25}FeN_3O_2$.

Ferrocene building block, A. NMR characterization.

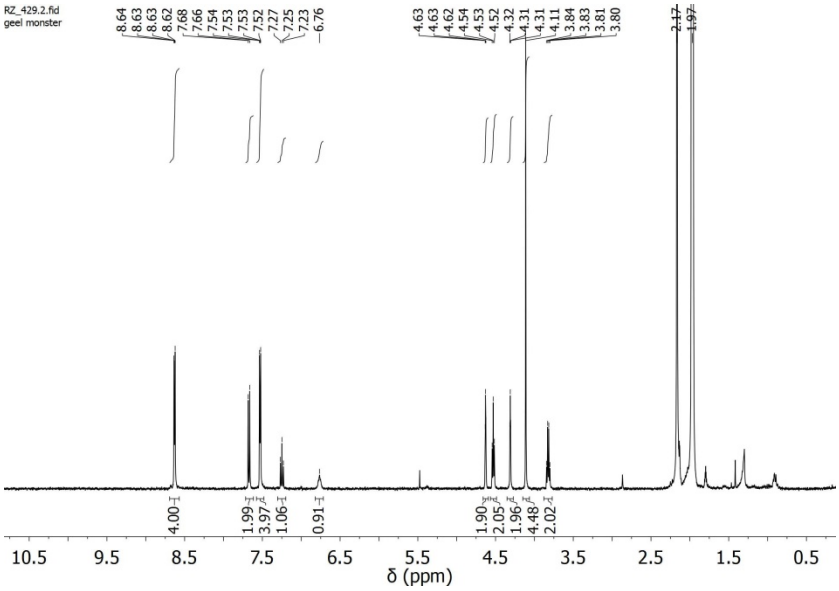

Figure S1. Ferrocene building block **A**, ^{1}H NMR in CD_3CN.

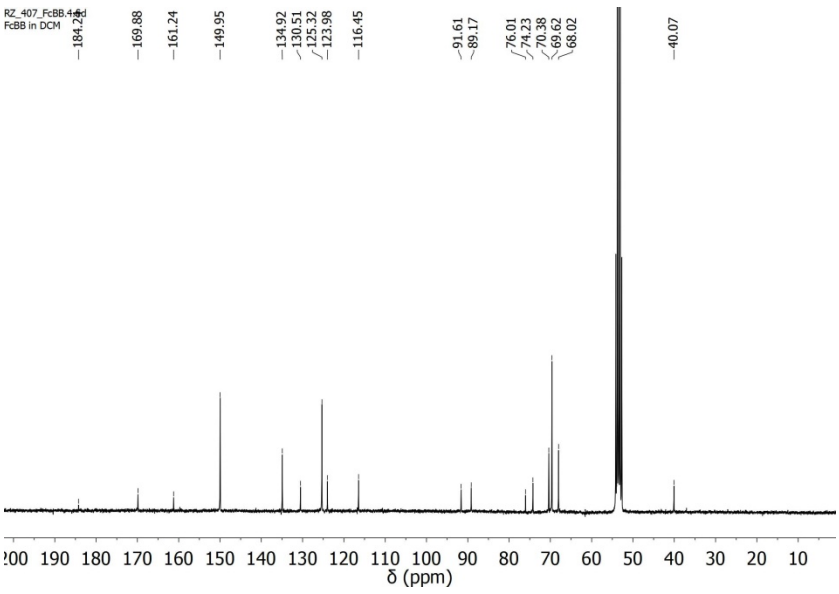

Figure S2. Ferrocene building block **A**, ^{13}C NMR in CD_2Cl_2.

Crystallographic details FcBB, **A**; CCDC number: 1922848

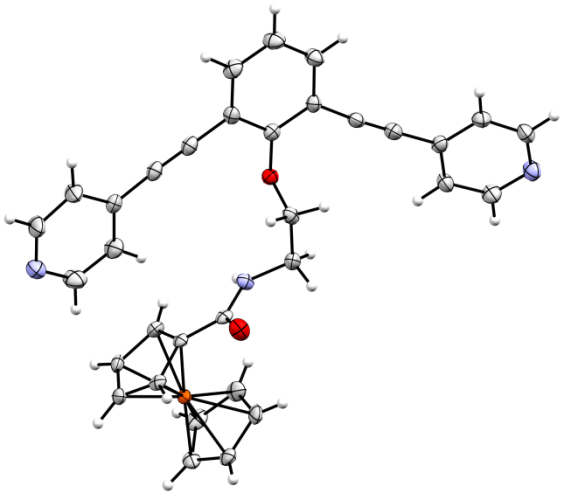

$C_{33}H_{25}FeN_3O_2$, Fw = 551.41, yellow needle, 0.20 × 0.11 × 0.10 mm, Tetragonal, $I4_1/a$ (No: 88), a = 24.833 (3), c = 17.086 (3) Å, V = 10537 (3) $Å^3$, Z = 16, D_x = 1.390 g/cm^3, μ = 0.61 mm^{-1}. 41611 reflections were measured up to a resolution of $(\sin \theta/\lambda)_{max}$ = 0.595 $Å^{-1}$. 4633 reflections were unique (R_{int} = 0.116), of which 3205 were observed [I>2σ(I)]. 355 parameters were refined with 0 restraints. R1/wR2 [I > 2σ(I)]: 0.0366/0.0865 R1/wR2 [all refl.]: 0.0731/0.0744. S = 0.99. Residual electron density between −0.36 and 0.25 $e/Å^3$.

Figure S3. X-ray crystal structure of FcBB **A**. Ellipsoids are set at 50% probability.

Synthesis and characterization of TTFBB B

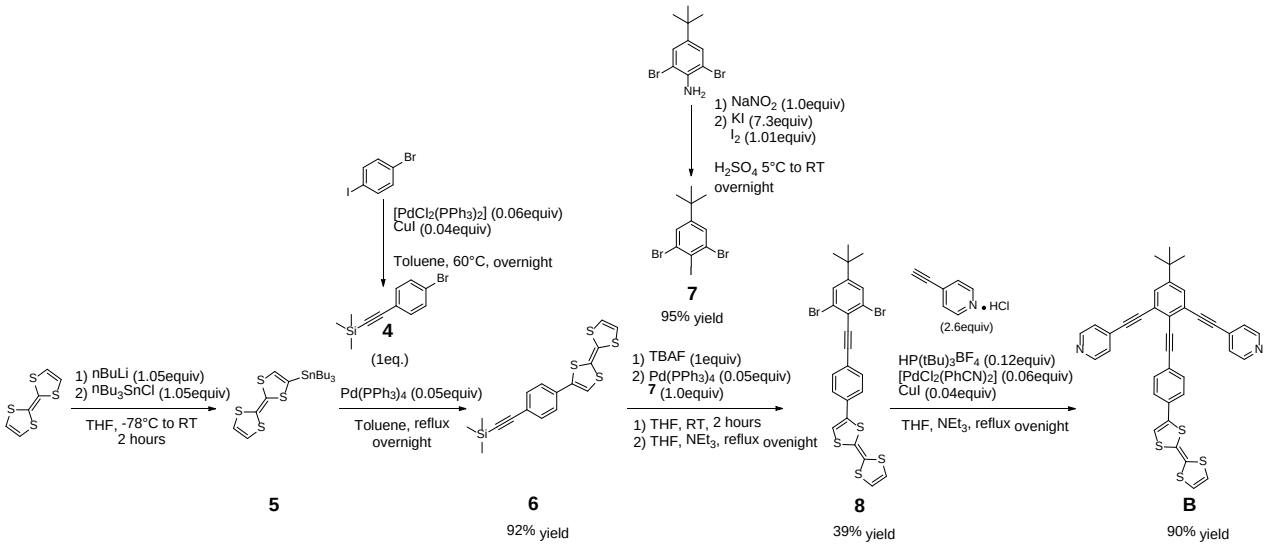

Scheme S3. Synthetic route for the preparation of TTFBB **B**.

Synthesis of compound 5: compound **5** was prepared according to a modified literature procedure.[5] An argon flushed Schlenk roundbottom flask was charged with 700 mg (3.42 mmol) of TTF and 20 mL of dry THF. The solution was cooled to -78 °C in a dry ice/acetone bath then 1.37 mL (1.05 equiv, 3.59 mmol) of nBuLi 2.5 M were added dropwise during the course of 15 minutes. The solution was left stirring under these condition for 60 min then 975 µL (1.05 equiv, 3.59 mmol) of $SnBu_3Cl$. The solution was stirred for an additional 30 min before it was allowed to warm to room temperature over the course of 2 hours. The reaction was quenched with 100 mL of water and extracted with ethyl acetate (3×50 mL). The combined organic layers were dried over $MgSO_4$ and the volatiles removed under vacuum to afford 1.81 g of the crude product, which was used without further purification. **^{1}H NMR (CD_2Cl_2, ppm)** δ 6.31(s, 2H), δ 6.14(s, 1H), δ 1.53 (m, 6H), δ 1.34 (m, 6H), δ 1.09 (m, 6H), δ 0.90 (t, J = 6.5 Hz, 9H).

Synthesis of compound 6: A roundbottom Schlenk flask was charged with crude **5**, 1.81 g (1 equiv, 3.65 mmol), 0.926 g of 1-bromo-4-[2-(trimethylsilyl)ethynyl]benzene (1 equiv, 3.65 mmol) and 0.211 g of $[Pd(PPh_3)_4]$ (5 mol%). The flask was purged with argon before 100 mL of degassed toluene were added. The mixture was refluxed overnight then cooled to room temperature and the solvent removed under reduced pressure. The residue was dissolved in a minimal amount of hexane:dichloromethane 8:2 and chromatographed over silica gel to afford a bright orange compound in 92% yield, 1.208 g. **^{1}H NMR (CD_2Cl_2, ppm)** δ 7.43 (m, 4H), δ 6.66 (s, 1H), δ 6.42 (s, 2H), δ 0.22 (s, 9H).

Synthesis of compound 7: A roundbottom flask was charged with H_2SO_4 (20 mL) and cooled in an ice bath for 15 minutes. Subsequently, 2.471 g of $NaNO_2$ (1.01 equiv, 35.86 mmol) were carefully added to the flask, maintaining the temperature below 5 °C. A solution of 10 g of 2,6-dibromo-4-*tert*-butyl aniline (1 equiv, 32.57 mmol) in 100 mL of acetic acid was added dropwise over the course of 3 hours, with the temperature always maintained below 5 °C. After the addition, the mixture was allowed to warm to room temperature and stirred for an additional 4

hours. After this time, a solution of 39.32 g of KI (7.3 equiv, 236.86 mmol) and 8.26 g I_2 (1 equiv, 32.57 mmol) in 75 mL of water was added and the mixture stirred overnight at room temperature. The resulting mixture was quenched by pouring it in 1.5 L of a 15% solution of sodium hydroxide and then extracted with ethyl acetate (4×150 mL). The organic phase was washed with water (2×100 mL) and brine (2×100 mL), dried over $MgSO_4$ and the volatiles removed under vacuum. The residue was purified by silica column chromatography with petroleum ether to afford a white solid 12.90 g, 95% yield. **^{1}H NMR (CD_2Cl_2, ppm)** δ 7.63 (s, 2H), δ 1.31 (s, 9H).

Synthesis of compound 8: A roundbottom Schlenk flask was charged with **6**, 1.208 g (1 equiv, 3.21 mmol) and 20 mL of degassed THF. To this solution 3.2 mL of tetrabutylammonium fluoride (1 M solution, 1 equiv, 3.21 mmol) was added and the solution was stirred at room temperature in the dark for 2 hours. The completeness of the reaction was check by TLC, after which the volatiles were removed under vacuum. To the same flask, 1.334 g of compound **7** (1 equiv, 3.21 mmol) and 0.350 mg of [$Pd(PPh_3)_4$] (10 mol%) were added. The flask was purged with argon before 60 mL of degassed THF and 20 mL of degassed triethylamine were added. The mixture was refluxed overnight then cooled to room temperature, quenched by addition of water and extracted with ethyl acetate (3x100 mL). The organics were then dried over $MgSO_4$ and the volatiles removed under vacuum. The residue was purified by silica column chromatography with dichloromethane:hexane 1:2 to afford a red crystalline solid 0.740 g, 39% yield. **^{1}H NMR (CD_2Cl_2, ppm)** δ 7.66 (s, 2H), δ 7.64 (m, 2H), δ 7.47 (m, 2H), δ 6.71 (s, 1H), δ 6.42 (s, 2H), δ 1.34 (s, 9H).

Synthesis of TTFBB, B: A roundbottom Schlenk flask was charged with **8**, 0.740 g (1 equiv, 1.24 mmol), 0.452 g of 4-ethynylpyridine hydrochloride (2.6 equiv, 3.29 mmol) and 9.5 mg of CuI (0.05 mmol). The flask was flushed with argon before a degassed mixture of 40 mL of THF and 20 mL of triethylamine was added. A separate Schlenk flask was charged with 28.6 mg of [$Pd(PhCN)_2Cl_2$] (6 mol%) and 43.3 mg of $P(tBu)_3$·HCl (0.12 mol%). To this mixture, 5 mL of triethylamine and 10 mL of THF were added. The mixture was stirred for five minutes before it was transferred to the first flask by syringe. The mixture was refluxed overnight then cooled to room temperature, quenched with water and extracted with dichloromethane (4×50 mL). The organics were washed with water (2×50 mL) and brine (2×50 mL) then dried over $MgSO_4$ and the volatiles removed under vacuum. The residue was purified by silica column chromatography with dichloromethane:methanol 94:6 to afford a red crystalline solid 0.715 g, 90% yield. **^{1}H NMR (CD_2Cl_2, ppm)** δ 8.66 (m, 4H), δ 7.72 (s, 2H), δ 7.60 (m, 2H), δ 7.48 (m, 4H), δ 7.46 (m, 2H), δ 6.72 (s, 1H), δ 6.43 (s, 2H), δ 1.41 (s, 9H). **^{13}C NMR (CD_2Cl_2, ppm)** δ 151.80, 149.49, 134.95, 132.45, 131.79, 130.46, 130.07, 126.12, 124.74, 122.64, 119.05, 118.98, 115.25, 97.07, 91.94, 90.49, 88.04, 34.72, 30.52. **HR ESI-MS** (*m*/*z*) found 638.0976 expected 638.0979, $C_{38}H_{26}N_2S_4$.

TTF building block, **B**.

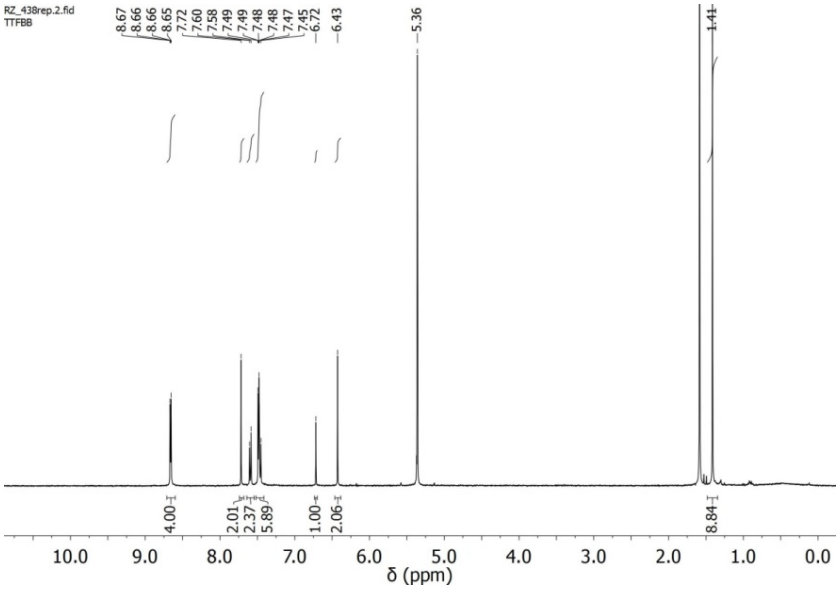

Figure S4. TTF building block B, ^{1}H NMR in CD_2Cl_2.

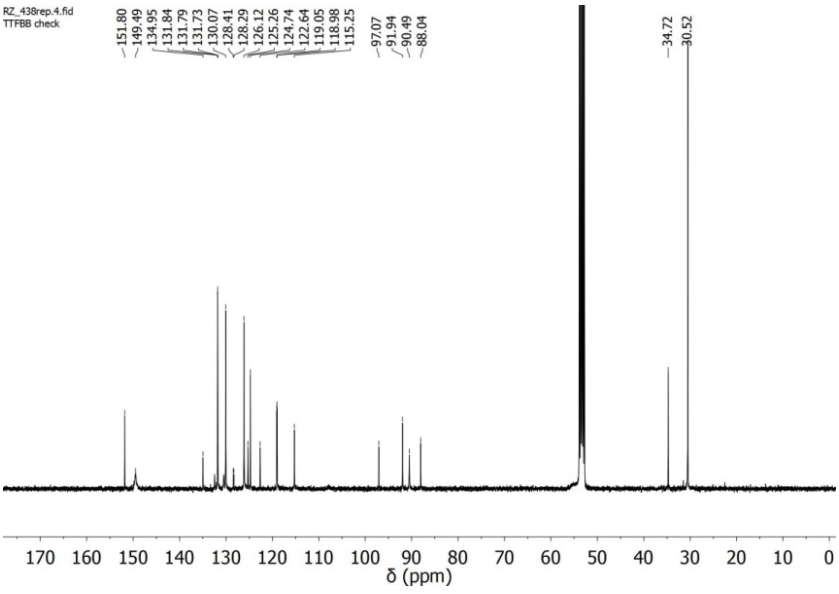

Figure S5. TTF building block **B**, ^{13}C NMR in CD_2Cl_2.

Crystallographic details TTFBB, **B**; CCDC number: 1922846.

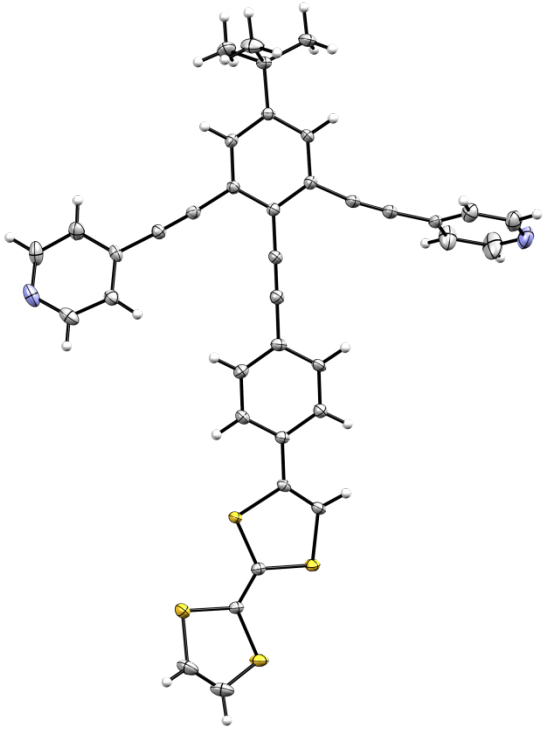

$C_{38}H_{26}N_2S_4$, Fw = 638.85, orange plate, 0.56 × 0.35 × 0.20 mm, Triclinic, *P* (No: 2), a = 9.1542 (3), b = 10.4410 (4), c = 17.0912 (6) Å, α = 78.573 (2), β = 86.194 (2), γ = 82.405 (2) °, V = 1585.77 (10) $Å^3$, Z = 2, D_x = 1.338 g/cm^3, μ = 0.33 mm^{-1}. 36086 reflections were measured up to a resolution of $(\sin \theta/\lambda)_{max}$ = 0.627 $Å^{-1}$. 6546 reflections were unique (R_{int} = 0.065), of which 4874 were observed [I>2σ(I)]. 400 parameters were refined with 0 restraints. R1/wR2 [I > 2σ(I)]: 0.0392/0.0910 R1/wR2 [all refl.]: 0.0652/0.1069. S = 0.94. Residual electron density between −0.35 and 0.46 e/$Å^3$.

Figure S6. X-ray crystal structure of TTFBB **B**. Ellipsoids are set at 50% probability.

Synthesis and characterization of twisted TTFBB C

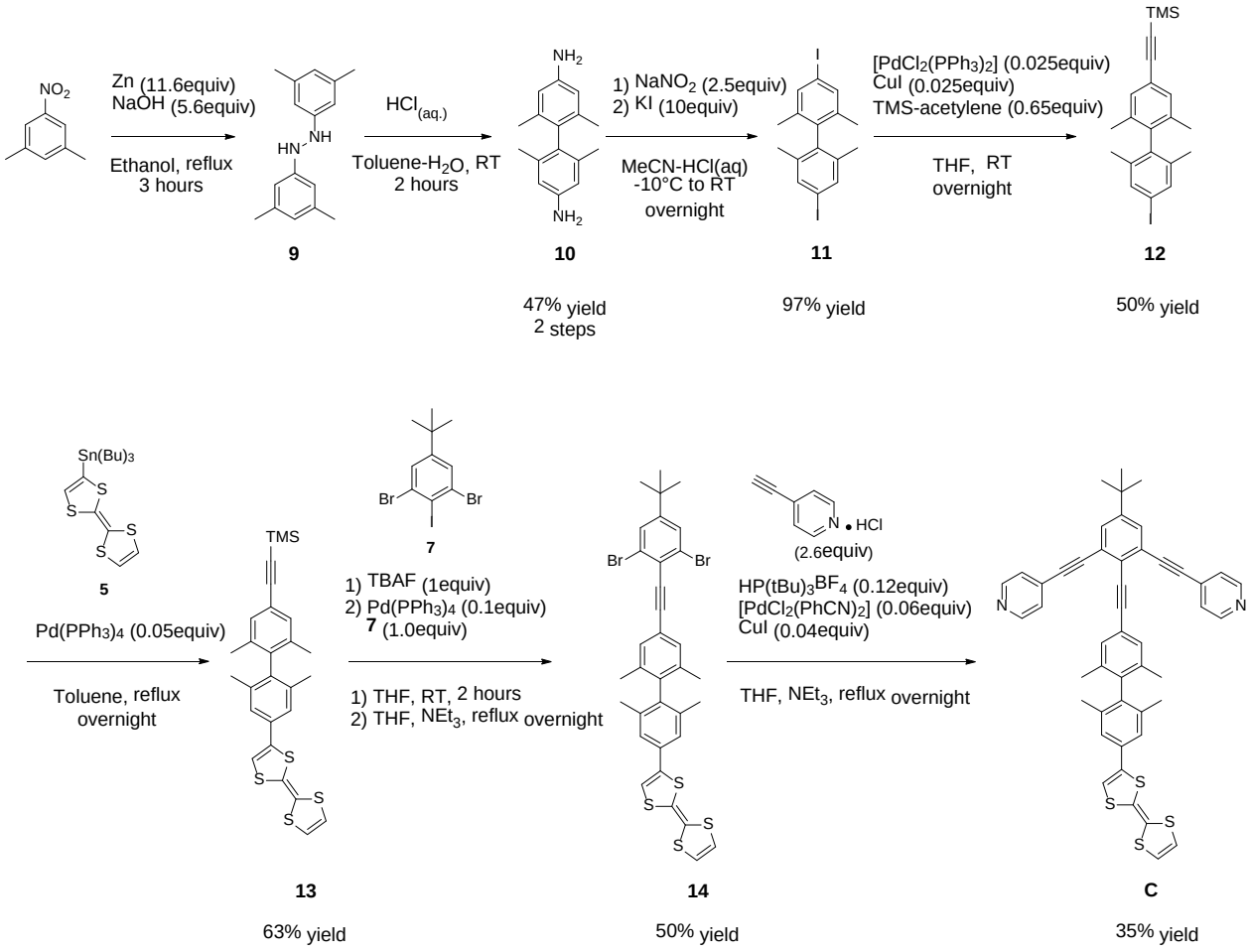

Scheme S4. Synthetic route for the preparation of TwistedTTFBB **C**.

Synthesis of compound 9: This compound was prepared according to a modified literature procedure.[6] A roundbottom Schlenk flask equipped with a condenser and a dropping funnel was charged with 10g of 3,5-dimethylnitrobenzene (1 equiv, 66.15 mmol) and 25 g of zinc powder (5.8 equiv, 384 mmol). The flask was flushed with argon before 60 mL of degassed ethanol was added. The mixture was heated to reflux, after which a degassed solution of 15 g of NaOH (5.6 equiv, 375 mmol) in 50 mL of water was carefully added dropwise over the course of 1 hour. After the addition was completed the mixture was refluxed for an additional 2 hours, followed by the addition of an extra 10 g of zinc powder and continued reflux for another 2 hours. The mixture was allowed to cool to room temperature before the addition of 200 mL of diethyl ether , followed by filtration of the mixture filtered over Celite. The solution obtained was washed with water (3×100 mL), the organics dried over magnesium sulfate and the volatiles removed under vacuum. The crude product containing few impurities was used in the next step without further purification. **^{1}H NMR (CD_2Cl_2, ppm)** δ 7.57 (s 2H), δ 6.51 (s, 4H), δ 5.63 (br s, 2H) δ 2.27 (s, 12H).

Synthesis of compound 10: Crude **9** was dissolved in 100 mL of toluene and to this solution was added 100 mL 6 M HCl and the mixture stirred vigorously at room temperature for 2 hours. The organic layer was discarded and the aqueous phase was washed with ethyl acetate (3×50 mL). The pH of the aqueous phase was adjusted to about 14 by addition of 5 M NaOH causing the formation of white precipitate which was extracted with ethyl acetate (3×100 mL). The organic layer was washed with slightly basic water (3×50 mL) dried over magnesium sulfate and the volatiles removed under vacuum to afford an off-white solid 7.45 g, 47% yield over two steps, which was used without further purification in the next step. **^{1}H NMR (CD_2Cl_2, ppm)** δ 6.50 (s, 4H), δ 3.49 (br s, 4H) 1.84 (s, 12H).

Synthesis of compound 11: This compound was prepared according to a modified literature procedure.[7] Crude compound **10**, 2.9 g (1 equiv, 12.1 mmol) was dissolved in acetonitrile 100 mL before the addition of 100 mL of 2 M HCl. The solution was cooled to −10° C in an ice-salt bath. 2.09 g of solid $NaNO_2$ (2.5 equiv, 30.25 mmol) were added portionwise over the course of 30 minutes whilst maintaining the temperature around −10° C. After the addition was complete, the mixture was stirred for 30 minutes at −10 °C before 20 g of KI (10 equiv, 120 mmol) was slowly added. The mixture was allowed to warm to room temperature over the course of 1 hour and stirred overnight at room temperature. Orange precipitate forms and it is collected by filtration, dissolved in ethyl acetate and washed with water (3×50 mL). The organic layer is dried over magnesium sulfate and the volatiles removed under vacuum to afford 5.45 g of product in 97% yield. This material was used in the next step without further purification. **^{1}H NMR (CD_2Cl_2, ppm)** δ 7.54 (s, 4H), δ 1.87 (s, 12H).

Synthesis of compound 12: A roundbottom Schlenk flask was charged with **11**, 2.50 g (1 equiv, 5.41 mmol), 5 mg of CuI (0.025 mmol) and $[Pd(PPh_3)_2Cl_2]$ 17.5 mg (0.025 mmol). The flask flushed with argon before a degassed mixture of 180 mL of THF and 20 mL of triethylamine was added. To this mixture, trimethylsilylacetylene 0.5 mL (0.65 equiv, 3.5 mmol) was added and the mixture stirred at room temperature overnight. The volatiles were removed under vacuum and the residue was purified by silica column chromatography with dichloromethane:hexane 1:2 to afford about 1.4 g of the unreacted excess of starting material **11**, then the desired product as white crystalline solid 0.750 g, 49.6% yield. **^{1}H NMR (CD_2Cl_2, ppm)** δ 7.54 (s, 2H), δ 7.27 (s, 2H), δ 1.88 (s, 6H), δ 1.86 (s, 6H), δ 0.28 (s, 9H).

Synthesis of compound 13: A roundbottom Schlenk flask was charged with **12**, 0.750 g (1 equiv, 1.74 mmol), $[Pd(PPh_3)_4]$ 100 mg (5 mol%) and crude compound **5**, 1 g (1.1 equiv, 2.0 mmol). The flask flushed with argon before degassed toluene, 50 mL was added. The mixture was refluxed overnight, allowed to cool to room temperature before the volatiles were removed under vacuum. The residue was purified by silica column chromatography with dichloromethane:hexane 1:1 to afford the desired product as yellow solid, 0.560 g, 63.4% yield. **^{1}H NMR (CD_2Cl_2, ppm)** δ 7.29 (s, 2H), δ 7.24 (s, 2H), δ 6.62 (s, 1H), δ 6.42 (s, 2H), δ 1.92 (s, 6H), δ 1.90 (s, 6H), δ 0.29 (s, 9H).

Synthesis of compound 14: A roundbottom Schlenk flask was charged with **13**, 560 mg (1 equiv, 1.10 mmol) and 20 mL of degassed THF. To this solution 1.1 mL of tetrabutylammonium fluoride (1 M solution, 1 equiv, 1.1 mmol) were added and the solution was stirred at room temperature in the dark for 1 hour. The completeness of the reaction was check by TLC. To the same flask under continuous argon purging, 0.552 g of compound **7** (1.2 equiv, 1.32 mmol), 130

mg of [$Pd(PPh_3)_4$] (10 mol%) and a degassed mixture of THF 40 mL and triethylamine 20 mL were added. The mixture was refluxed overnight then cooled to room temperature, quenched by addition of water and extracted with ethyl acetate (3×100 mL). The organics were then dried over $MgSO_4$ and the volatiles removed under vacuum. The residue was purified by silica column chromatography with dichloromethane:hexane 1:2 to afford a yellow solid 0.405 g, 50% yield. **^{1}H NMR (CD_2Cl_2, ppm)** δ 7.66 (s, 2H), δ 7.44 (s, 2H), δ 7.26 (s, 2H), δ 6.63 (s, 1H), δ 6.42 (s, 2H), δ 1.95 (s, 12H), 1.35 (s, 9H).

Synthesis of twistedTTFBB, C: A roundbottom Schlenk flask was charged with **14**, 0.400 g (1 equiv, 0.55 mmol), 0.200 g of 4-ethynylpyridine hydrochloride (2.6 equiv, 1.43 mmol) and 4.1 mg of CuI (0.05 mmol). The flask was flushed with argon before a degassed mixture of 40 mL of THF and 20 mL of triethylamine was added. A separate Schlenk flask was charged with 12.6 mg of [$Pd(PhCN)_2Cl_2$] (6 mol%) and 19.2 mg of $P(tBu)_3$·HCl (0.12 mol%). To this mixture, 5 mL of triethylamine and 10 mL of THF were added. The mixture was stirred for five minutes before it was transferred to the first flask by syringe. The mixture was refluxed overnight then cooled to room temperature, quenched with water and extracted with dichloromethane (4×50 mL). The organics were washed with water (2x50 mL) and brine (2×50 mL) then dried over $MgSO_4$ and the volatiles removed under vacuum. The residue was purified by silica column chromatography with dichloromethane:methanol 94:6 to afford a yellow powder 0.150 g, 35.4% yield. **^{1}H NMR (CD_2Cl_2, ppm)** δ 8.65 (m, 4H), δ 7.72 (s, 2H), δ 7.53 (m, 4H), δ 7.42 (s, 2H), δ 7.27 (s, 2H), δ 6.64 (s, 1H), δ 6.42 (s, 2H), δ 1.97 (s, 6H), δ 1.91 (s, 6H), δ 1.42 (s, 9H). **^{13}C NMR (CD_2Cl_2, ppm)** δ 151.44, 149.77, 140.51, 139.55, 136.08, 135.83, 131.11, 130.86, 130.60, 129.98, 125.97, 125.33, 124.60, 121.39, 119.03, 118.98, 112.88, 111.00, 108.89, 98.28, 92.27, 90.23, 86.14, 34.69, 30.53, 19.37, 19.27. **HR FD-MS** (*m*/*z*) found 770.1898 expected 770.1918, $C_{48}H_{38}N_2S_4$.

twistedTTF building block C

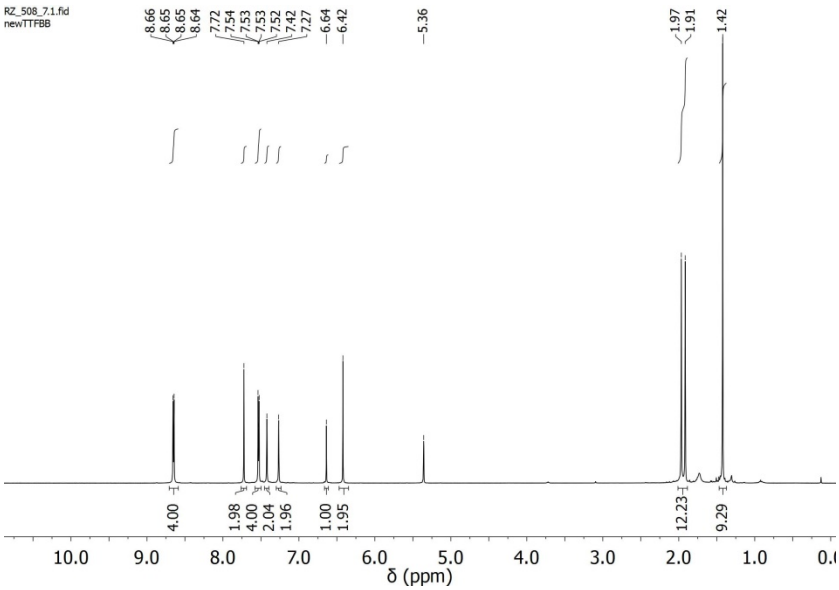

Figure S7. TwistedTTF building block **C**, ^{1}H NMR in CD_2Cl_2.

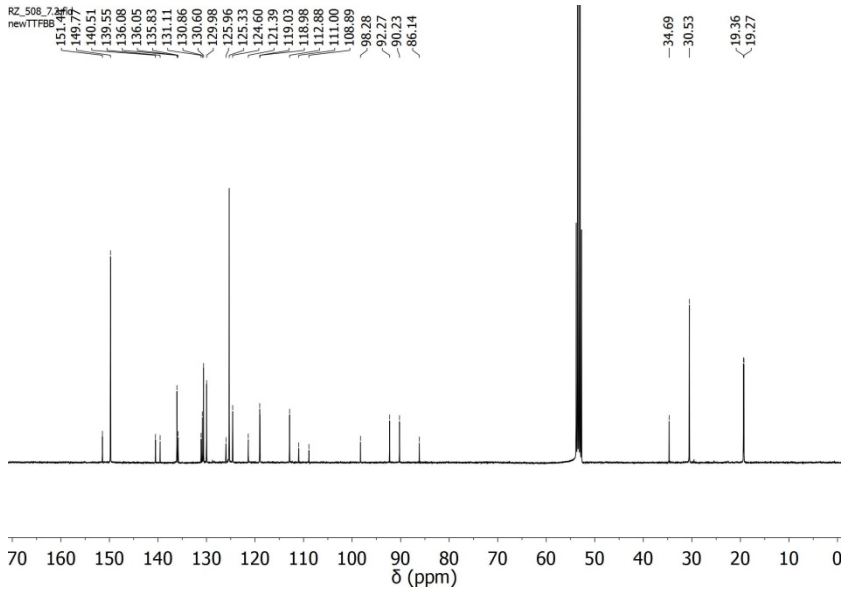

Figure S8. TwistedTTF building block **C**, ^{13}C NMR in CD_2Cl_2.

Crystallographic details twistedTTFBB, **C**; CCDC number: 1922847

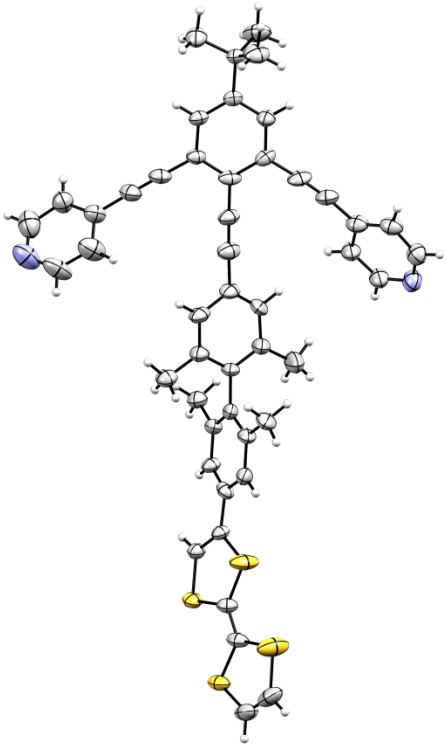

$C_{48}H_{38}N_2S_4$, Fw = 771.04, yellow needle, 0.58 × 0.30 × 0.21 mm, Orthorhombic, *Pbcn* (No: 60), a = 22.841 (1), b = 9.4123 (4), c = 42.3819 (18) Å, V = 9111.5 (7) $Å^3$, Z = 8, D_x = 1.124 g/cm^3, μ = 0.24 mm^{-1}. 61958 reflections were measured up to a resolution of $(\sin \theta/\lambda)_{max}$ = 0.597 $Å^{-1}$. 8072 reflections were unique (R_{int} = 0.061), of which 5799 were observed [I>2σ(I)]. 494 parameters were refined with 0 restraints. R1/wR2 [I > 2σ(I)]: 0.1061/0.3004 R1/wR2 [all refl.]: 0.1400/0.3116. S = 2.06. Residual electron density between −0.55 and 0.51 $e/Å^3$.

Figure S9. X-ray crystal structure of twistedTTFFBB **C**. Ellipsoids are set at 50% probability.

Synthesis and characterization of BBH E

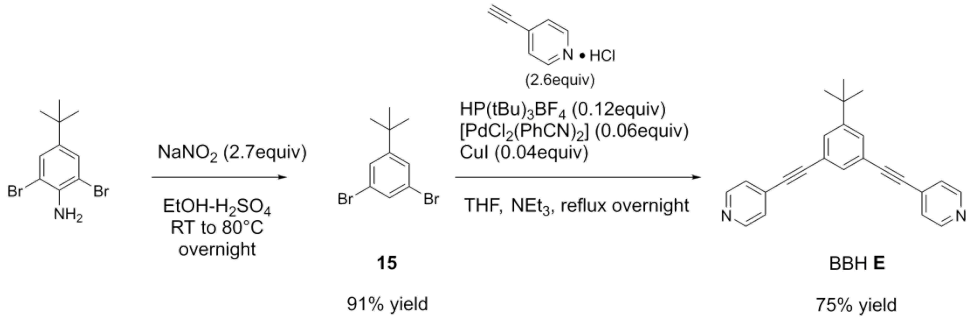

Scheme S5. Synthetic route for the preparation of BBH, **E.**

Synthesis of compound 15: 5 g of 2,6-dibromo-4-*tert*-butylbenzenamine (1 equiv, 16.3 mmol) were dissolved in 200 mL of ethanol and the solution heated to 50 °C. 25 mL of concentrated H_2SO_4 were added dropwise to this solution and the temperature was raised to 70 °C. 3.1 g of $NaNO_2$ (2.7 equiv, 44.6 mmol) were added portionwise over the course of 2 hours. After the addition was completed the temperature was raised to 80°C and the mixture stirred at this temperature overnight. The mixture was then poured over ice and extracted with ethyl acetate (3x100 mL). The organics were washed with brine (2×50 mL) and dried over $MgSO_4$, filtered and evaporated under reduced pressure. The residue was purified by silica gel column chromatography (petroleum ether 40-60°C) to afford 4.32 g, 91%. **^{1}H NMR (CD_2Cl_2, ppm)** δ 7.53 (m, 1H), δ 7.52 (m, 2H), δ 1.33 (s, 9H).

Synthesis of BBH, E: A roundbottom Schlenk flask was charged with **15**, 2.52 g (1 equiv, 8.63 mmol), 3.13 g of 4-ethynylpyridine hydrochloride (2.6 equiv, 22.44 mmol) and 66 mg of CuI (0.05 mmol). The flask was flushed with argon before a degassed mixture of 40 mL of toluene and 20 mL of triethylamine was added. A separate Schlenk flask was charged with 198 mg of $[Pd(PhCN)_2Cl_2]$ (6 mol%) and 300 mg of $P(tBu)_3$·HCl (0.12 mol%). To this mixture, 5 mL of triethylamilne and 10 mL of toluene were added. The mixture was stirred for five minutes before it was transferred to the first flask by syringe. The mixture was heated overnight at 60°C, then cooled to room temperature, quenched with water and extracted with dichloromethane (4×100 mL). The organics were washed with water (2×50 mL) and brine (2×50 mL) then dried over $MgSO_4$ and the volatiles removed under vacuum. The residue was purified by gradient silica column chromatography with dichloromethane:acetone 9:1. The desired product eluted with dichloromethane:acetone 2:1 to afford an off-white crystalline solid 2.19 g, 75.5% yield. **^{1}H NMR (CD_2Cl_2, ppm)** δ 8.60 (br, 4H), δ 7.64 (s, 2H), δ 7.58 (s, 1H), δ 7.42 (m, 4H), δ 1.35 (s, 9H). **^{13}C NMR (CD_2Cl_2, ppm)** δ 154.1, 151.8, 151.8, 133.9, 132.7, 131.8, 131.8, 127.4, 127.3, 124.2, 94.8, 88.7, 36.6, 32.7. **HR FD-MS** (m/z) found 336.1620 expected 336.1626, $C_{24}H_{20}N_2$.

Synthesis and characterization of ferrocenyl sulfonate tetrabutylammonium

Synthesis of compound 16, ferrocenyl sulfonic acid: Ferrocene (1 equiv, 2 g, 10.7 mmol) was suspended in 60 mL of acetic anhydride and the mixture cooled with ice. To this was added 0.71 mL of $ClSO_3H$ (1.25 g, 1 equiv, 10.7 mmol) dropwise over the course of 1 hour. The mixture was allowed to warm to room temperature and stirred for additional 2 hours then poured over ice, stirred for 1 hour and extracted with diethyl ether. The volatiles were removed under vacuum and the residue recrystallized from toluene/pentane mixture to afford the desired compound, 2.5 g, 90% yield. **^{1}H NMR (D_2O, ppm)** δ 4.56 (br, 2H), δ 4.37 (br, 7H).

Synthesis of compound 17, ferrocenyl sulfonate tetrabutylammonium: Ferrocene sulfonic acid 300 mg (1 equiv, 1.13 mmol) was dissolved in methanol prior to the additionof 1.13 mL of a 1 M solution of tetrabutylammonium hydroxide (1 equiv, 1.13 mmol). The mixture was stirred for 10 minutes before the volatiles were removed under vacuum. This compound was found to be very hygroscopic and always affording oil upon vacuum removal of solvents, therefore some water was added and the sample was freeze-dried affording an orange solid. **^{1}H NMR (CD_3CN, ppm)** δ 4.40 (t, *J* = 1.9 Hz, 2H), 4.24 (s, 5H), 4.09 (t, *J* = 1.9 Hz, 2H), 3.31 – 2.97 (m, 8H), 1.97 (m, 8H), 1.62 (m, 8H), 1.38 (m, 8H), 0.99 (t, *J* = 7.3 Hz, 12H). **HR ESI(neg,)-MS** (m/z) found 264.9616 expected 264.9622, (m) $C_{10}H_9FeO_3S$. Found 772.2029 expected 772.2093, (2m + TBA) $C_{36}H_{54}Fe_2NO_6S_2$.

Cages synthesis and characterization

Cages containing FcBB A

Cage $[Pd_{12}A_{24}]^{24+}$

Preparation: A Schlenk flask was charged with 22.04 mg (1 equiv, 40 µmol) of FcBB **A**, and 12.33 mg $[Pd(PF_6)_2(MeCN)_4]$ (0.55 equiv, 22 µmol). The flask was flushed with nitrogen before 4 ml of degassed CD_3CN were added. The resulting mixture was heated under N_2 at 60 °C overnight.

For MS analysis the same procedure was carried out but $[Pd(PF_6)_2(MeCN)_4]$ was replaced by $[Pd(BF_4)_2(MeCN)_4]$.

NMR Spectroscopy

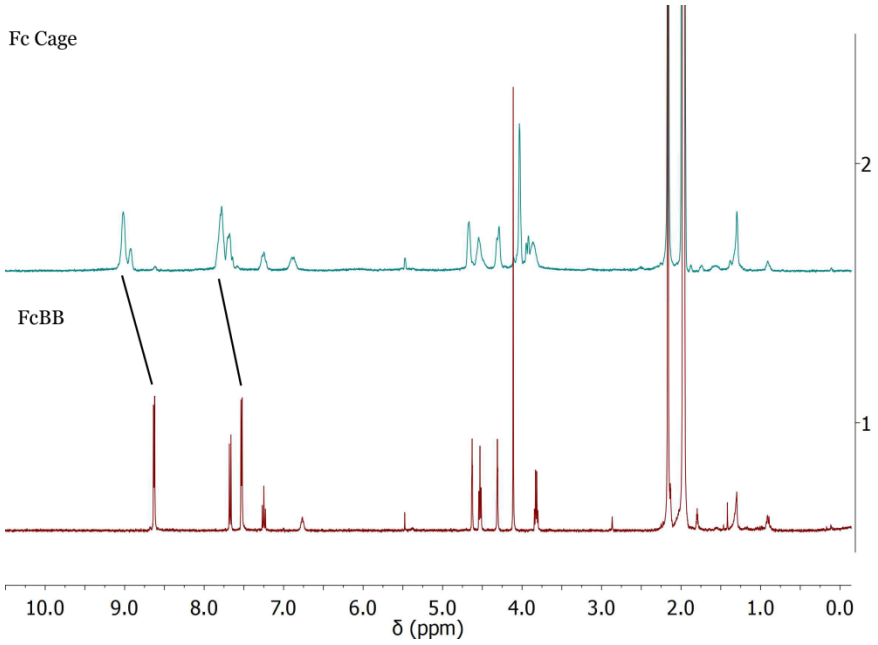

Figure S10. NMR spectra of FcBB **A** in CD_3CN (bottom) and its palladium ferrocene cage, $(Pd_{12}\mathbf{A}_{24})^{24+}$ in CD_3CN (top). The shift of the pyridine peaks upon metal coordination is indicated by the black lines.

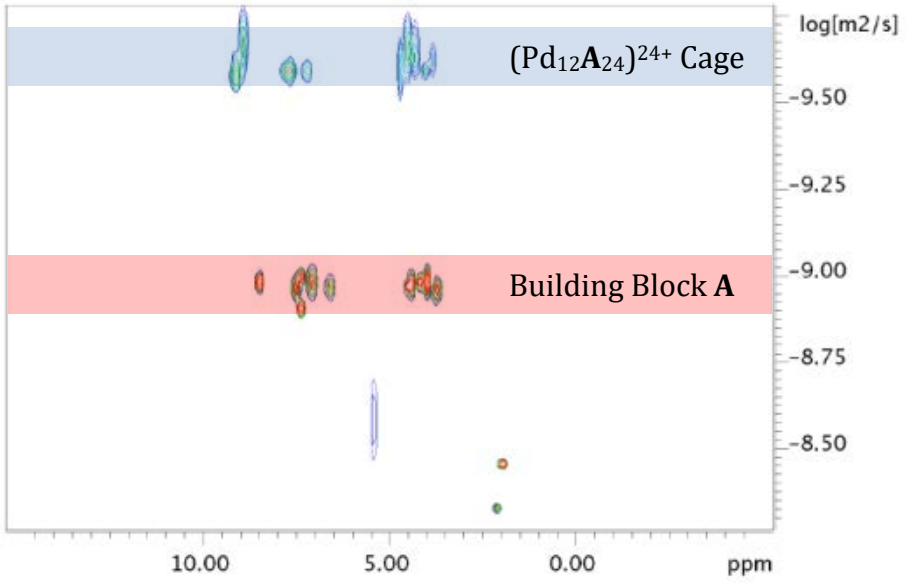

Figure S11. ^{1}H DOSY NMR overlay for FcBB **A**, showing a single diffusing species with a logD of -8.9 m^2s^{-1} and a palladium cage $(Pd_{12}\mathbf{A}_{24})^{24+}$, showing a single diffusing species with a logD of -9.6 m^2s^{-1}, in CD_3CN at 25 °C.

CSI-MS characterization

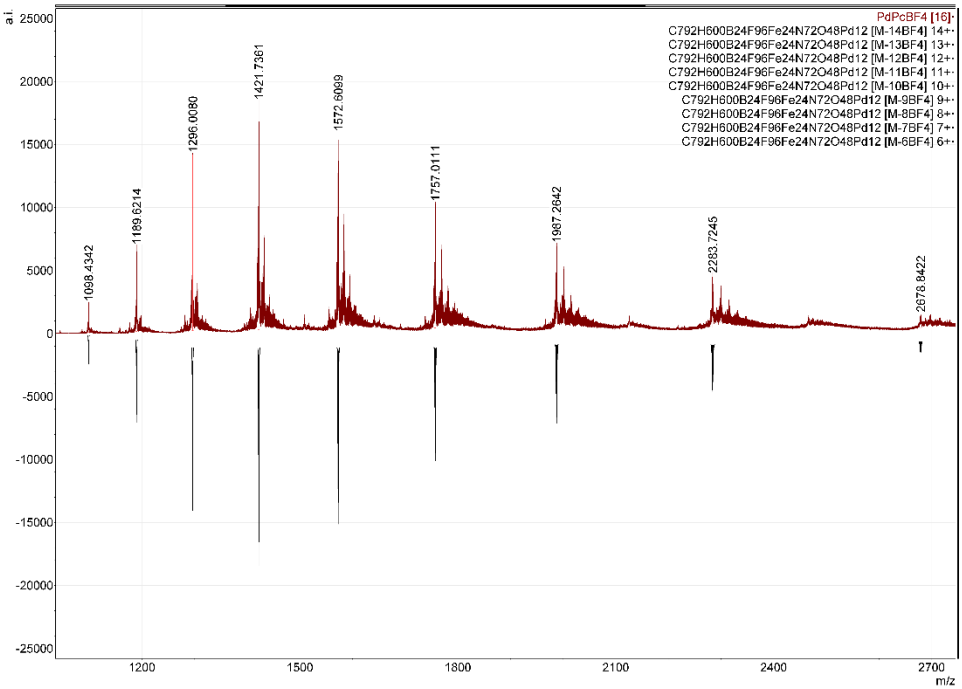

Figure S12. Full CSI-MS spectrum for cage sample $(Pd_{12}\mathbf{A}_{24})(BF_4)_{24}$ in CD_3CN.

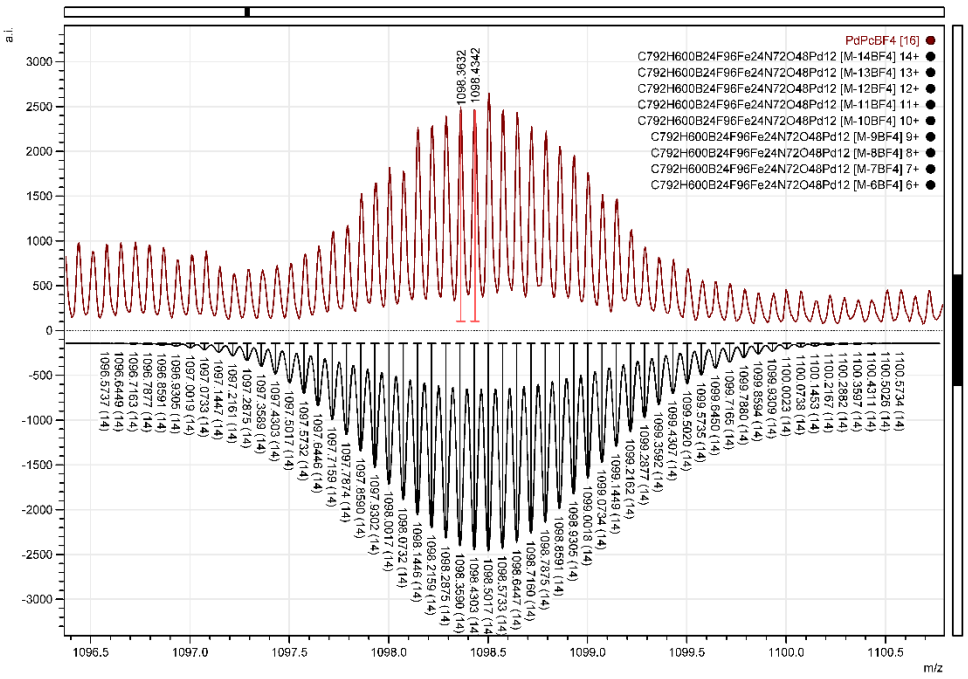

Figure S13. CSI-MS peak for $[(Pd_{12}\mathbf{A}_{24})(BF_4)_{15}]^{14+}$ in CD_3CN, *m/z* 1098.4342; calculated *m/z* 1098.4303.

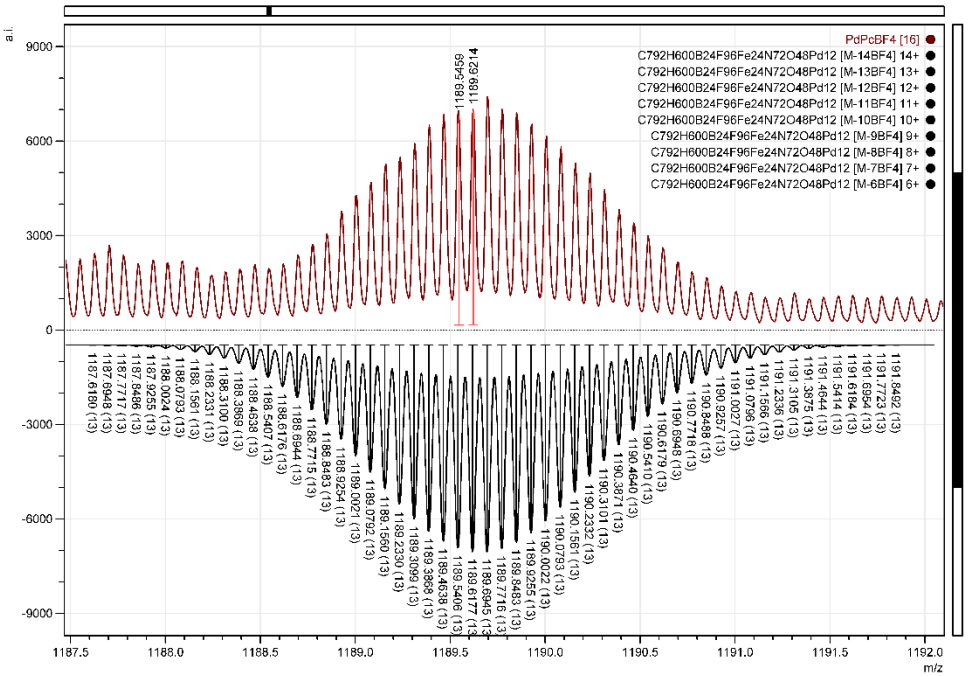

Figure S14. CSI-MS peak for $[(Pd_{12}\mathbf{A}_{24})(BF_4)_{14}]^{13+}$ in CD_3CN, *m/z* 1189.6214; calculated *m/z* 1189.6177.

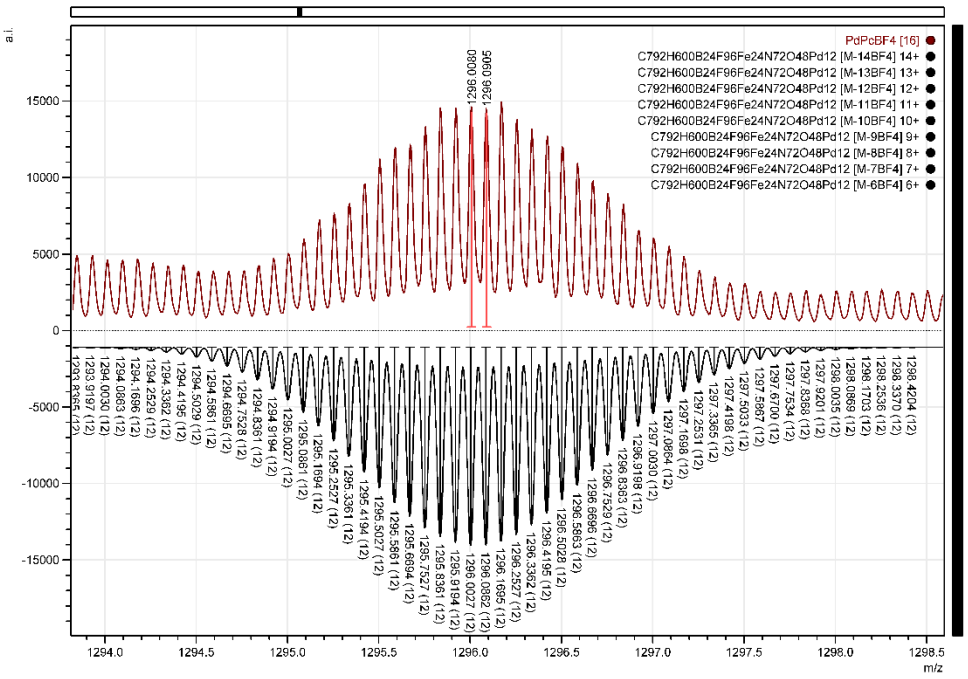

Figure S15. CSI-MS peak for $[(Pd_{12}\mathbf{A}_{24})(BF_4)_{13}]^{12+}$ in CD_3CN, *m/z* 1296.0905; calculated *m/z* 1296.0862.

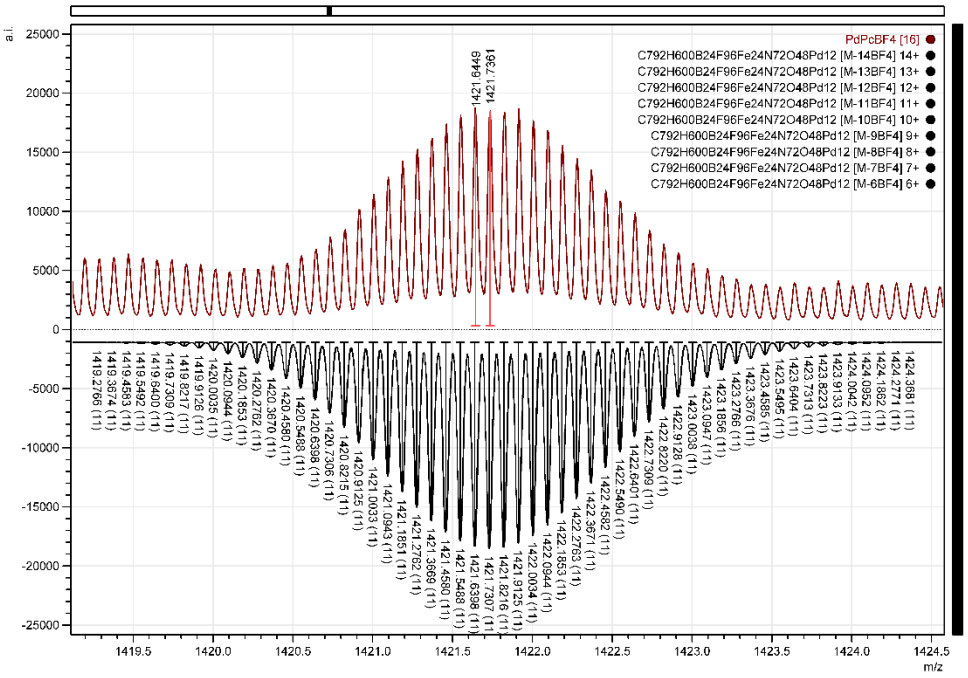

Figure S16. CSI-MS peak for $[(Pd_{12}\mathbf{A}_{24})(BF_4)_{11}]^{11+}$ in CD_3CN, *m/z* 1421.7361; calculated *m/z* 1421.7307.

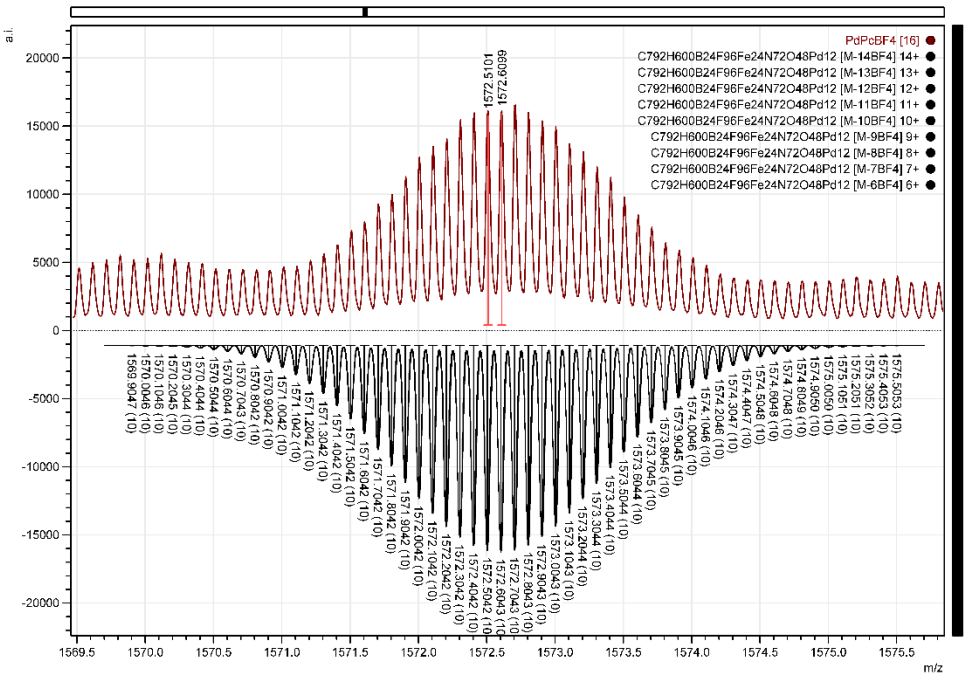

Figure S17. CSI-MS peak for $[(Pd_{12}\mathbf{A}_{24})(BF_4)_{10}]^{10+}$ in CD_3CN, *m/z* 1572.6099; calculated *m/z* 1572.6043.

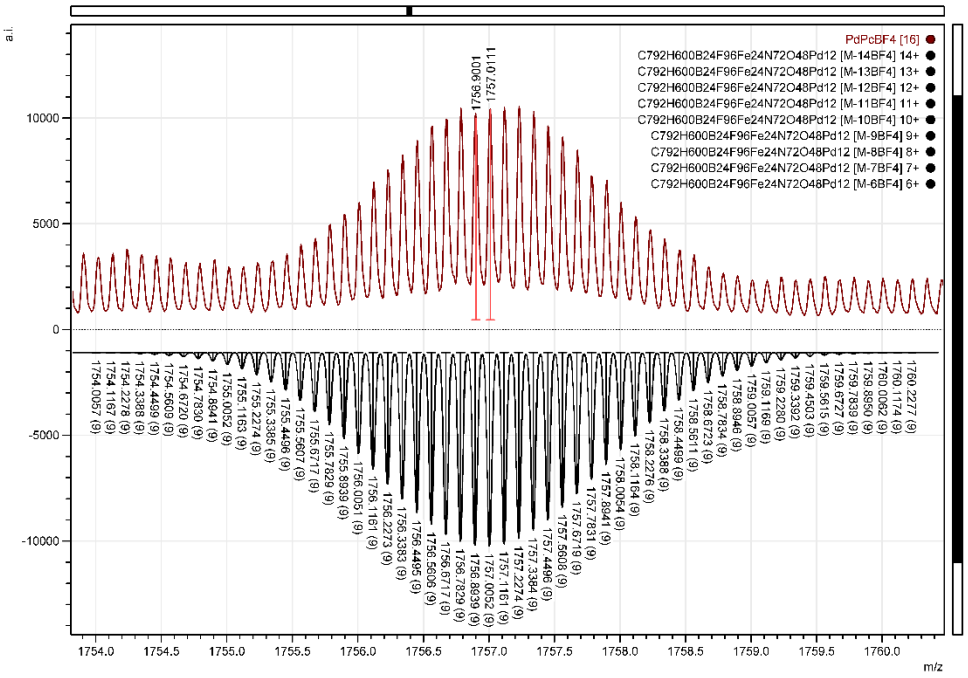

Figure S18. CSI-MS peak for $[(Pd_{12}\mathbf{A}_{24})(BF_4)_{10}]^{9+}$ in CD_3CN, *m/z* 1757.0111; calculated *m/z* 1757.0052.

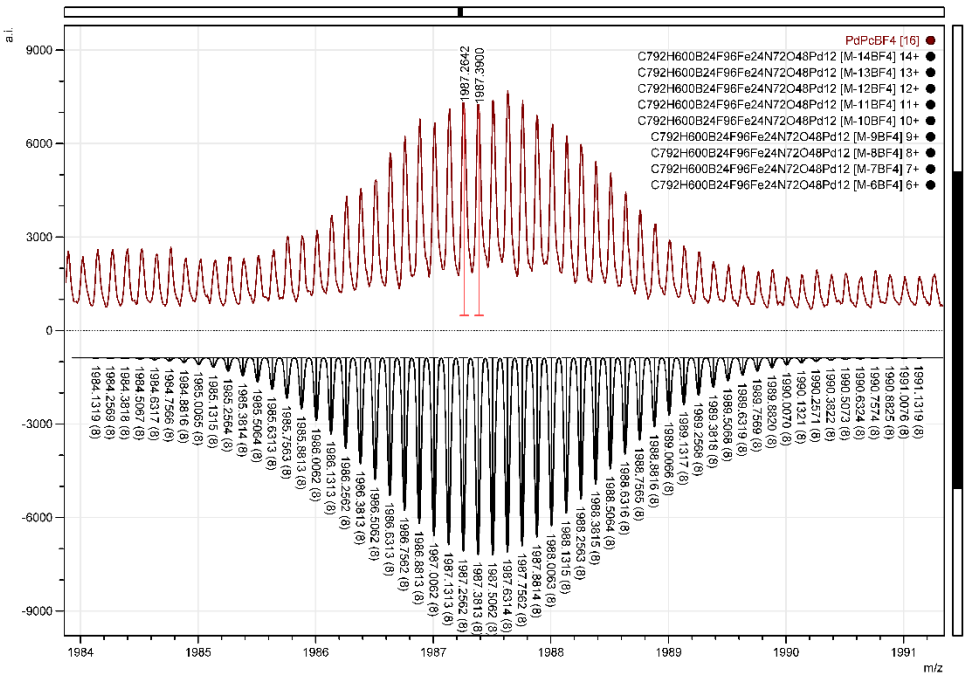

Figure S19. CSI-MS peak for $[(Pd_{12}\mathbf{A}_{24})(BF_4)_{10}]^{8+}$ in CD_3CN, *m/z* 1987.3900; calculated *m/z* 1987.3813.

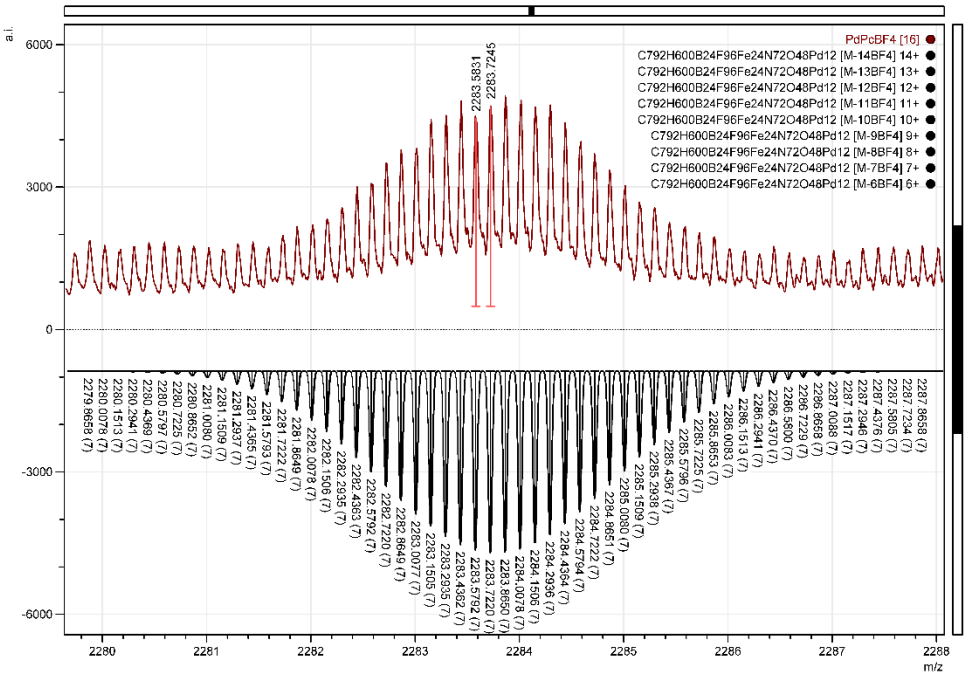

Figure S20. CSI-MS peak for $[(Pd_{12}\mathbf{A}_{24})(BF_4)_{10}]^{7+}$ in CD_3CN, *m/z* 2283.7245; calculated *m/z* 2283.7220.

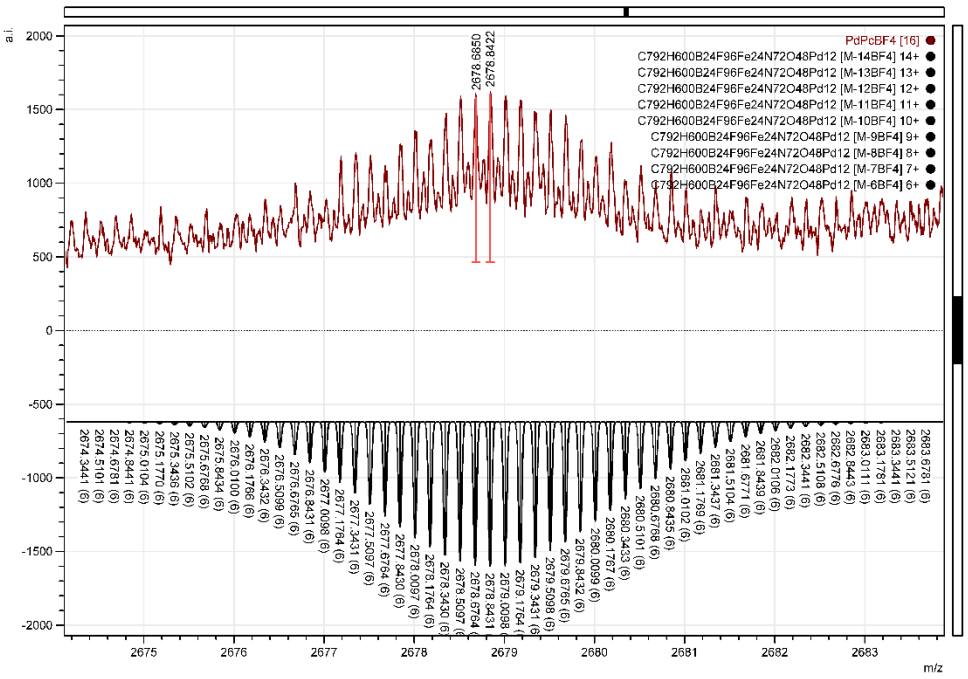

Figure S21. CSI-MS peak for $[(Pd_{12}\mathbf{A}_{24})(BF_4)_{10}]^{6+}$ in CD_3CN, *m/z* 2678.8422; calculated *m/z* 2648.8431.

Cage $[Pd_{12}E_{23}A_1]^{24+}$

Preparation: A Schlenk flask was charged with 0.918 mg (1 equiv, 1.66 µmol) of FcBB **A**, 12.886 mg (11 equiv, 38.33 µmol) of BBH **E** and 12.33 mg $[Pd(PF_6)_2(MeCN)_4]$ (0.55 equiv, 22 µmol). The flask was flushed with nitrogen before 4 ml of degassed CD_3CN were added. The resulting mixture was heated under N_2 at 60 °C overnight.

NMR Spectroscopy

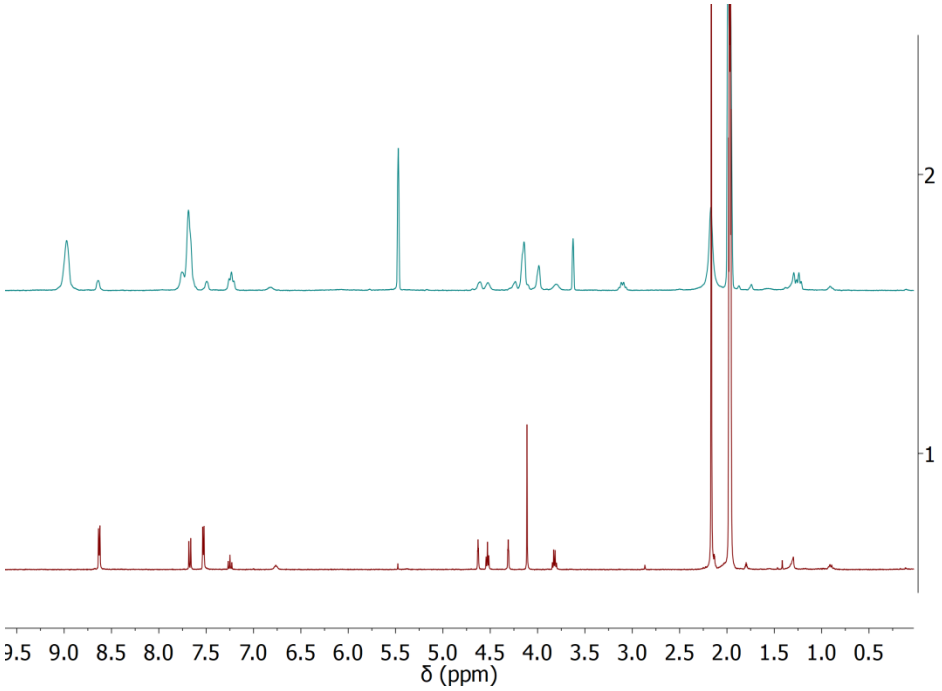

Figure S22. ^{1}H-NMR spectra of FcBB **A** in CD_3CN (bottom) and its palladium ferrocene cage, $(Pd_{12}\mathbf{E}_{23}\mathbf{A})^{24+}$ (top) in a 1:1 mixture of CD_3CN and CD_2Cl_2.

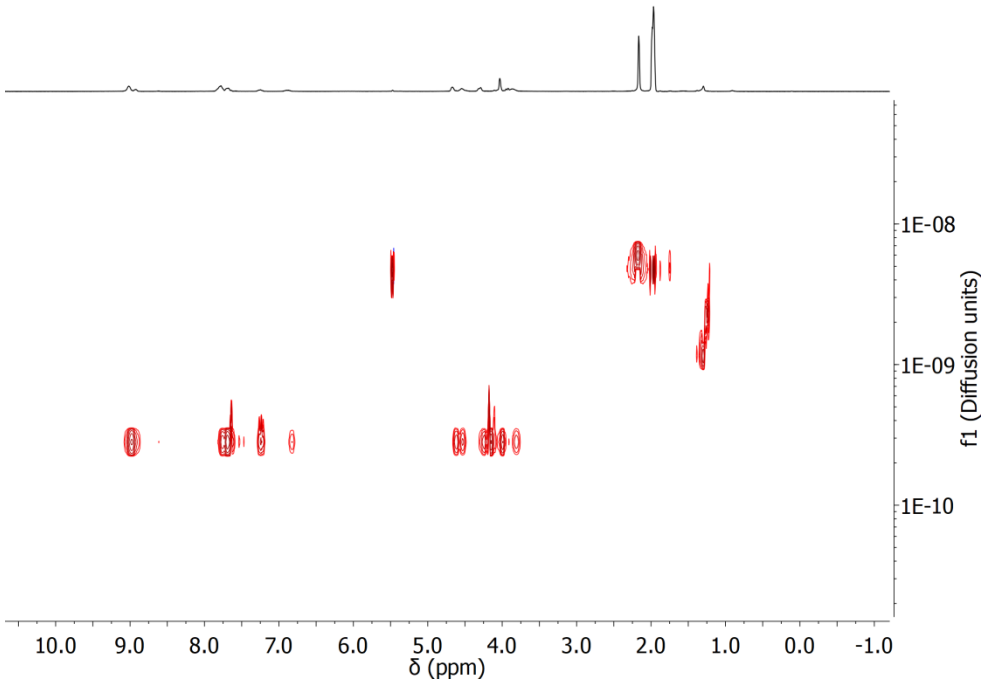

Figure S23. ^{1}H DOSY NMR for palladium cage $(Pd_{12}\mathbf{E}_{23}\mathbf{A})^{24+}$ in a 1:1 mixture of CD_3CN and CD_2Cl_2 showing a single diffusing species with a D value of $2.85 \cdot 10^{-10}$ m^2s^{-1} and logD of -9.54 m^2s^{-1} at 25 °C.

CSI-MS characterization

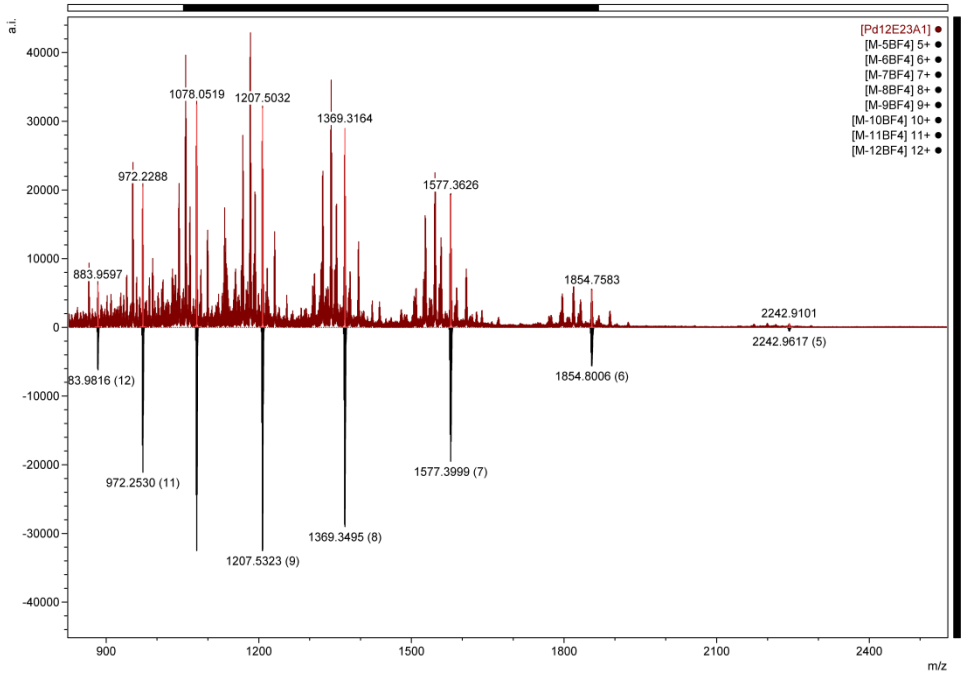

Figure S24. Full CSI-MS spectrum for cage sample (Pd$\mathbf{E}_{23}\mathbf{A}_1$)($PF_6^-$)$_{12}$ in CD_3CN.

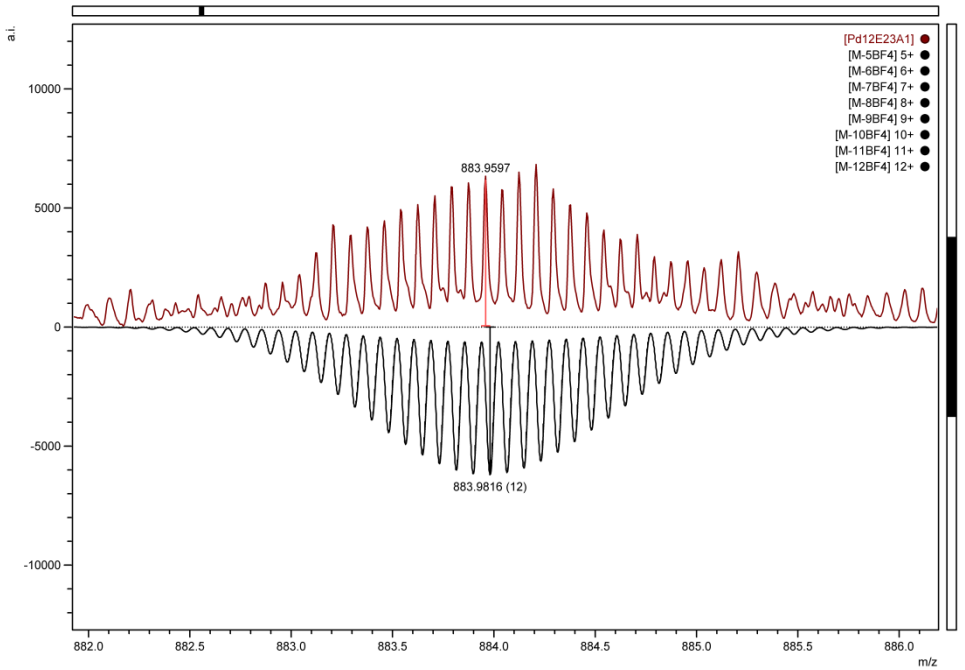

Figure S25. CSI-MS peak for [(Pd$_{12}\mathbf{E}_{23}\mathbf{A}_1$)($BF_4^-$)$_{12}$]$^{12+}$ in CD_3CN, *m/z* 883.9597; calculated *m/z* 883.9616.

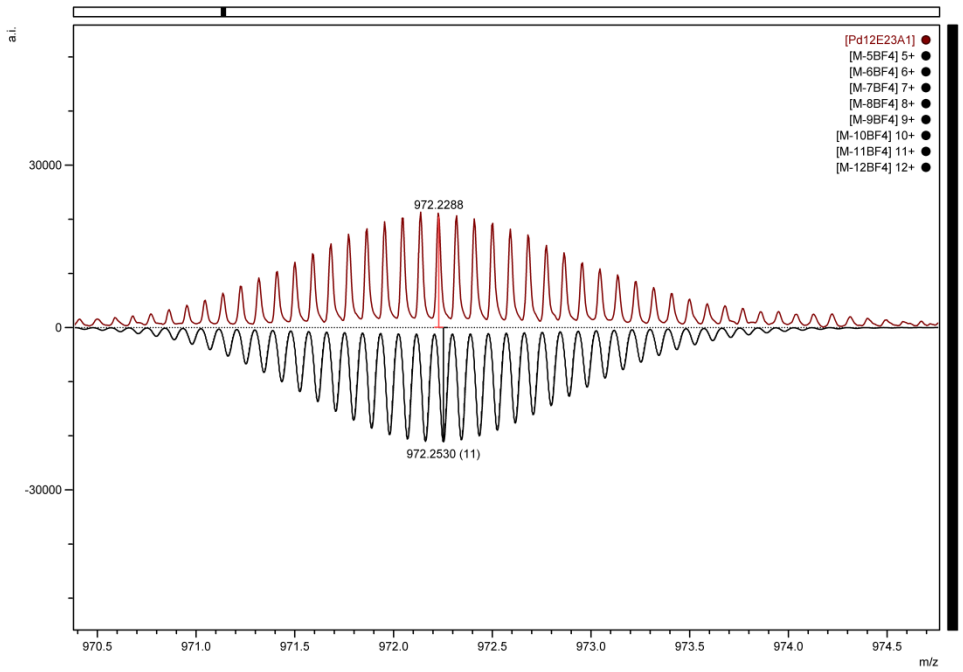

Figure S26. CSI-MS peak for $[(Pd_{12}\mathbf{E}_{23}\mathbf{A}_1)(BF_4^-)_{11}]^{11+}$ in CD_3CN, *m/z* 972.2288; calculated *m/z* 972.2530.

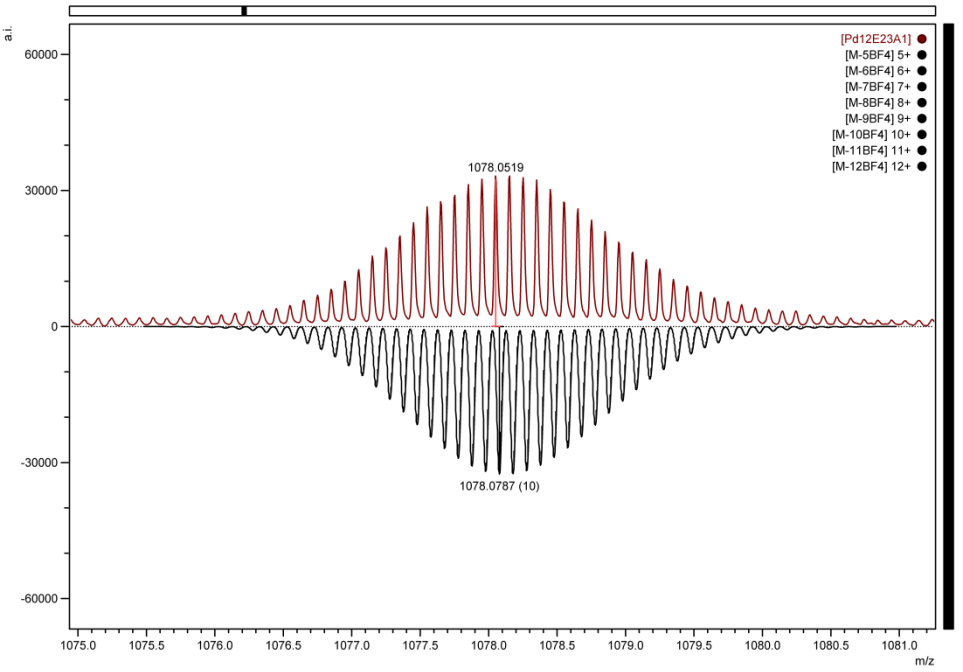

Figure S27. CSI-MS peak for $[(Pd_{12}\mathbf{E}_{23}\mathbf{A}_1)(BF_4^-)_{10}]^{10+}$ in CD_3CN, *m/z* 1078.0519; calculated *m/z* 1078.0787.

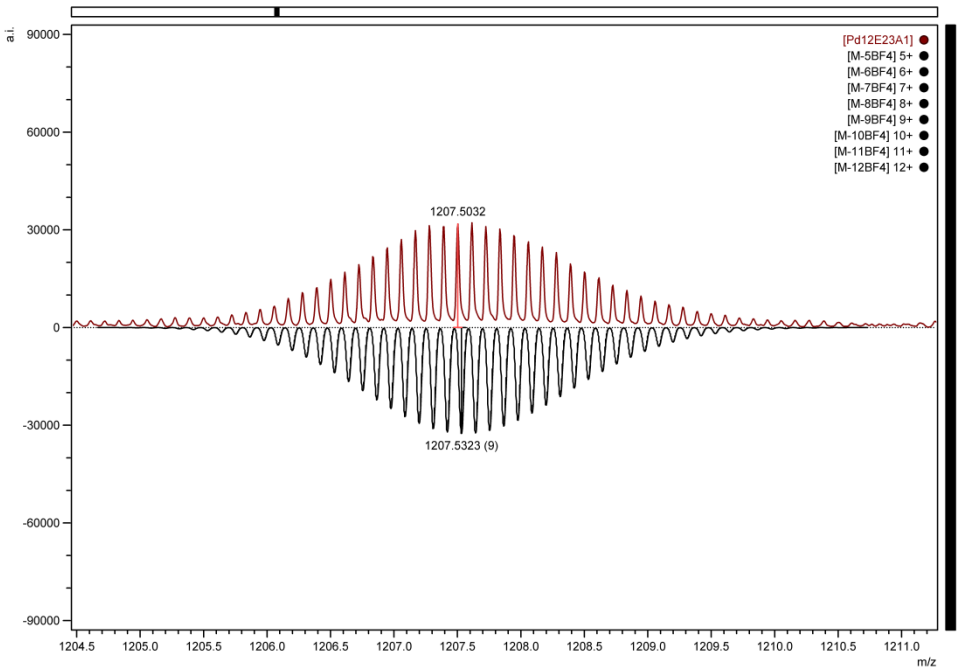

Figure S28. CSI-MS peak for $[(Pd_{12}\mathbf{E}_{23}\mathbf{A}_1)(BF_4^-)_9]^{9+}$ in CD_3CN, *m/z* 1207.5032; calculated *m/z* 1207.5323.

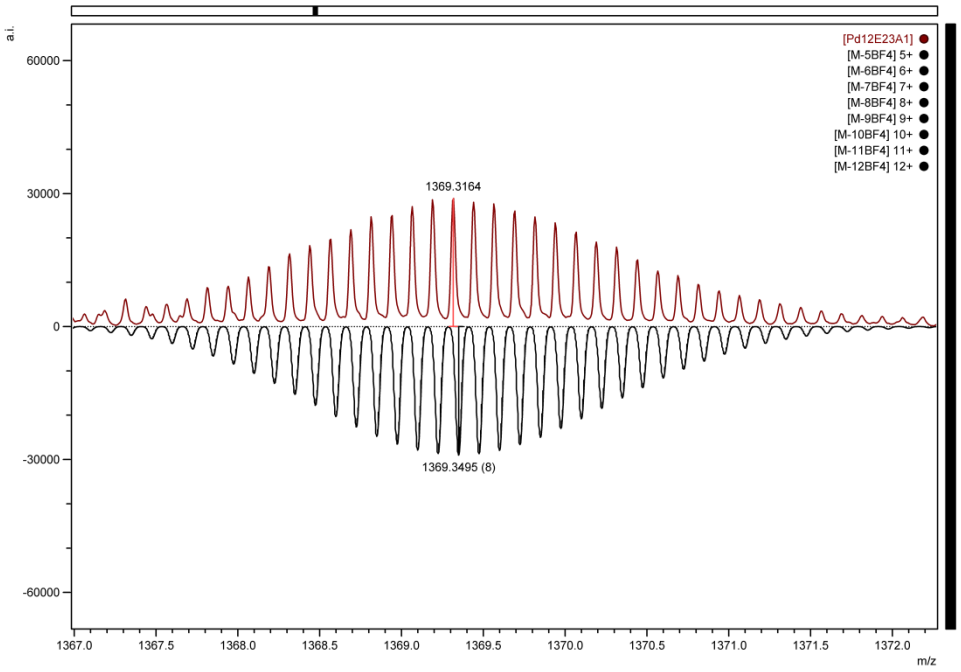

Figure S29. CSI-MS peak for $[(Pd_{12}\mathbf{E}_{23}\mathbf{A}_1)(BF_4^-)_8]^{8+}$ in CD_3CN, *m/z* 1369.3164; calculated *m/z* 1369.3495.

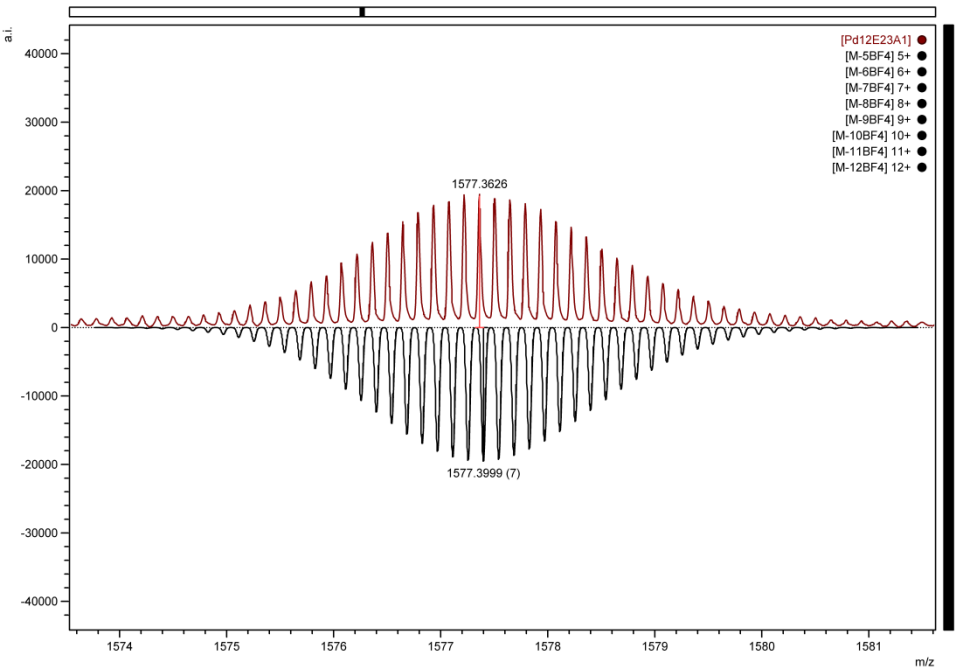

Figure S30. CSI-MS peak for $[(Pd_{12}\mathbf{E}_{23}\mathbf{A}_1)(BF_4^-)_7]^{7+}$ in CD_3CN, *m/z* 1577.3626; calculated *m/z* 1577.3999

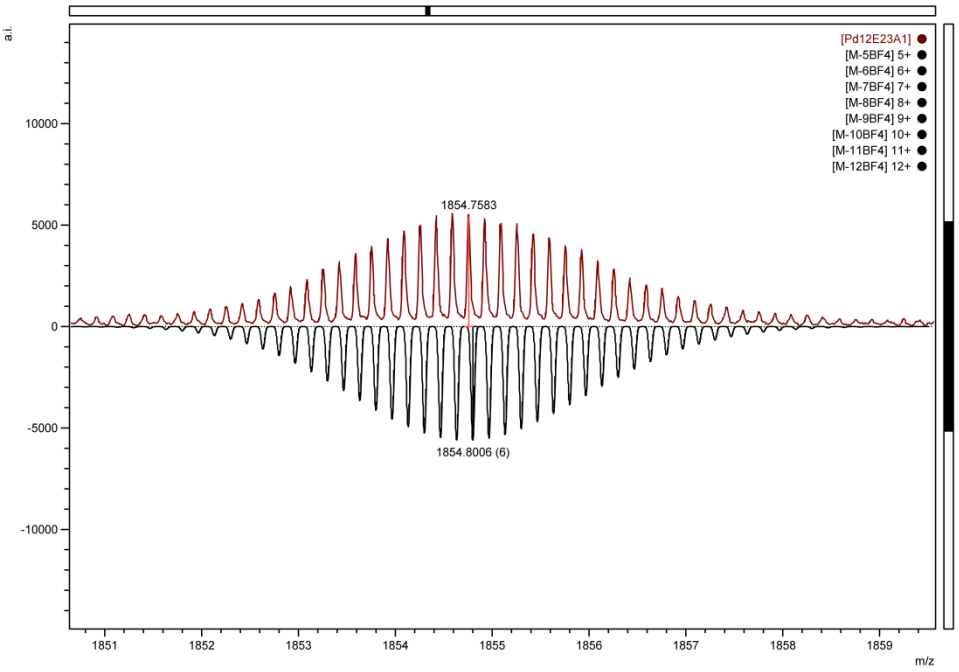

Figure S31. CSI-MS peak for $[(Pd_{12}\mathbf{E}_{23}\mathbf{A}_1)(BF_4^-)_6]^{6+}$ in CD_3CN, *m/z* 1854.7583; calculated *m/z* 1854.8006

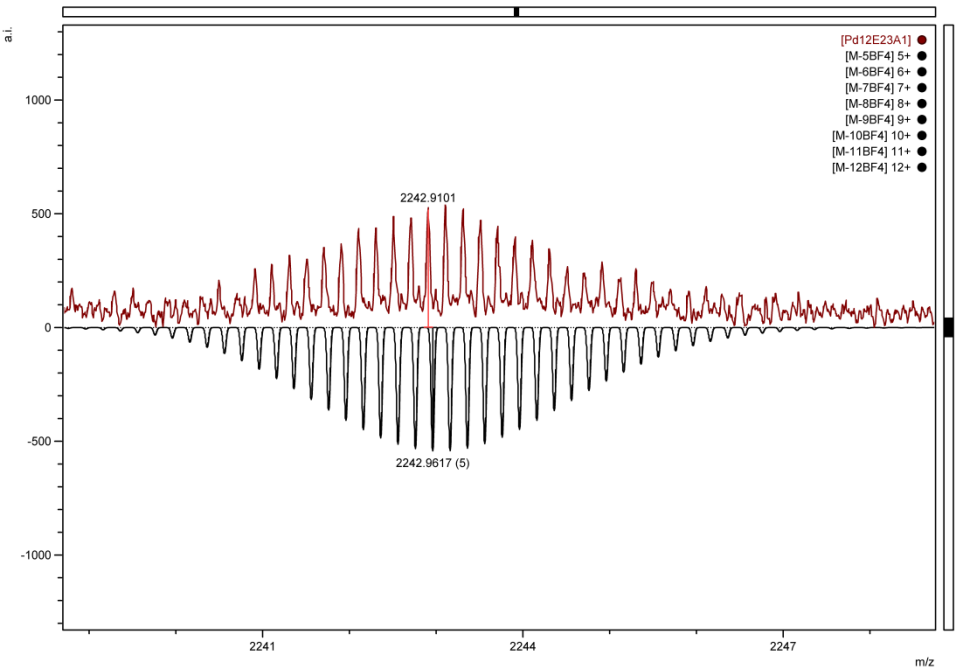

Figure S32. CSI-MS peak for $[(Pd_{12}\mathbf{E}_{23}\mathbf{A}_1)(BF_4^-)_5]^{5+}$ in CD_3CN, *m/z* 2242.9101; calculated *m/z* 2242.9617.

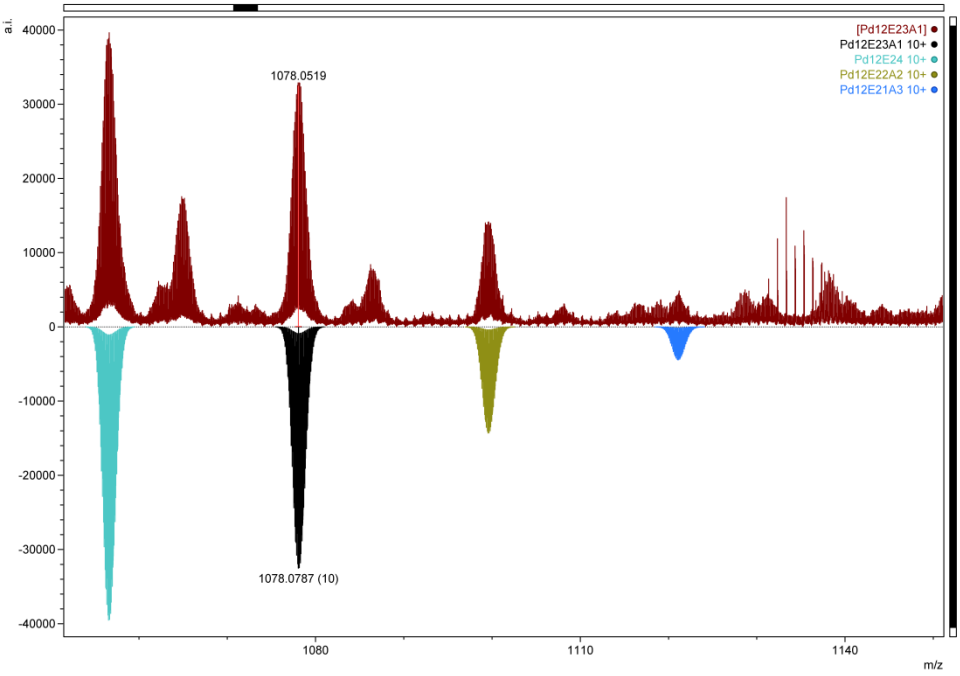

Figure S33. Full CSI-MS spectrum for cage sample $(Pd_{12}\mathbf{E}_{23}\mathbf{A}_1)(BF_4^-)_{24}$ in CD_3CN showing the presence of different species in solution: $[(Pd_{12}\mathbf{E}_{24})(BF_4^-)_{10}]^{10+}$ (cyan), $[(Pd_{12}\mathbf{E}_{23}\mathbf{A}_1)(BF_4^-)_{10}]^{10+}$ (black), $[(Pd_{12}\mathbf{E}_{22}\mathbf{A}_2)(BF_4^-)_{10}]^{10+}$ (yellow) and $[(Pd_{12}\mathbf{E}_{21}\mathbf{A}_3)(BF_4^-)_{10}]^{10+}$ (blue).

Cage $[Pt_6A_{12}]^{12+}$

Preparation: A Schlenk flask was charged with 22.04 mg (1 equiv, 40 µmol) of FcBB **A** and 14.28 mg $[Pt(PF_6)_2(MeCN)_4]$ (0.55 equiv, 22 µmol). The flask was flushed with nitrogen before 4 ml of degassed CD_3CN were added. The resulting mixture was heated under N_2 at 85 °C for 48h.

NMR spectroscopy

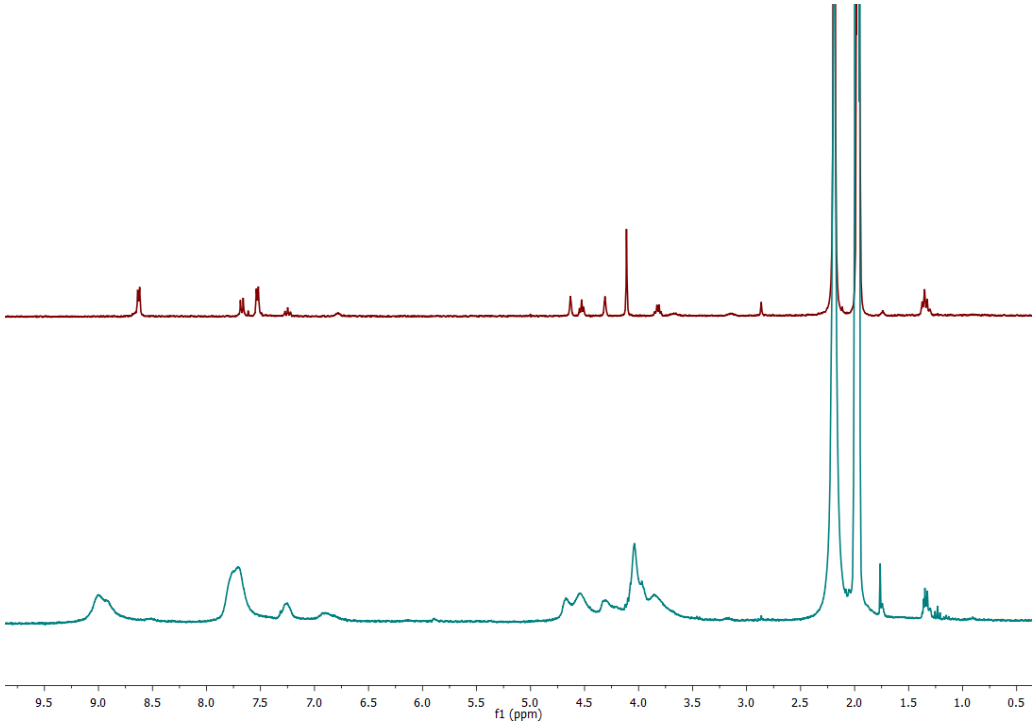

Figure S34. ^{1}H-NMR spectra of ferrocene building block **A** in CD_3CN (top) and its platinum ferrocene cage, $(Pt_6\mathbf{A}_{12})^{12+}$ in CD_3CN (bottom).

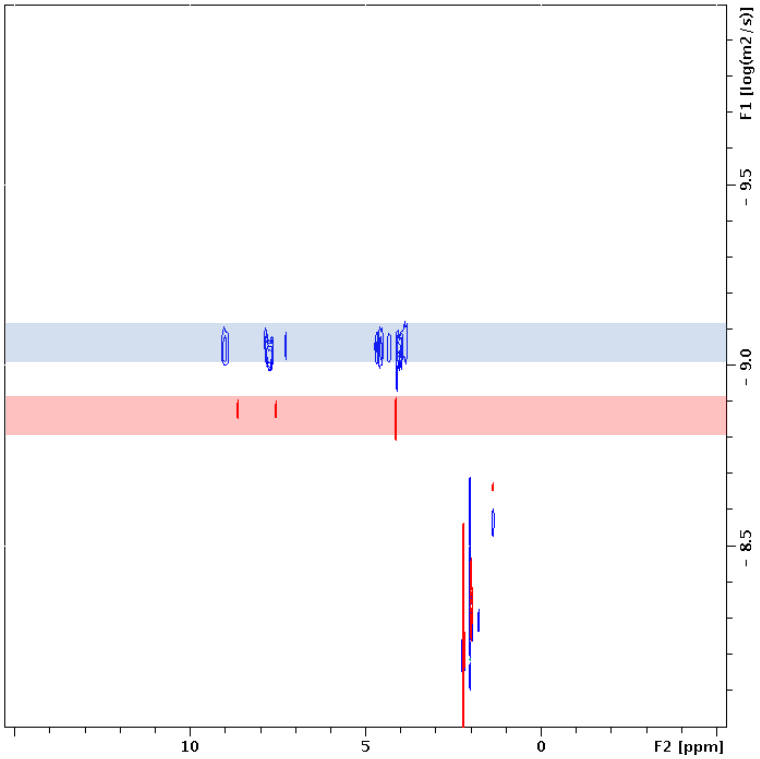

Figure S35. ^{1}H DOSY NMR overlay for FcBB **A**, showing a single diffusing species with a logD of -8.9 m^2s^{-1} and a platinum cage $(Pt_6\mathbf{A}_{12})^{12+}$, showing a single diffusing species with a logD of -9.15 m^2s^{-1}, in CD_3CN at 25 °C.

CSI-MS characterization

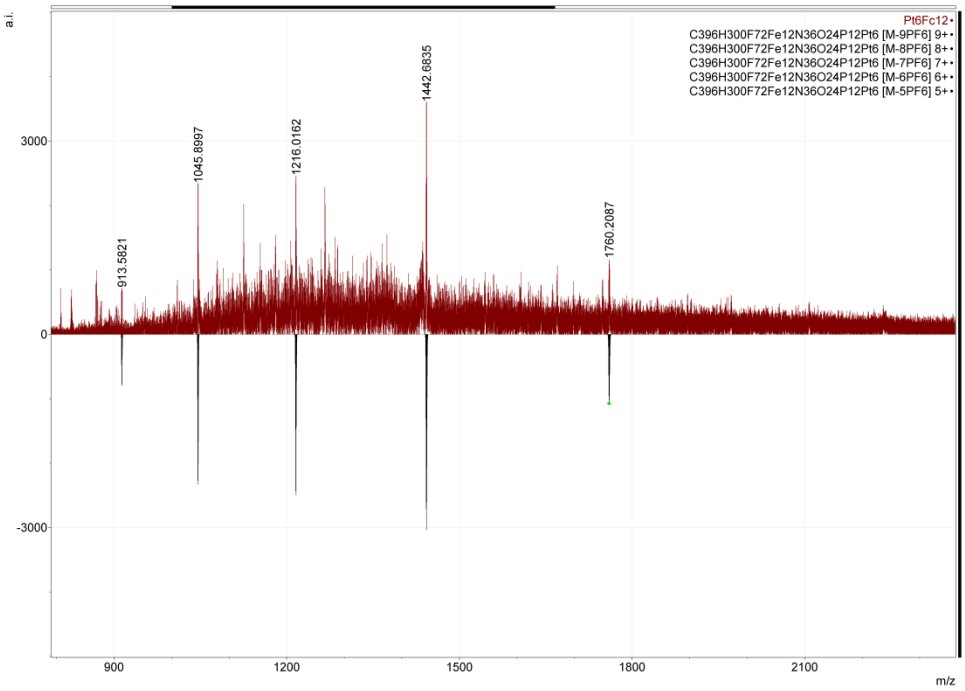

Figure S36. Full CSI-MS spectrum for cage sample $(Pt_6\mathbf{A}_{12})(PF_6^-)_{12}$ in CD_3CN.

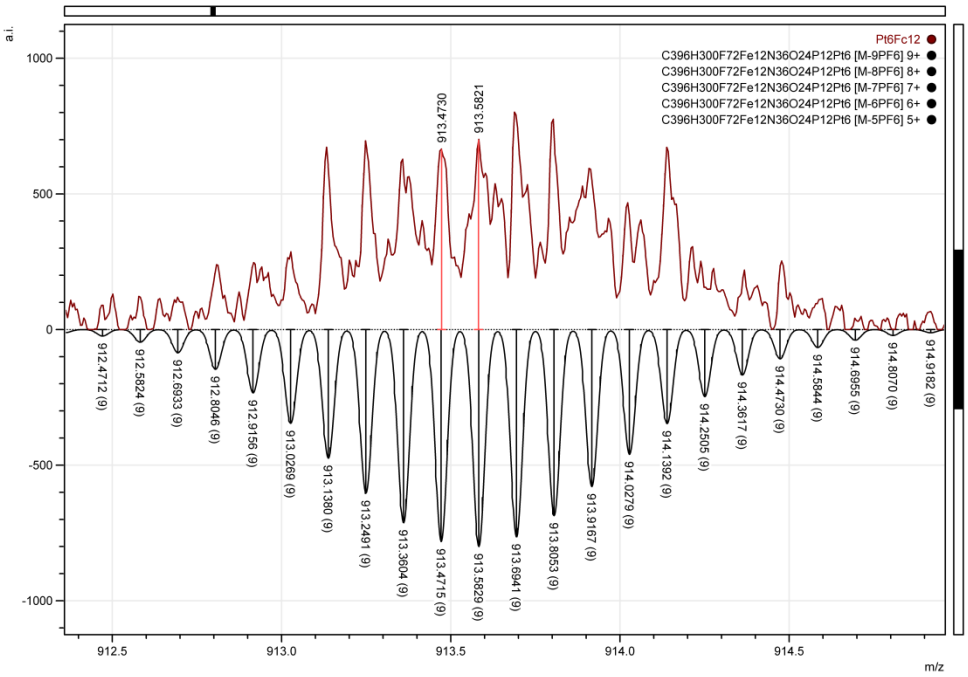

Figure S37. CSI-MS peak for $[(Pt_6\mathbf{A}_{12})(PF_6^-)_3]^{9+}$ in CD_3CN, *m/z* 913.5821; calculated *m/z* 913.5829.

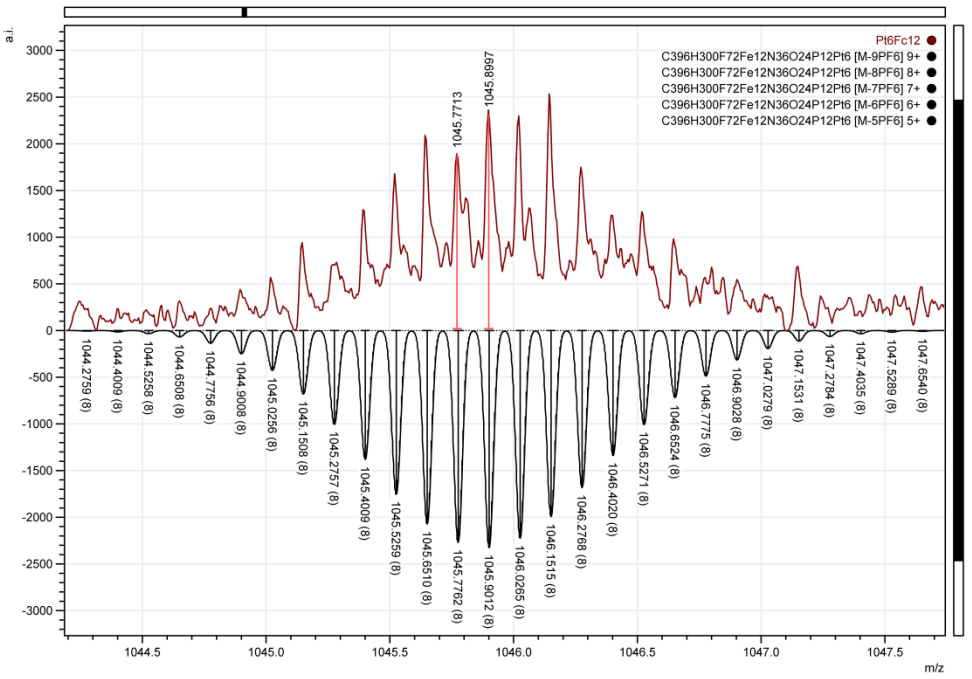

Figure S38. CSI-MS peak for $[(Pt_6\mathbf{A}_{12})(PF_6^-)_4]^{8+}$ in CD_3CN, *m/z* 1045.5997; calculated *m/z* 1045.9012.

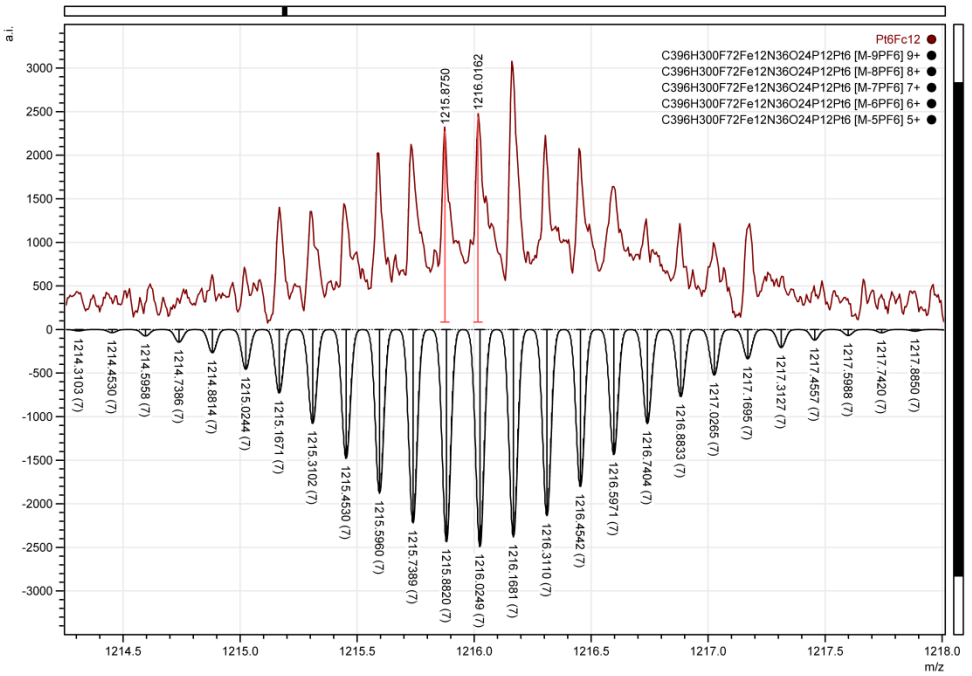

Figure S39. CSI-MS peak for $[(Pt_6\mathbf{A}_{12})(PF_6^-)_5]^{7+}$ in CD_3CN, *m/z* 1216.0162; calculated *m/z* 1216.0249.

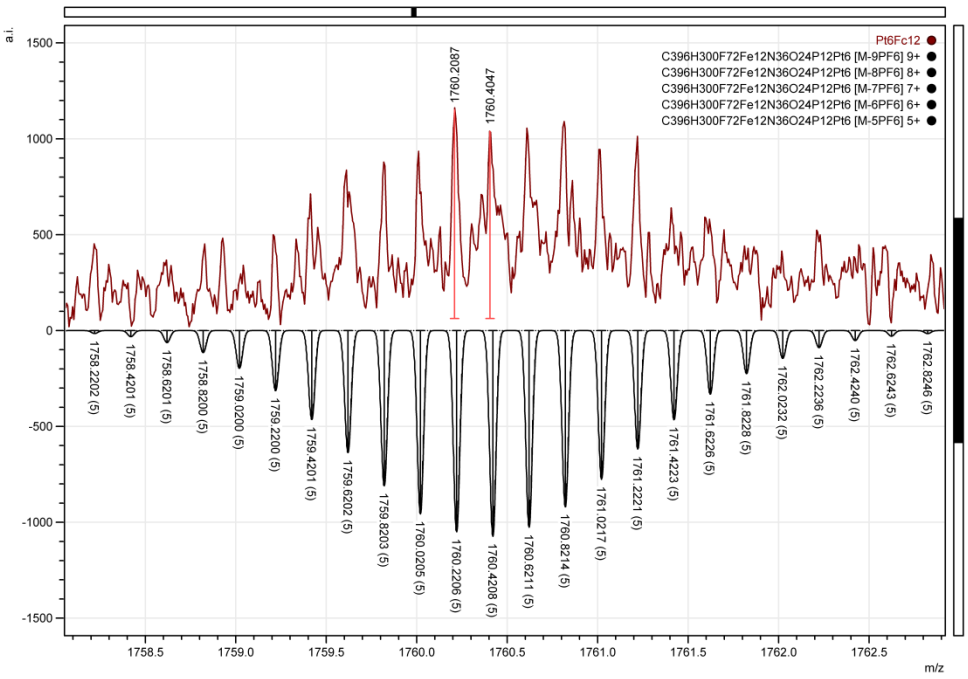

Figure S40. CSI-MS peak for $[(Pt_6\mathbf{A}_{12})(PF_6^-)_7]^{5+}$ in CD_3CN, *m/z* 1760.2087; calculated *m/z* 1760.2206.

Cage $[Pt_6E_{11}A_1]^{12+}$

Preparation: A Schlenk flask was charged with 1.836 mg (1 equiv, 3.33 µmol) of FcBB **A**, 12.326 mg (11 equiv, 36.66 µmol) of BBH **E** and 14.28 mg $[Pt(PF_6)_2(MeCN)_4]$ (0.55 equiv, 22 µmol). The flask was flushed with nitrogen before 4 ml of degassed CD_3CN were added. The resulting mixture was heated under N_2 at 85 °C for 48h.

For MS analysis the same procedure was carried out but $[Pt(PF_6)_2(MeCN)_4]$ was replaced by $[Pt(BF_4)_2(MeCN)_4]$.

NMR spectroscopy

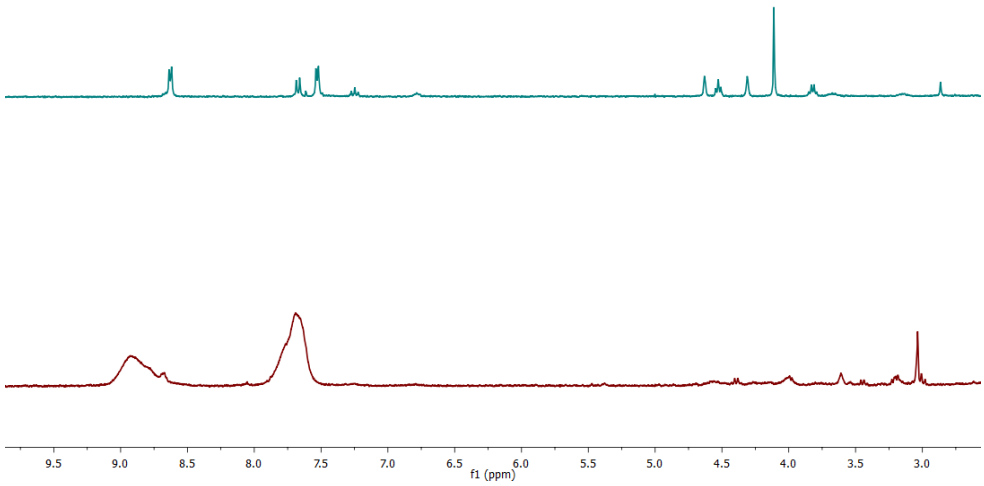

Figure S41. ^{1}H-NMR spectra of ferrocene building block **A** in CD_3CN (top) and its platinum ferrocene cage, $(Pt_6\mathbf{E}_{11}\mathbf{A}_1)^{12+}$ in CD_3CN (bottom).

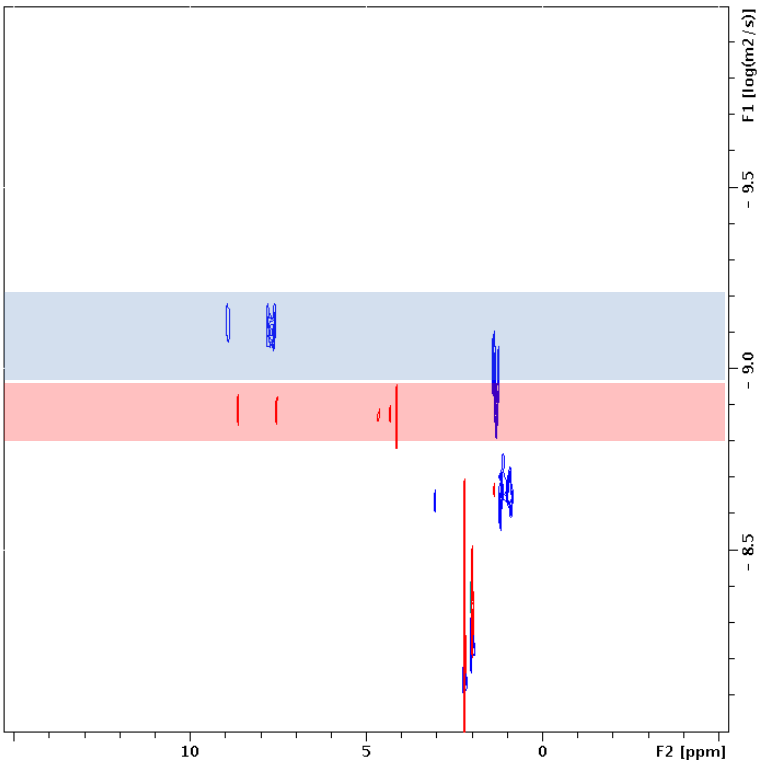

Figure S42. ^{1}H DOSY NMR overlay for FcBB **A**, showing a single diffusing species with a logD of -8.9 m^2s^{-1} and a platinum cage $(Pt_6\mathbf{E}_{11}\mathbf{A}_1)^{12+}$, showing a single diffusing species with a logD of -9.10 m^2s^{-1}, in CD_3CN at 25 °C.

CSI-MS characterization

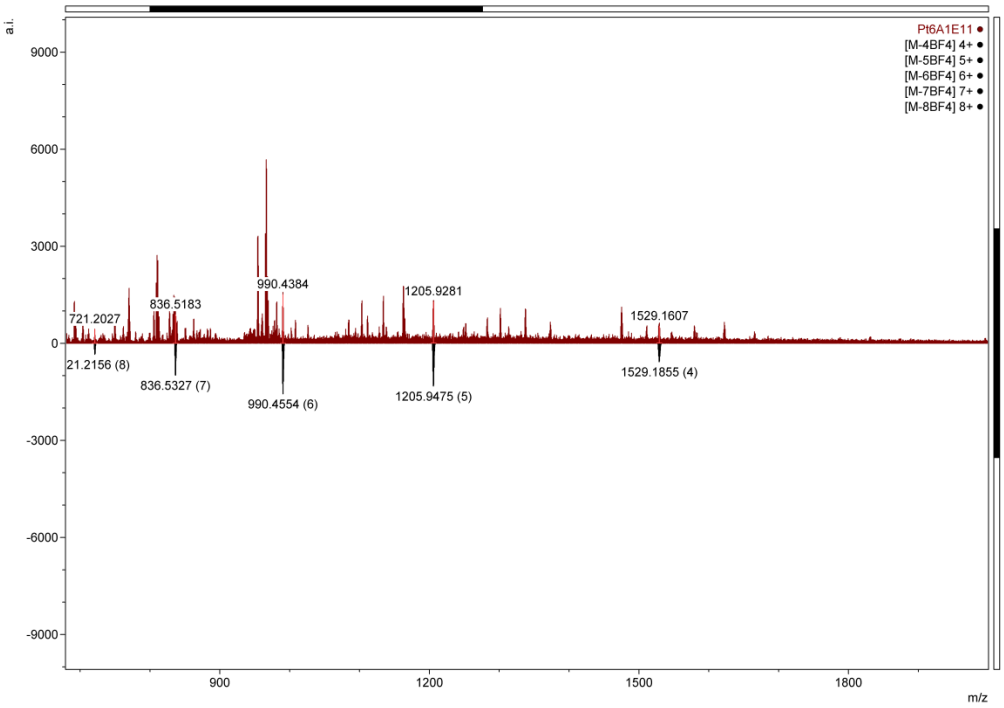

Figure S43. Full CSI-MS spectrum for cage sample $(Pt_6\mathbf{E}_{11}\mathbf{A}_1)(BF_4^-)_{12}$ in CD_3CN.

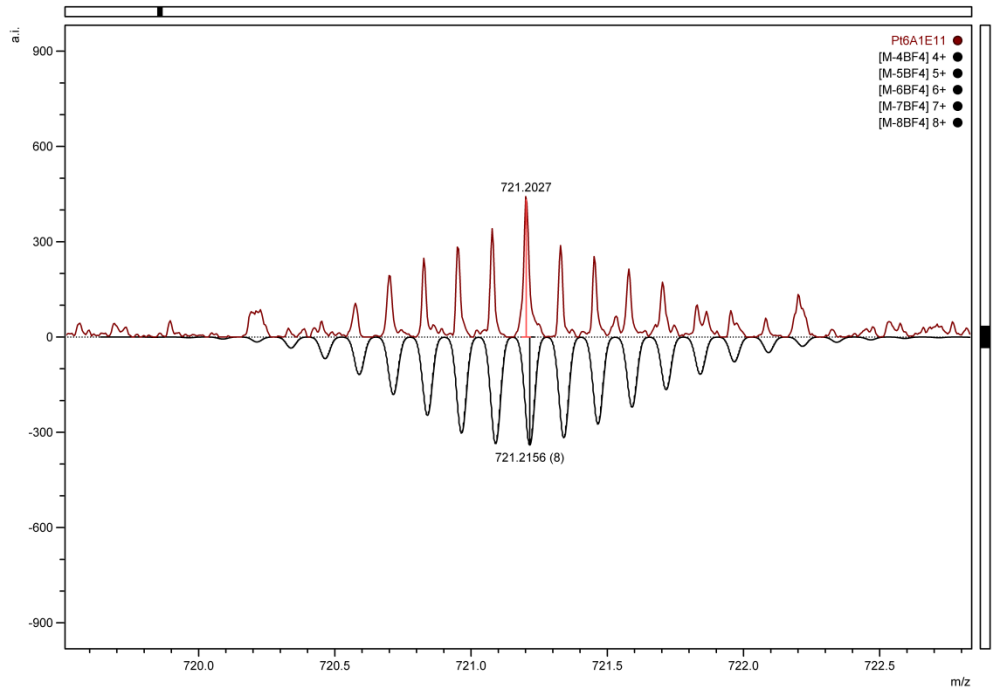

Figure S44. CSI-MS peak for $[(Pt_6\mathbf{E}_{11}\mathbf{A}_1)(BF_4^-)_4]^{8+}$ in CD_3CN, *m/z* 721.2027; calculated *m/z* 721.2156.

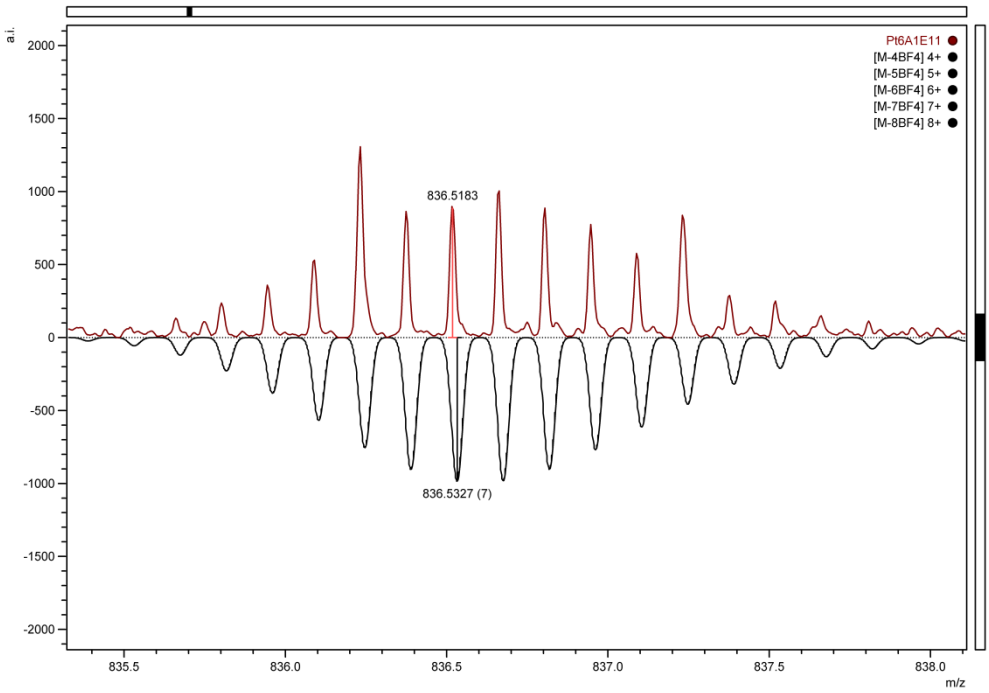

Figure S45. CSI-MS peak for $[(Pt_6\mathbf{E}_{11}\mathbf{A}_1)(BF_4^-)_5]^{7+}$ in CD_3CN, *m/z* 836.5183; calculated *m/z* 836.5327.

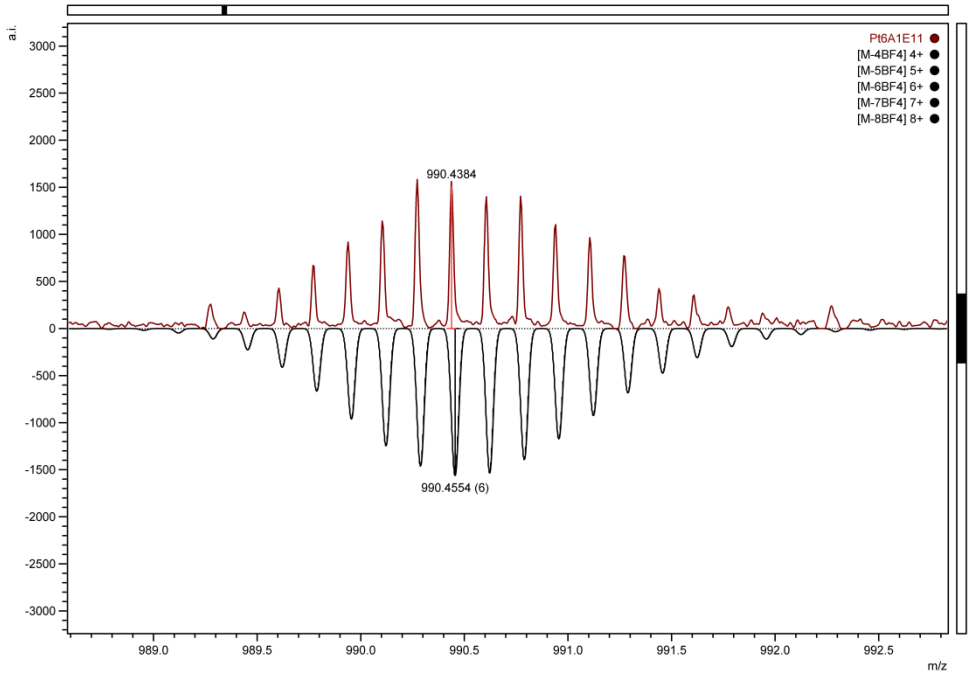

Figure S46. CSI-MS peak for $[(Pt_6\mathbf{E}_{11}\mathbf{A}_1)(BF_4^-)_6]^{6+}$ in CD_3CN, *m/z* 990.4384; calculated *m/z* 990.4554.

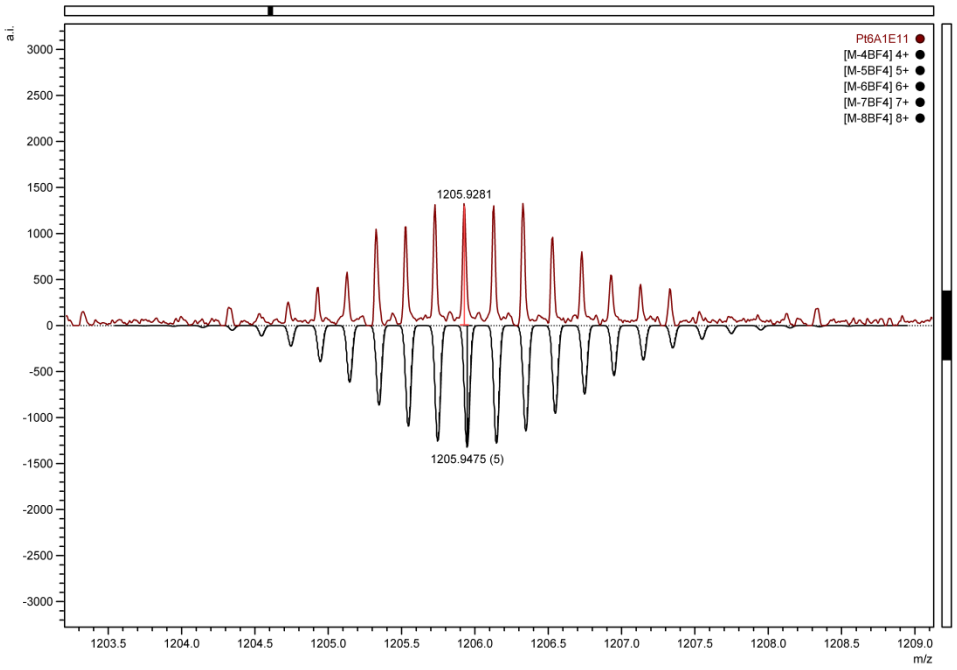

Figure S47. CSI-MS peak for $[(Pt_6\mathbf{E}_{11}\mathbf{A}_1)(BF_4^-)_7]^{5+}$ in CD_3CN, *m/z* 1205.9281; calculated *m/z* 122205.9475.

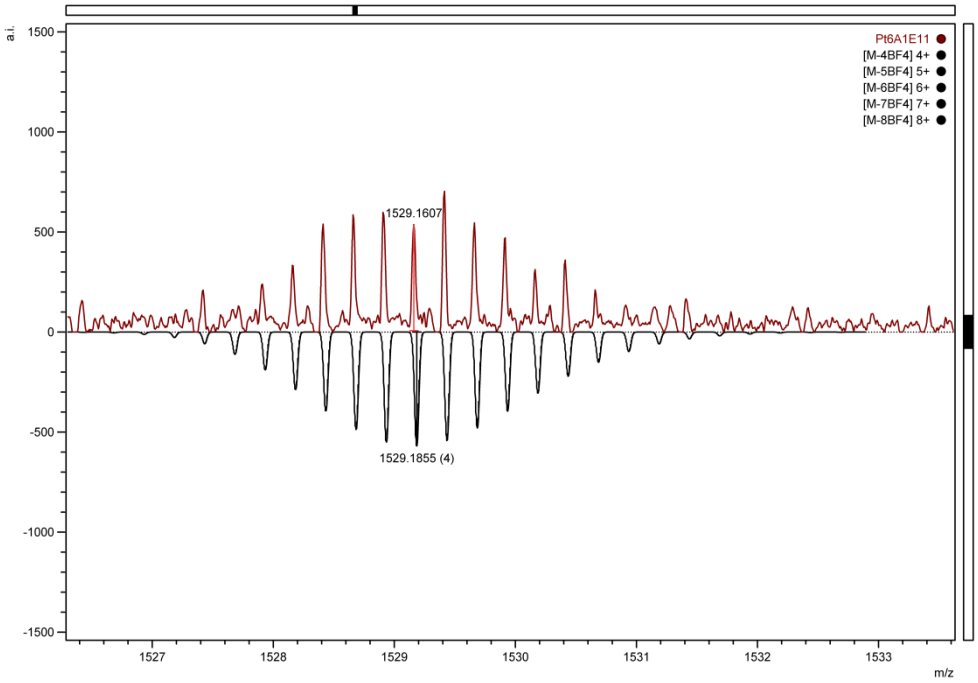

Figure S48. CSI-MS peak for $[(Pt_6\mathbf{E}_{11}\mathbf{A}_1)(BF_4^-)_8]^{4+}$ in CD_3CN, *m/z* 1529.1607; calculated *m/z* 1529.1855.

Cages containing TTFBB B

Cage $[Pt_6E_{11}B_1]^{12+}$

Preparation: A Schlenk flask was charged with 2.127 mg (1 equiv, 3.33 µmol) of TTFBB **B**, 12.326 mg (11 equiv, 36.66 µmol) of BBH **E** and 14.28 mg $[Pt(PF_6)_2(MeCN)_4]$ (0.55 equiv, 22 µmol). The flask was flushed with nitrogen before 4 ml of degassed CD_3CN were added. The resulting mixture was heated under N_2 at 85 °C for 48h.

For MS analysis the same procedure was carried out but $[Pt(PF_6)_2(MeCN)_4]$ was replaced by $[Pt(BF_4)_2(MeCN)_4]$.

NMR spectroscopy

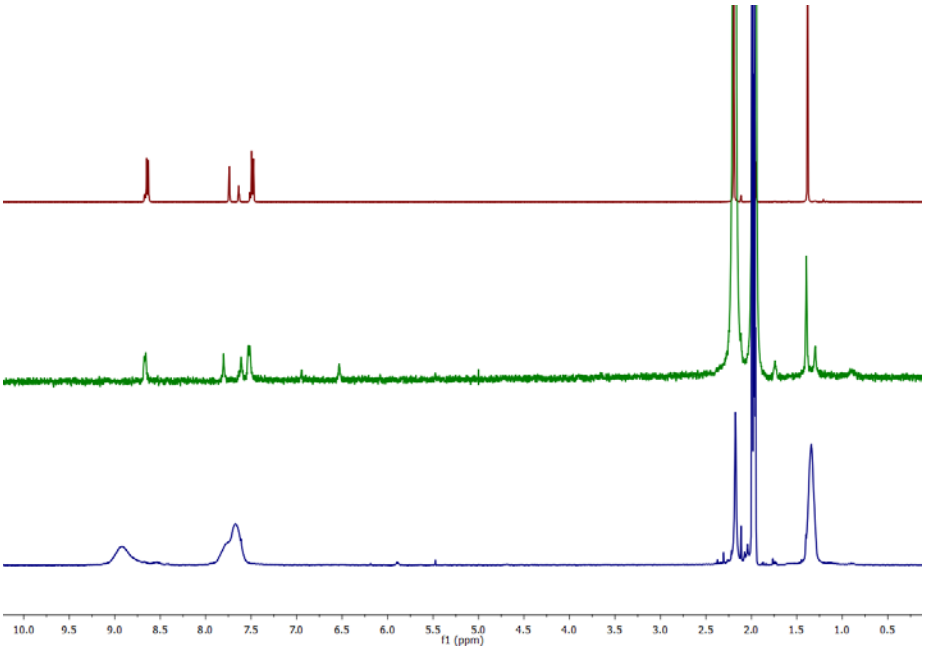

Figure S49. ^{1}H NMR spectra of non-functionalized building block BBH **E** (top), free TTFBB **B** (middle), and corresponding cage of the type $(Pt_6\mathbf{E}_{11}\mathbf{B}_1)^{12+}$ (bottom) in MeCN.

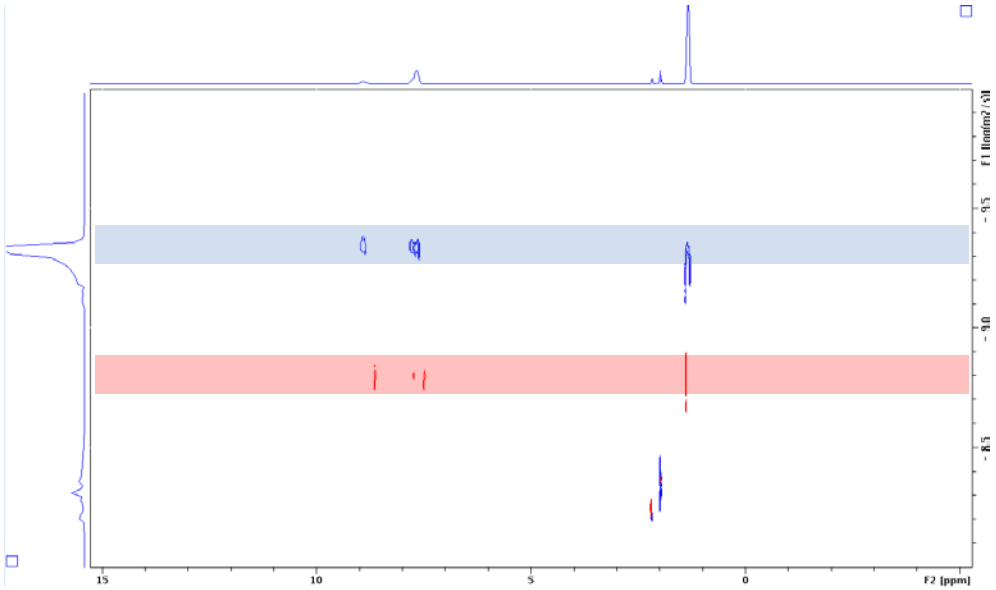

Figure S50. Overlay of two ^{1}H DOSY NMR spectra, showing the difference in logD value between the free diffusing TTFBB **B** (logD = -8.8) and a solution of its cage of the type $(Pt_6\mathbf{E}_{11}\mathbf{B}_1)^{12+}$ (logD = -9.4) in CD_3CN at 25 °C.

CSI-MS characterization

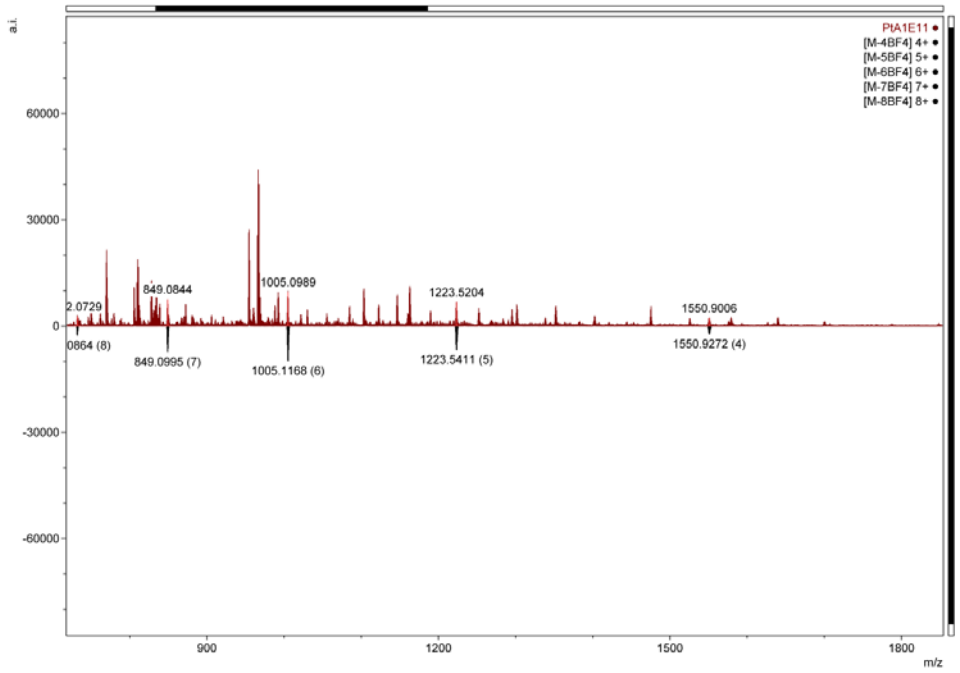

Figure S51. Full CSI-MS spectrum for cage sample $(Pt_6\mathbf{E}_{11}\mathbf{B}_1)(BF_4^-)_{12}$ in CD_3CN.

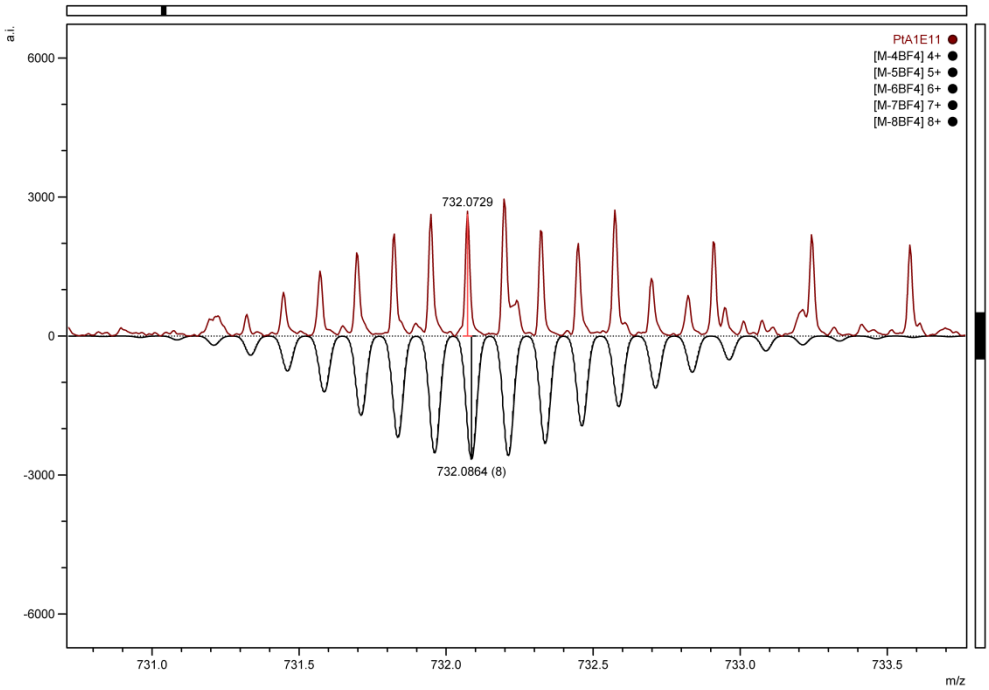

Figure S52. CSI-MS peak for $[(Pt_6\mathbf{E}_{11}\mathbf{B}_1)(BF_4^-)_4]^{8+}$ in CD_3CN, *m/z* 732.0729; calculated *m/z* 732.0864.

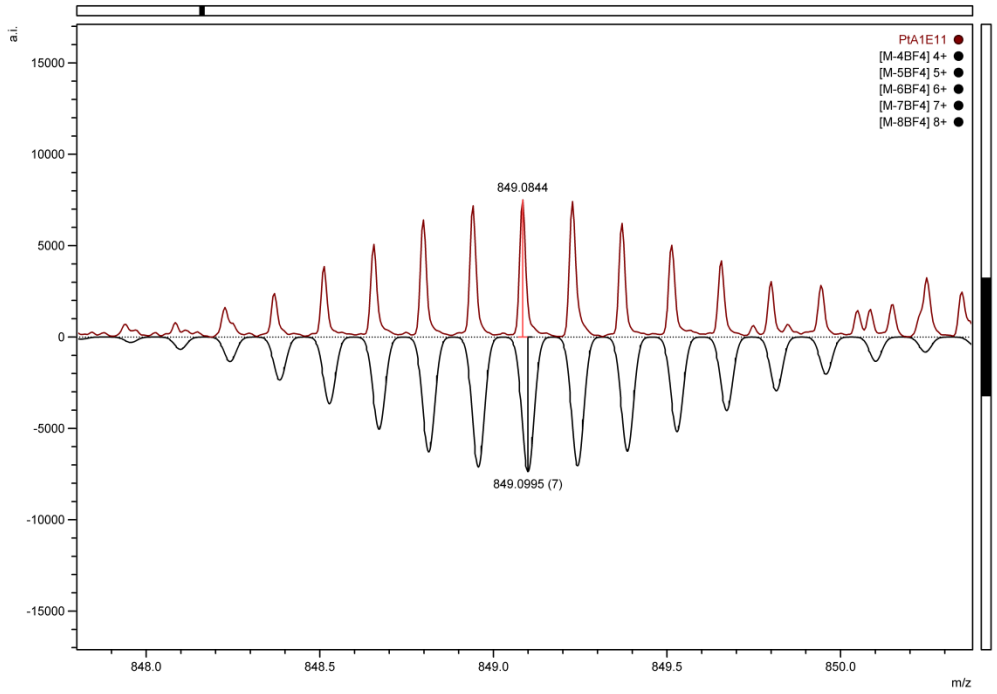

Figure S53. CSI-MS peak for $[(Pt_6\mathbf{E}_{11}\mathbf{B}_1)(BF_4^-)_5]^{7+}$ in CD_3CN, *m/z* 849.0844; calculated *m/z* 849.0995.

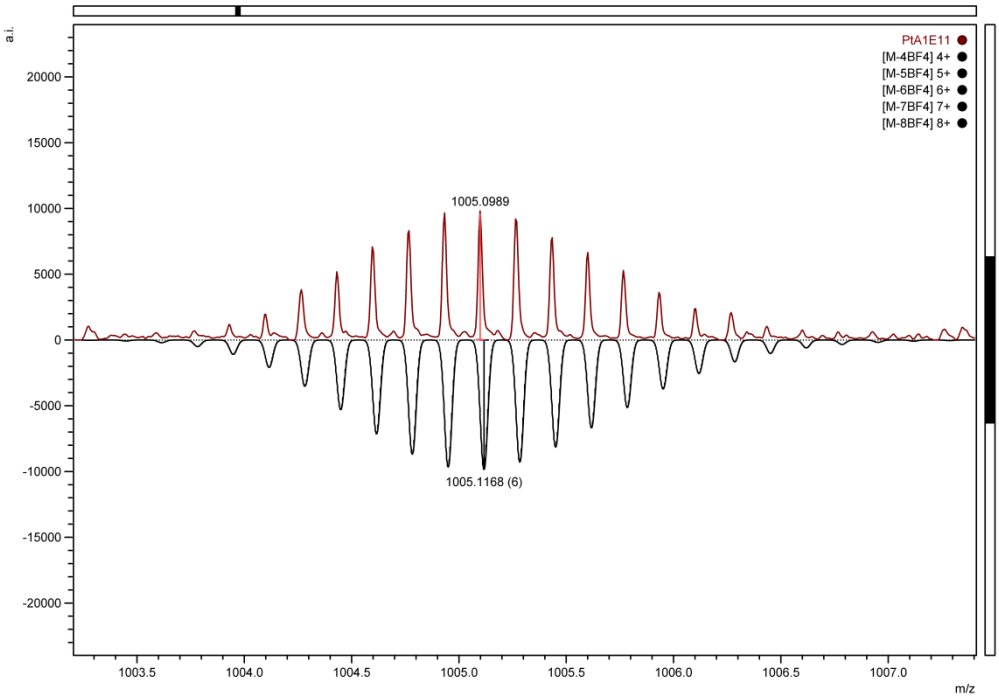

Figure S54. CSI-MS peak for $[(Pt_6\mathbf{E}_{11}\mathbf{B}_1)(BF_4^-)_6]^{6+}$ in CD_3CN, *m/z* 1005.0989; calculated *m/z* 1005.1168.

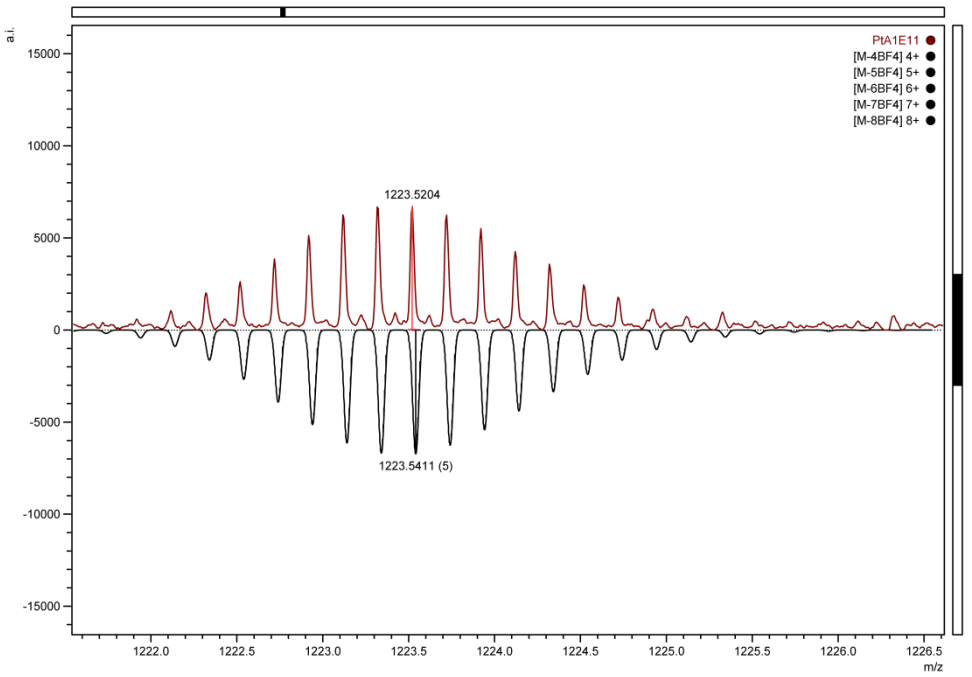

Figure S55. CSI-MS peak for $[(Pt_6\mathbf{E}_{11}\mathbf{B}_1)(BF_4^-)_7]^{5+}$ in CD_3CN, *m/z* 1223.5204; calculated *m/z* 1223.5411.

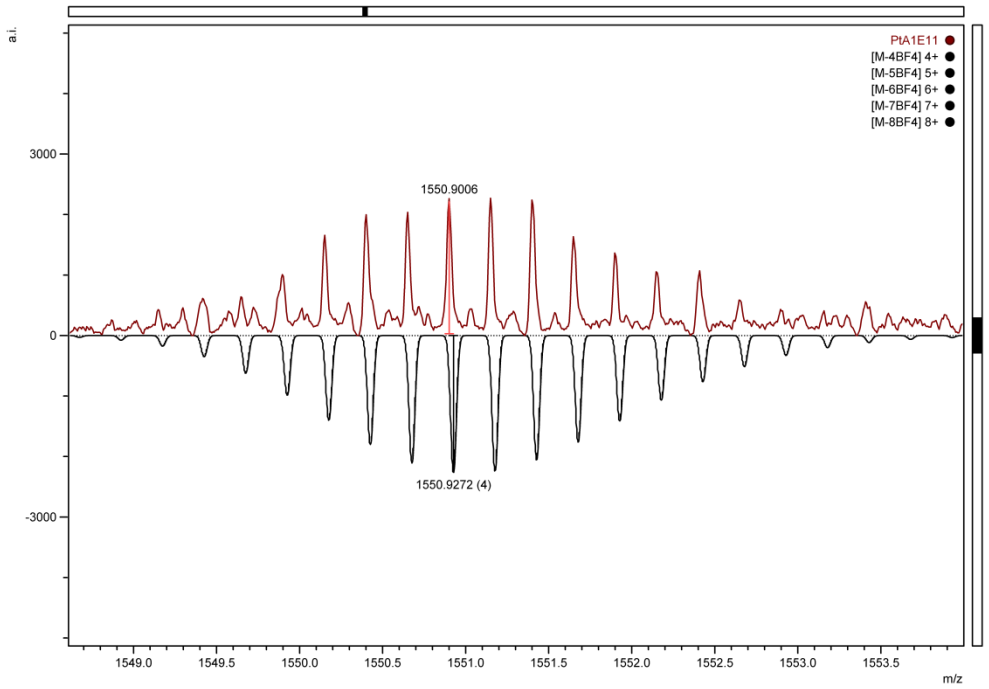

Figure S56. CSI-MS peak for $[(Pt_6\mathbf{E}_{11}\mathbf{B}_1)(BF_4^-)_8]^{4+}$ in CD_3CN, *m/z* 1550.9006; calculated *m/z* 1550.9272.

CSI-MS distribution of single composites from $(Pt_6E_{12-n}B_n)^{12+}$ with n=1

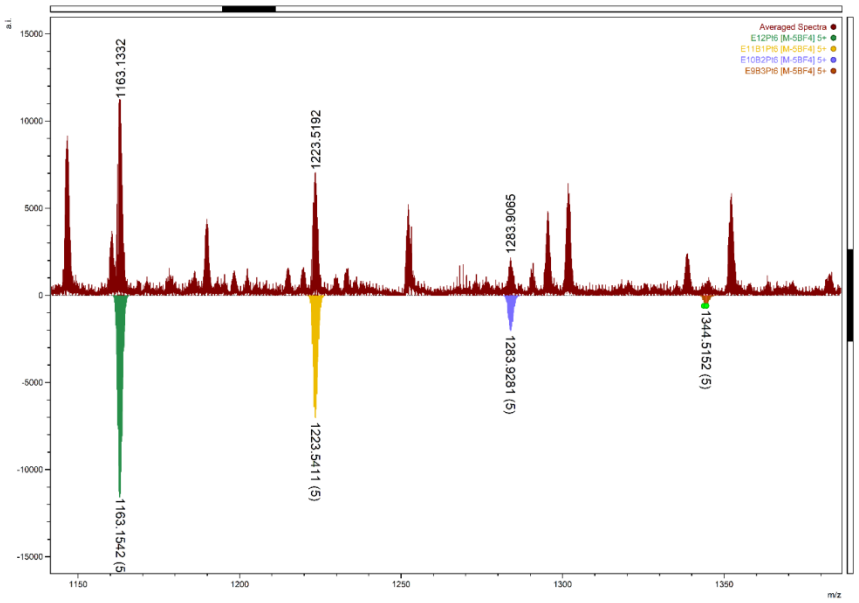

Figure S57. Full CSI-MS spectrum for cage sample $(Pt_6E_{11}B_1)(BF_4^-)_{12}$ in CD_3CN showing the presence of different species in solution: $[(Pt_6E_{12})(BF_4)_4]^{5+}$ *m/z* 1163.1332; calculated (green) *m/z* 1163.1542, $[(Pt_6E_{11}B_1)(BF_4)_4]^{5+}$ *m/z* 1223.5192; calculated (yellow) *m/z* 1223.5411, $[(Pt_6E_{10}B_2)(BF_4)_4]^{5+}$ *m/z* 1283.9065; calculated (blue) *m/z* 1283.19281. The experimental signal for $[(Pt_6E_9B_3)(BF_4)_4]^{5+}$ does not overlap the expected calculated pattern (orange). Proper quantification of the composition is not possible due to differences in ionizability of the different species under MS conditions. Zoom-in of the different species follow below.

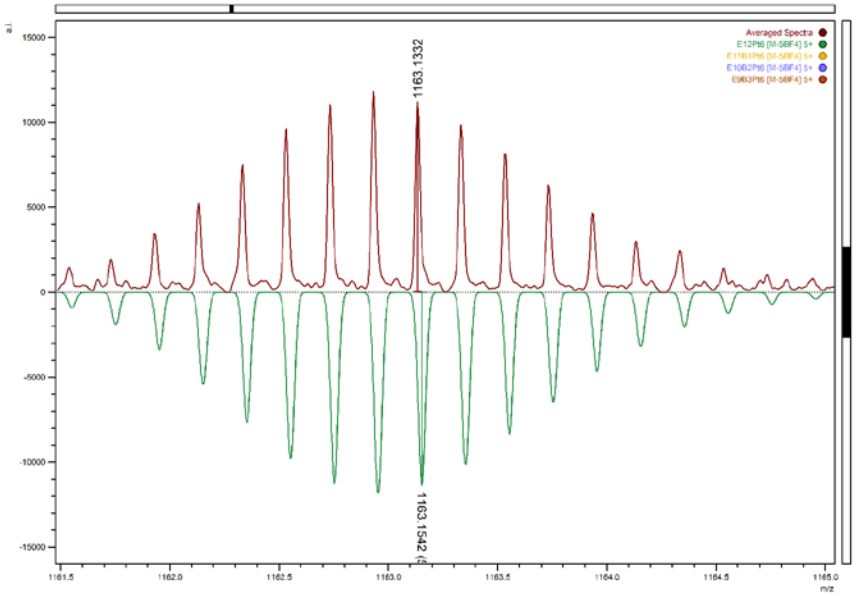

Figure S58. CSI-MS peak for $[(Pt_6E_{12})(BF_4)_4]^{5+}$ in MeCN, *m/z* 1163.1332 (red); calculated (green) *m/z* 1163.1542.

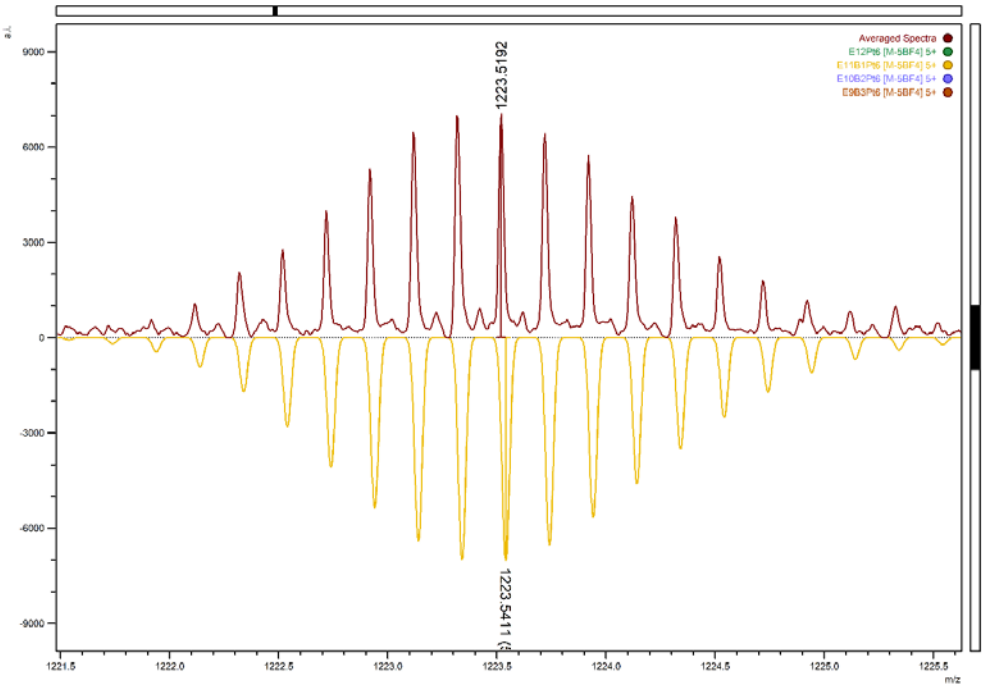

Figure S59. CSI-MS peak for $[(Pt_6\mathbf{E}_{11}\mathbf{B}_1)(BF_4)_4]^{5+}$ in MeCN, *m/z* 1223.5192 (red); calculated (yellow) *m/z* 1223.5411.

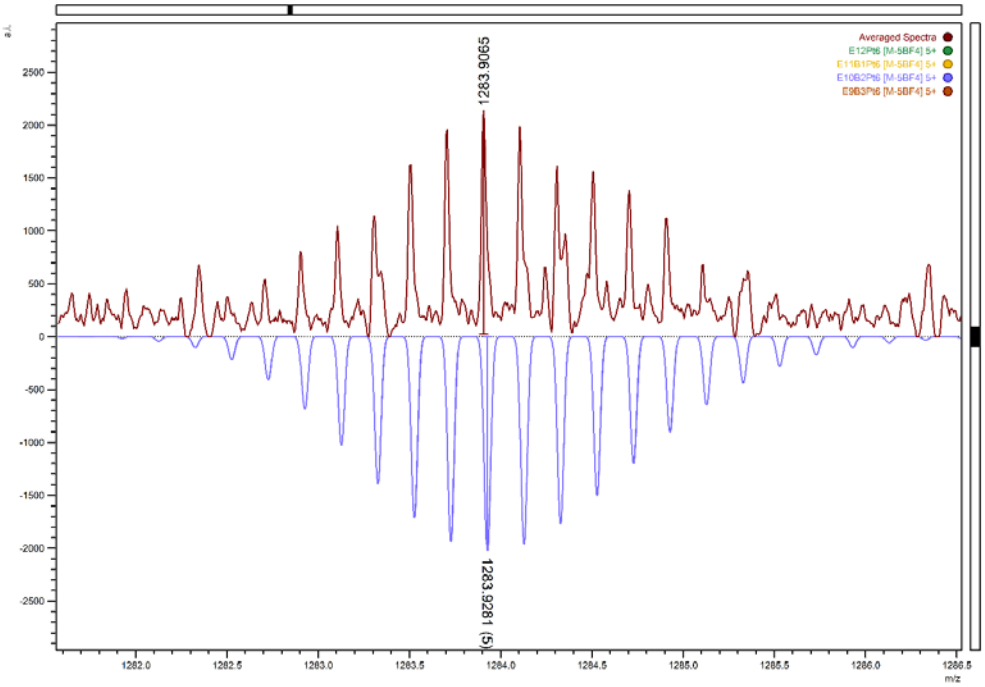

Figure S60. CSI-MS peak for $[(Pt_6\mathbf{E}_{10}\mathbf{B}_2)(BF_4)_4]^{5+}$ in MeCN *m/z* 1283.9065 (red); calculated (blue) *m/z* 1283.19281.

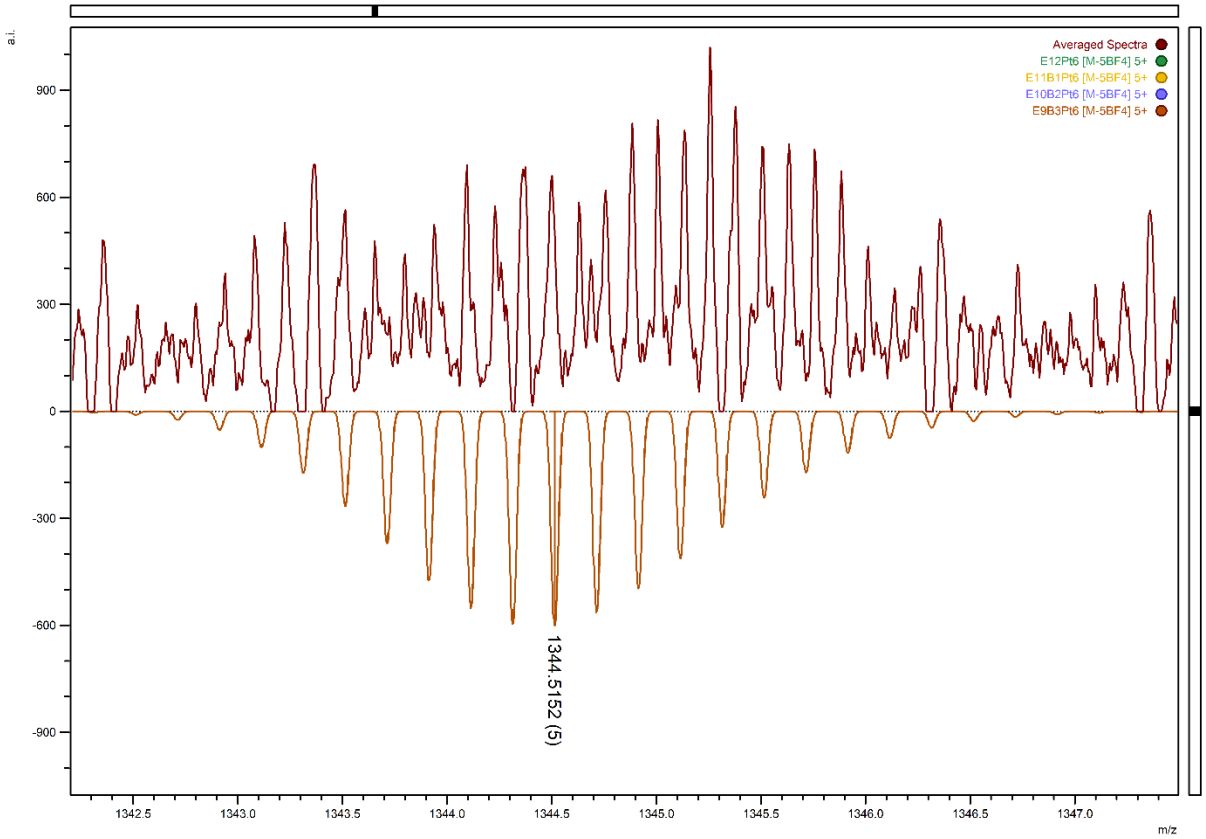

Figure S61. CSI-MS plot showing that measured pattern is not consistent with expected signal for $[(Pt_6\mathbf{E}_9\mathbf{B}_3)(BF_4)_4]^{5+}$ calculated *m/z* 1344.5152 (orange).

Cage $[Pt_6E_{10}B_2]^{12+}$

Preparation: A Schlenk flask was charged with 4.254 mg (1 equiv, 6.66 µmol) of TTFBB **B**, 11.205 mg (10 equiv, 33.33 µmol) of BBH **E** and 14.28 mg $[Pt(PF_6)_2(MeCN)_4]$ (0.55 equiv, 22 µmol). The flask was flushed with nitrogen before 4 ml of degassed CD_3CN were added. The resulting mixture was heated under N_2 at 85 °C for 48h.

For MS analysis the same procedure was carried out but $[Pt(PF_6)_2(MeCN)_4]$ was replaced by $[Pt(BF_4)_2(MeCN)_4]$.

NMR spectroscopy

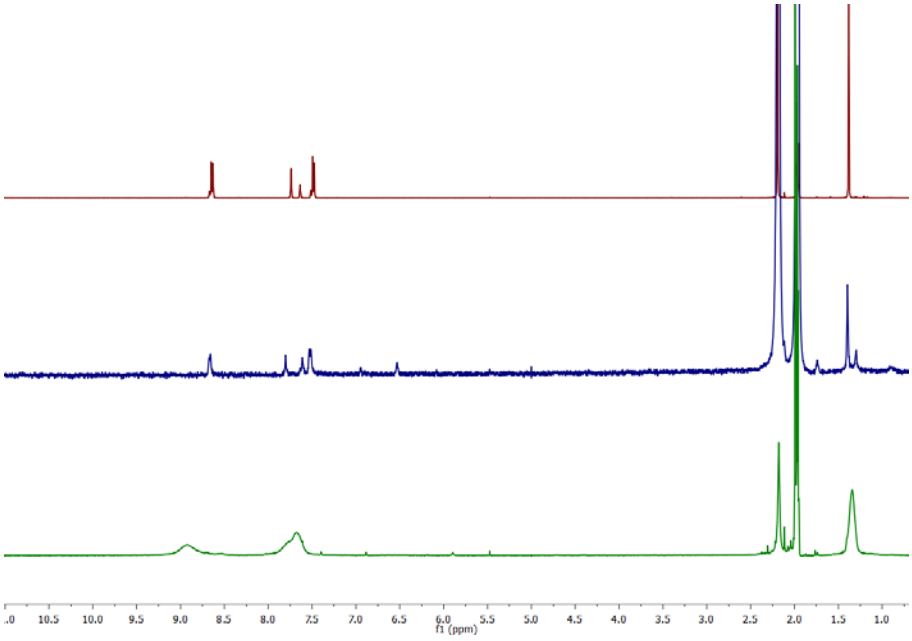

Figure S62. ^{1}H NMR spectra of non-functionalized building block BBH **E** (top), free TTFBB **B** (middle), and corresponding cage of the type $(Pt_6\mathbf{E}_{10}\mathbf{B}_2)^{12+}$ (bottom) in MeCN.

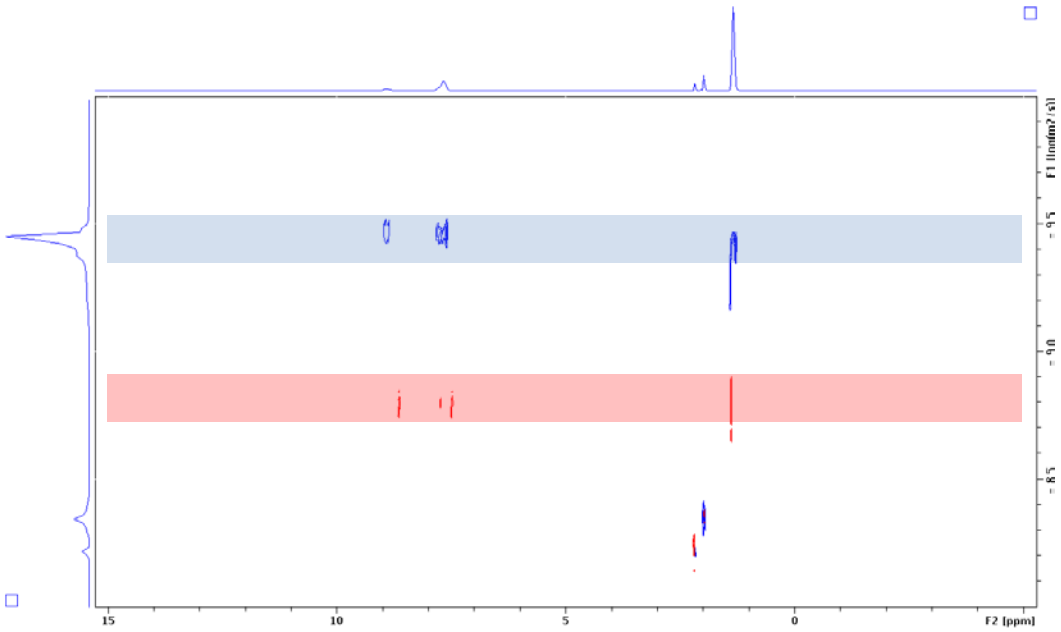

Figure S63. Overlay of two ^{1}H DOSY NMR spectra, showing the difference in logD value between the free diffusing TTFBB **B** (logD = -8.8) and a solution of its cage of the type $(Pt_6\mathbf{E}_{10}\mathbf{B}_2)^{12+}$ (logD = -9.5) in CD_3CN at 25 °C.

CSI-MS characterization

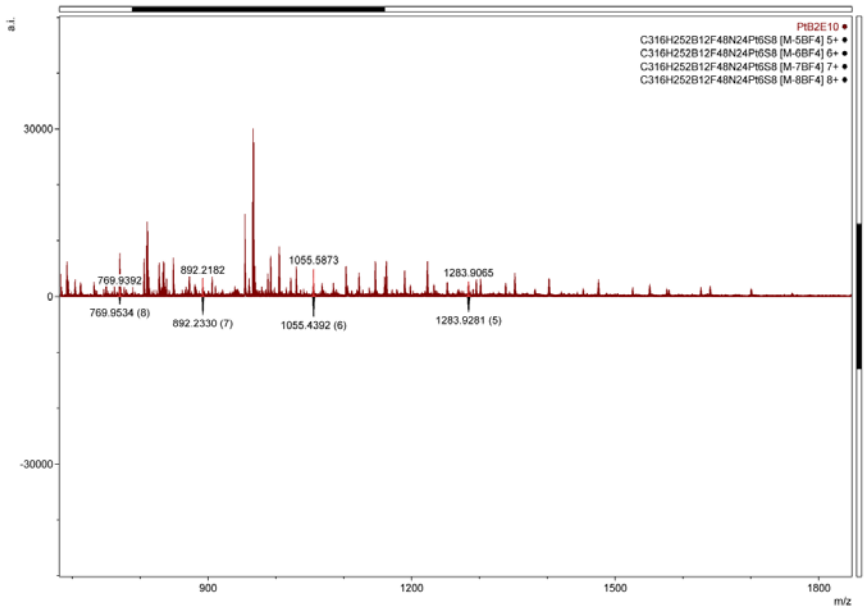

Figure S64. Full CSI-MS spectrum for cage sample $(Pt_6\mathbf{E}_{10}\mathbf{B}_2)(BF_4^-)_{12}$ in CD_3CN.

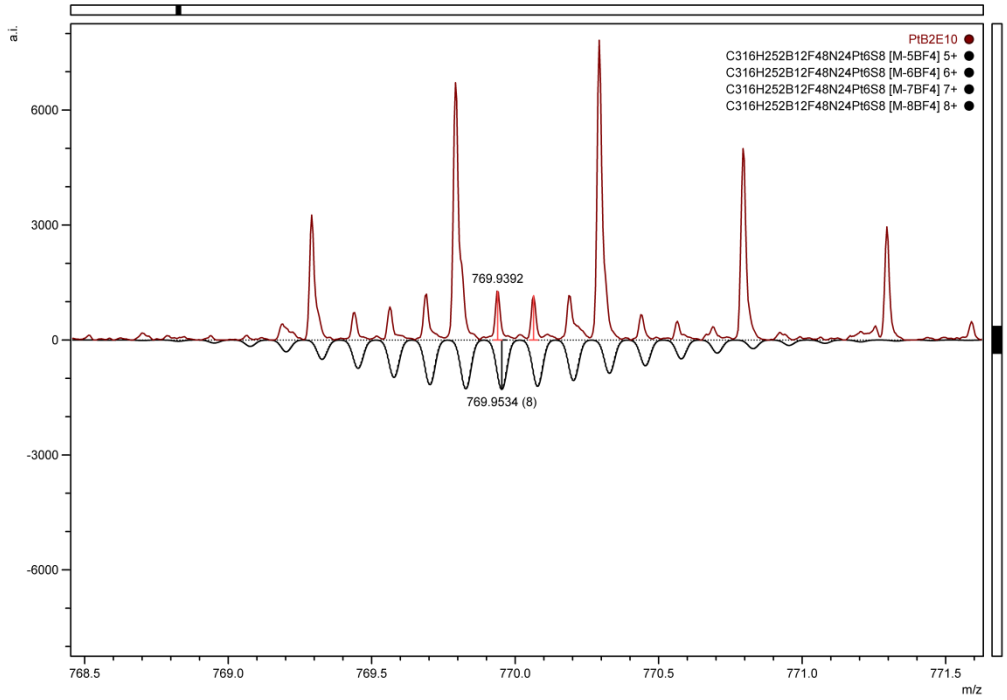

Figure S65. CSI-MS peak for $[(Pt_6\mathbf{E}_{10}\mathbf{B}_2)(BF_4^-)_4]^{8+}$ in CD_3CN, *m/z* 769.9392; calculated *m/z* 769.9534.

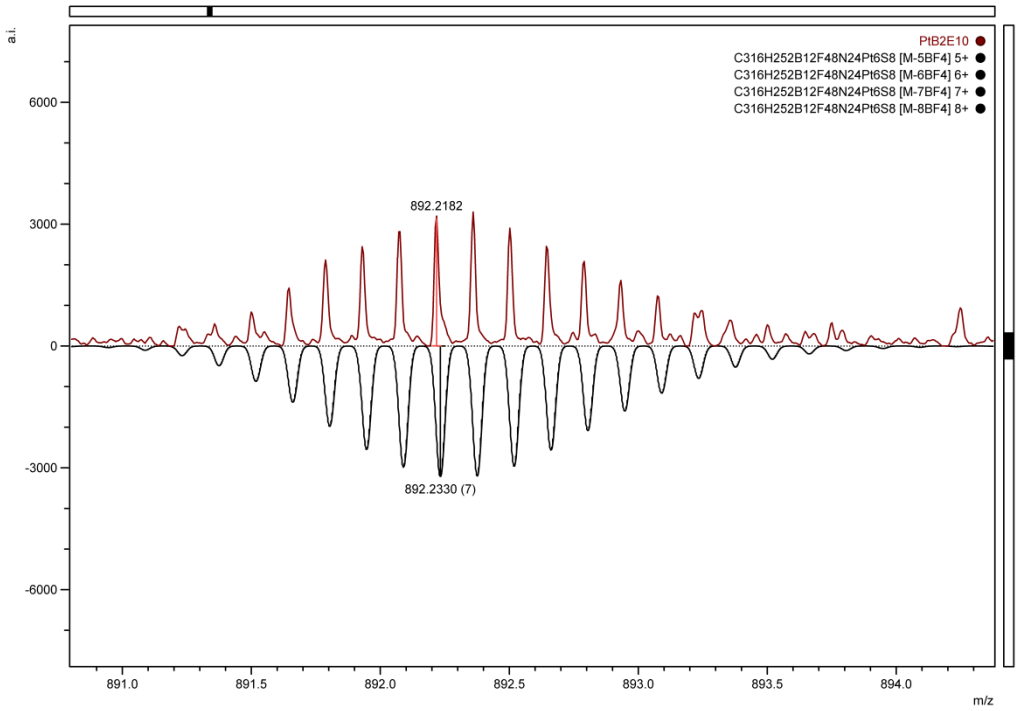

Figure S66. CSI-MS peak for $[(Pt_6\mathbf{E}_{10}\mathbf{B}_2)(BF_4^-)_5]^{7+}$ in CD_3CN, *m/z* 892.2182; calculated *m/z* 892.2330.

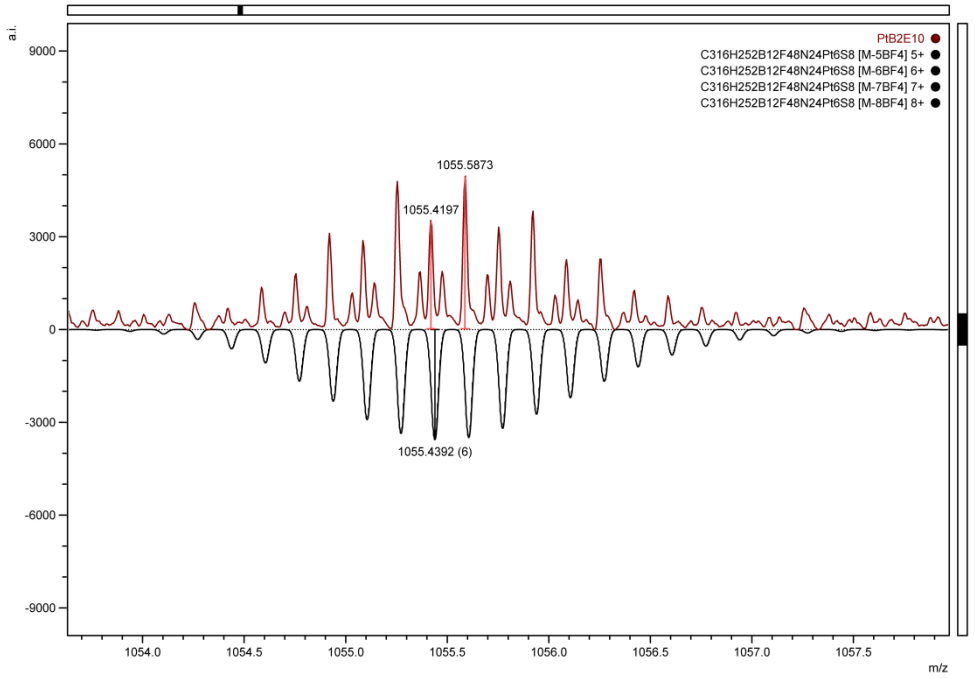

Figure S67. CSI-MS peak for $[(Pt_6\mathbf{E}_{10}\mathbf{B}_2)(BF_4^-)_6]^{6+}$ in CD_3CN, *m/z* 1055.4197; calculated *m/z* 1055.4392.

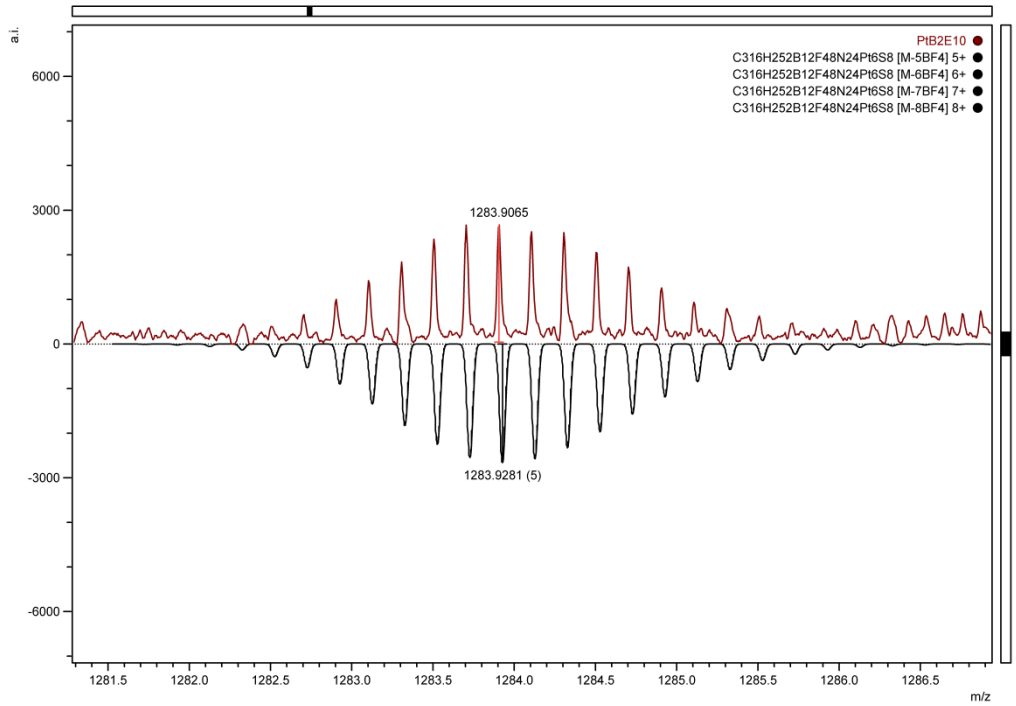

Figure S68. CSI-MS peak for $[(Pt_6\mathbf{E}_{10}\mathbf{B}_2)(BF_4^-)_7]^{5+}$ in CD_3CN, *m/z* 1283.9065; calculated *m/z* 1283.9281.

CSI-MS distribution of single composites from $(Pt_6E_{12-n}B_n)^{12+}$ with n=2

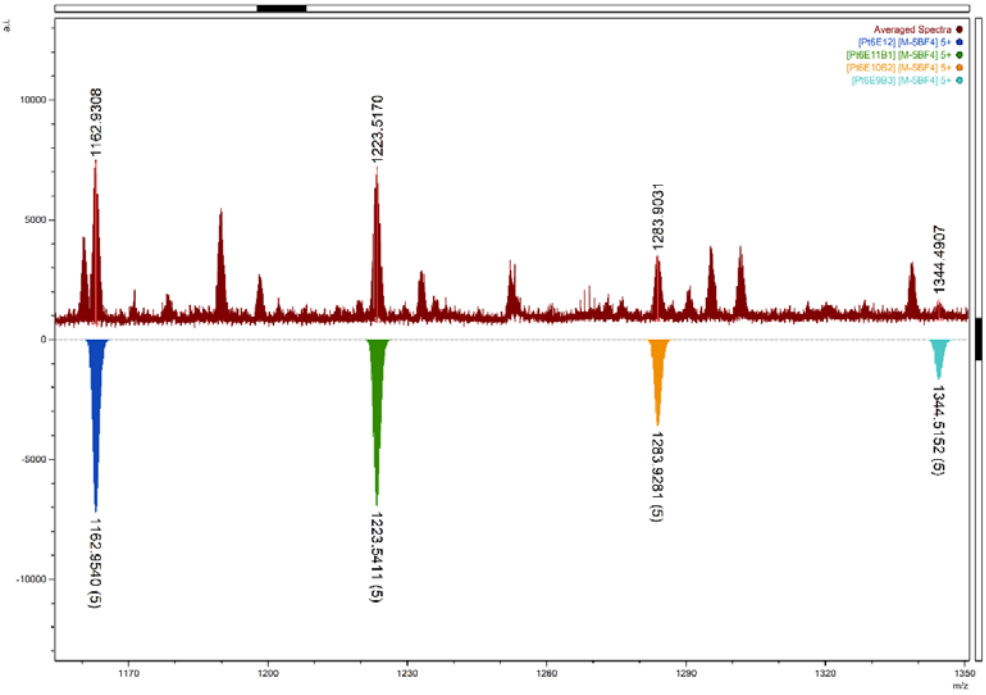

Figure S69. Full CSI-MS spectrum for cage sample $(Pt_6\mathbf{E}_{10}\mathbf{B}_2)(BF_4^-)_{12}$ in CD_3CN showing the presence of different species in solution: $[(Pt_6\mathbf{E}_{12})(BF_4)_4]^{5+}$ *m/z* 1162.9308; calculated (blue) *m/z* 1162.9540, $[(Pt_6\mathbf{E}_{11}\mathbf{B}_1)(BF_4)_4]^{5+}$ *m/z* 1223.5170; calculated (green) *m/z* 1223.5411, $[(Pt_6\mathbf{E}_{10}\mathbf{B}_2)(BF_4)_4]^{5+}$ *m/z* 1283.9031; calculated (blue) *m/z* 1283.9281; $[(Pt_6\mathbf{E}_9\mathbf{B}_3)(BF_4)_4]^{5+}$ *m/z* 1344.4907; calculated (cyan) *m/z* 1344.5152. Proper quantification of the composition is not possible due to differences in ionizability of the different species under MS conditions. Zoom-in of the different are consistent with those shown above in Figure S46 to Figure S49 while zoom-in of $[(Pt_6\mathbf{E}_9\mathbf{B}_3)(BF_4)_4]^{5+}$ and $[(Pt_6\mathbf{E}_9\mathbf{B}_3)(BF_4)_7]^{7+}$ are shown below.

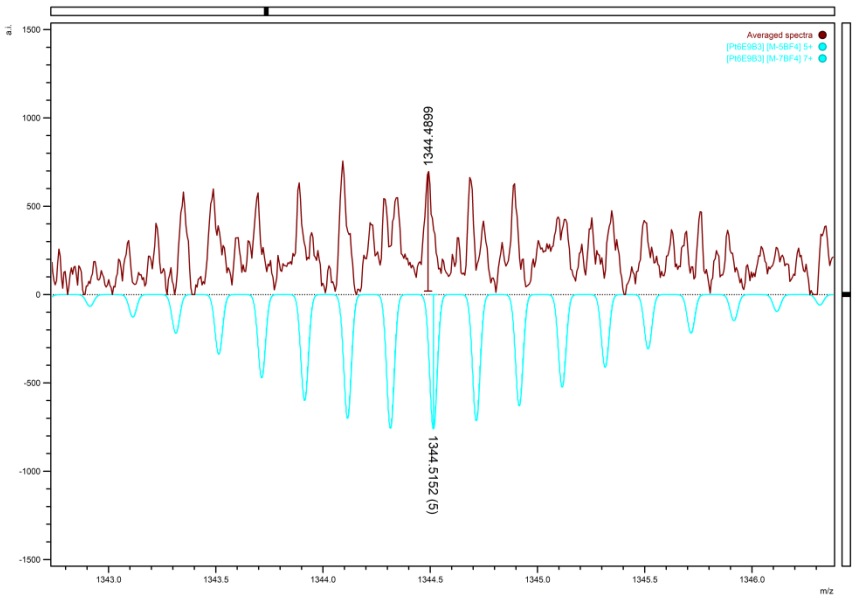

Figure S70. CSI-MS peak for $[(Pt_6\mathbf{E}_9\mathbf{B}_3)(BF_4)_4]^{5+}$ in MeCN *m/z* 1344.4899 (red); calculated (cyan) *m/z* 1344.5152.

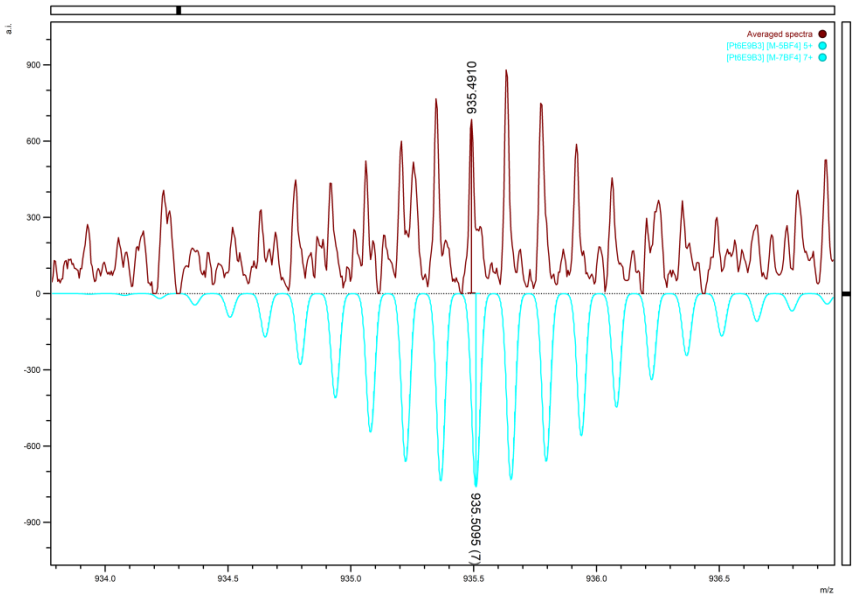

Figure S71. CSI-MS peak for $[(Pt_6\mathbf{E}_9\mathbf{B}_3)(BF_4)_7]^{7+}$ in MeCN *m/z* 935.4910 (red); calculated (cyan) *m/z* 935.5095.

Cage containing twistedTTFBB C

Cage $[Pt_6E_{11}C_1]^{12+}$

Preparation: A Schlenk flask was charged with 2.567 mg (1 equiv, 3.33 µmol) of TTFBB **B**, 12.326 mg (11 equiv, 36.66 µmol) of BBH **E** and 14.28 mg $[Pt(PF_6)_2(MeCN)_4]$ (0.55 equiv, 22 µmol). The flask was flushed with nitrogen before 4 ml of degassed CD_3CN were added. The resulting mixture was heated under N_2 at 85 °C for 48h.

For MS analysis the same procedure was carried out but $[Pt(PF_6)_2(MeCN)_4]$ was replaced by $[Pt(BF_4)_2(MeCN)_4]$.

NMR spectroscopy

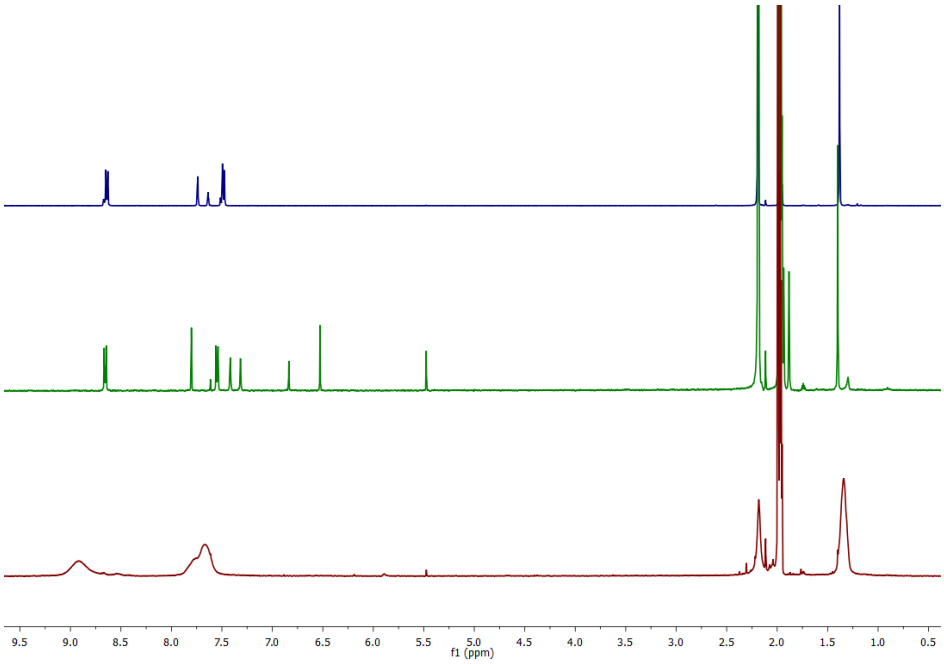

Figure S72. ^1H NMR spectra of non-functionalized building block BBH **E** (top), free twistedTTF building block **C** (middle), and corresponding cage of the type $(Pt_6\mathbf{E}_{11}\mathbf{C})^{12+}$ (bottom) in MeCN.

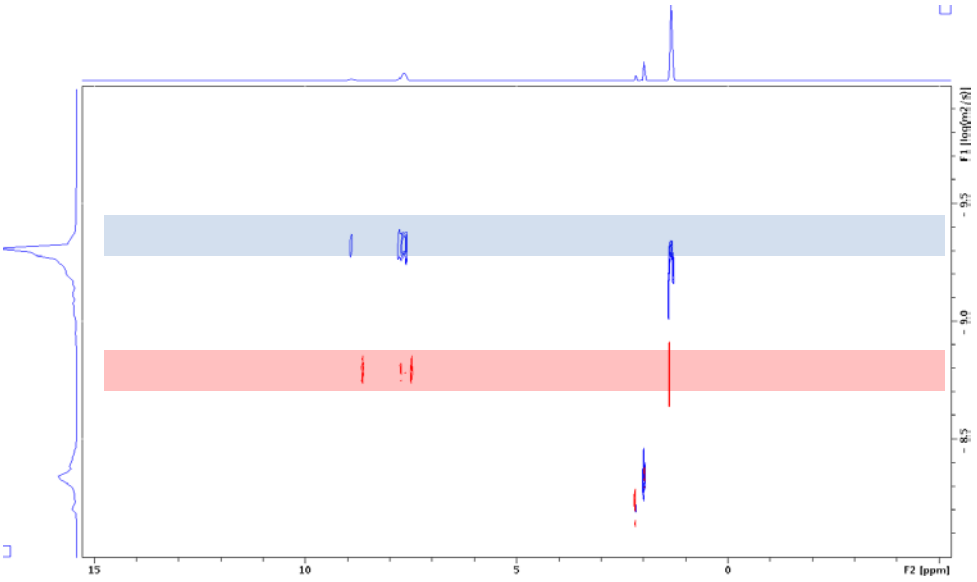

Figure S73. Overlay of two ^{1}H DOSY NMR spectra, showing the difference in logD value between the free diffusing twistedTTFBB **C** (logD = -8.8) and a solution of its cage of the type $(Pt_6\mathbf{E}_{11}\mathbf{C}_1)^{12+}$ (logD = -9.4) in CD_3CN at 25 °C.

CSI-MS characterization

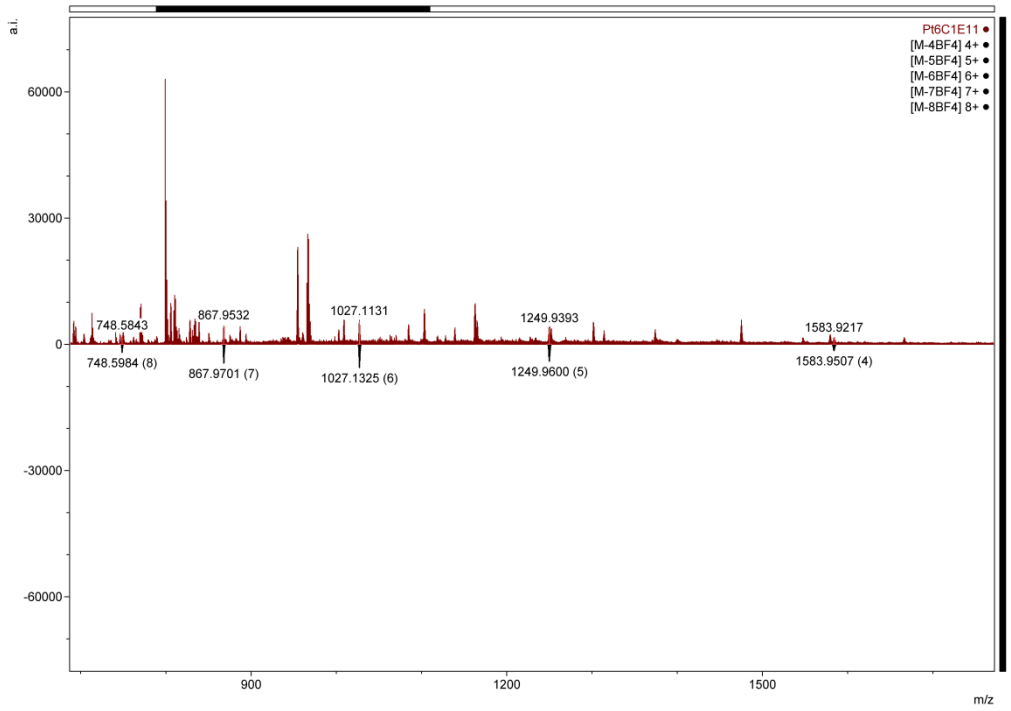

Figure S74. Full CSI-MS spectrum for cage sample $(Pt_6\mathbf{E}_{11}\mathbf{C}_1)(BF_4^-)_{12}$ in CD_3CN.

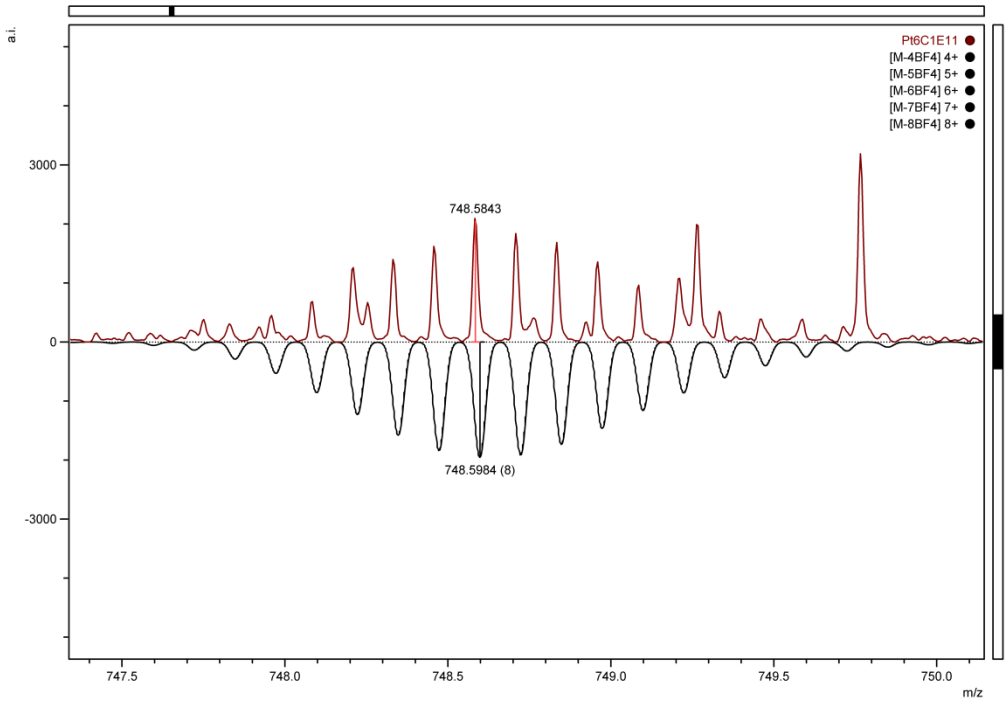

Figure S75. CSI-MS peak for $[(Pt_6\mathbf{E}_{11}\mathbf{C}_1)(BF_4^-)_4]^{8+}$ in CD_3CN, *m/z* 748.5843; calculated *m/z* 748.5984.

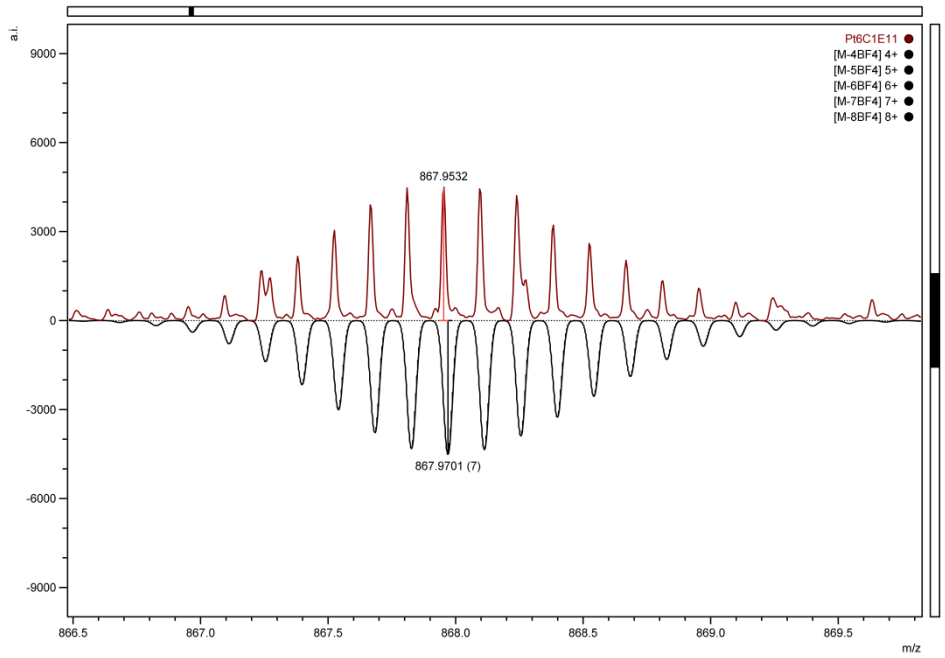

Figure S76. CSI-MS peak for $[(Pt_6\mathbf{E}_{11}\mathbf{C}_1)(BF_4^-)_5]^{7+}$ in CD_3CN, *m/z* 867.9532; calculated *m/z* 867.9701.

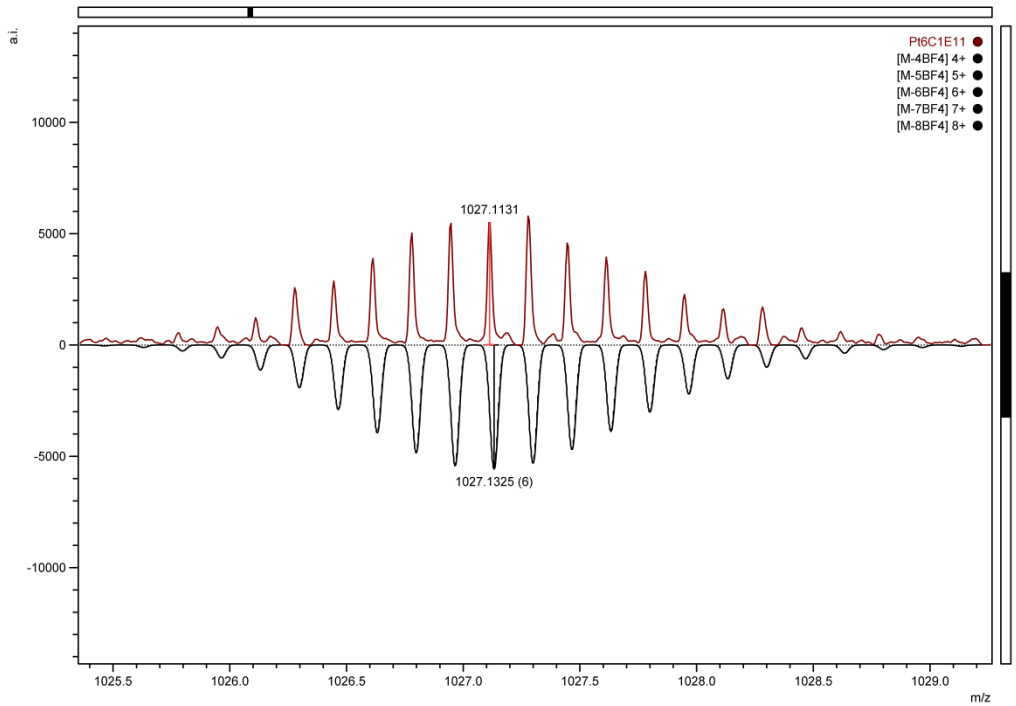

Figure S77. CSI-MS peak for $[(Pt_6\mathbf{E}_{11}\mathbf{C}_1)(BF_4^-)_6]^{6+}$ in CD_3CN, *m/z* 1027.1131; calculated *m/z* 1027.1325.

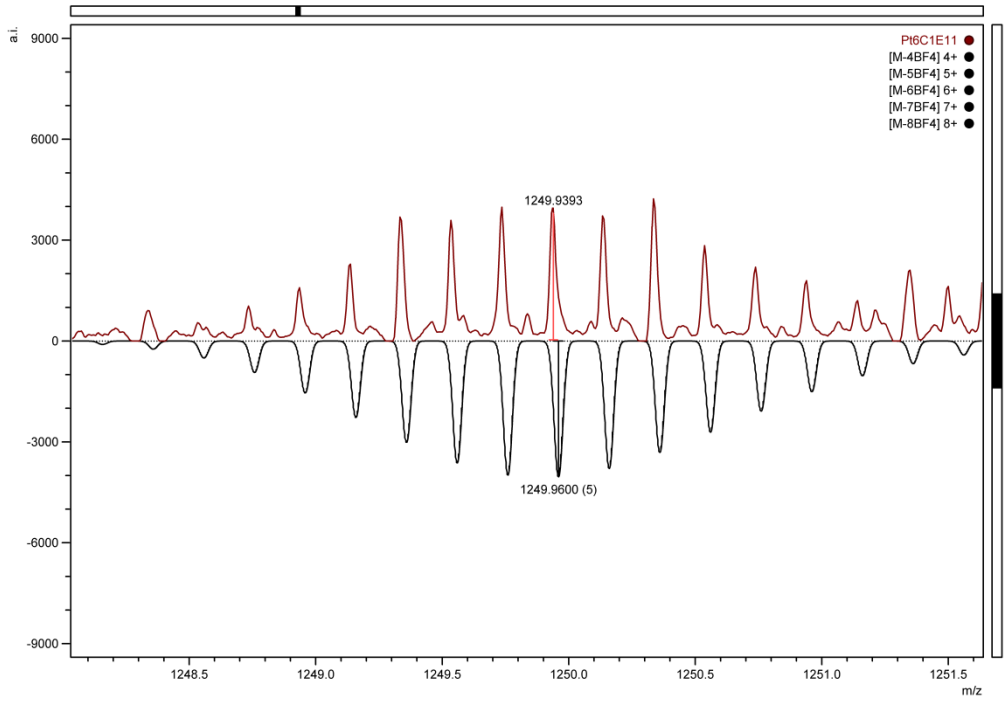

Figure S78. CSI-MS peak for $[(Pt_6\mathbf{E}_{11}\mathbf{C}_1)(BF_4^-)_7]^{5+}$ in CD_3CN, *m/z* 1249.9393; calculated *m/z* 1249.9600.

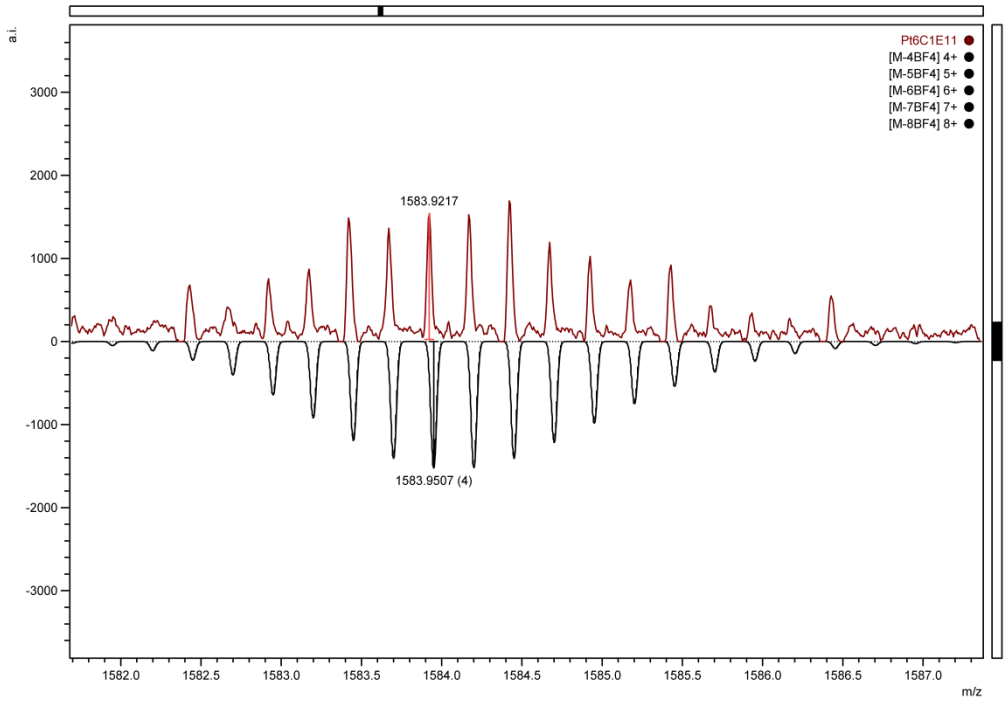

Figure S79. CSI-MS peak for $[(Pt_6\mathbf{E}_{11}\mathbf{C}_1)(BF_4^-)_8]^{4+}$ in CD_3CN, *m/z* 1583.9217; calculated *m/z* 1583.9507.

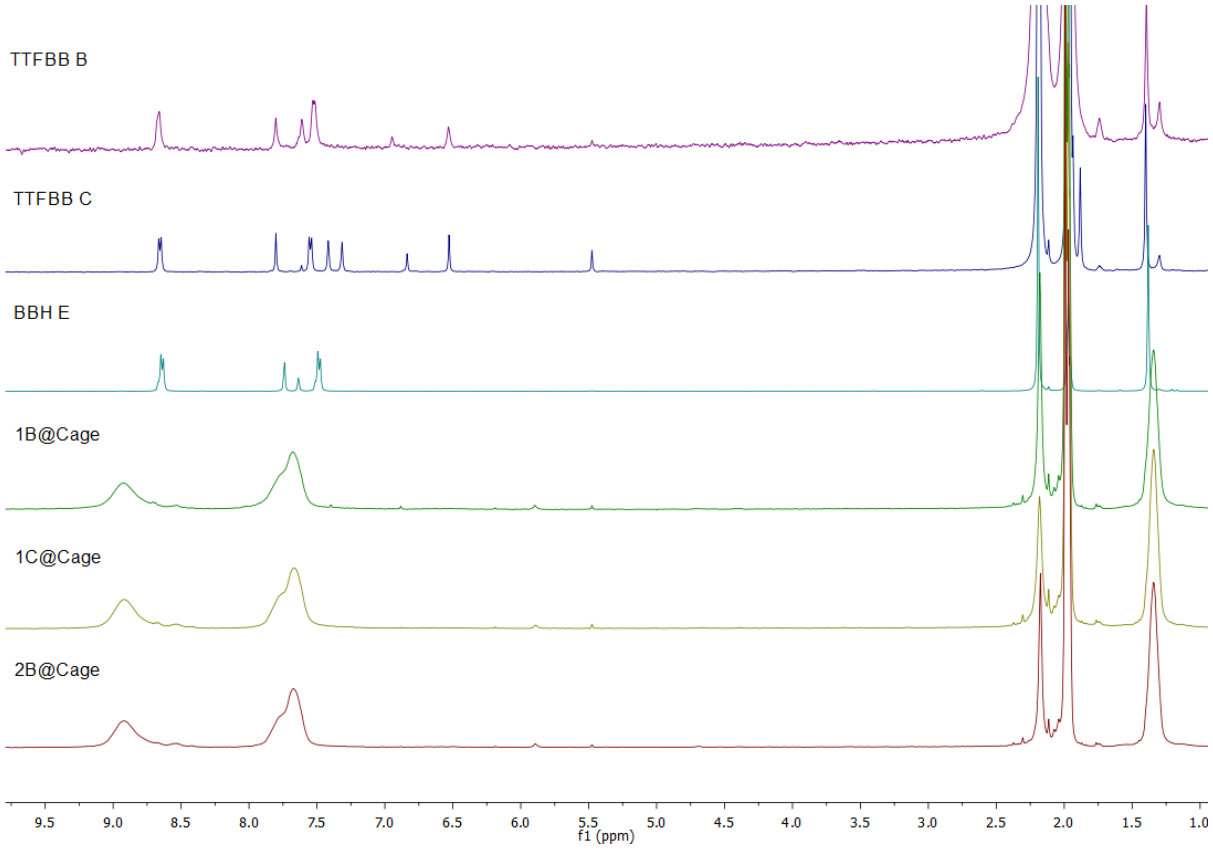

Figure S80. ^{1}H NMR overview of TTF containing building blocks and cages. From top ^{1}H NMR spectra of free TTFBB **B**, free twistedTTFBB **C**, non-functionalized building block BBH **E** and their corresponding cages of the type $(Pt_6\mathbf{E}_{11}\mathbf{B})^{12+}$, $(Pt_6\mathbf{E}_{11}\mathbf{C})^{12+}$ and bottom $(Pt_6\mathbf{E}_{10}\mathbf{B}_2)^{12+}$.

Cage containing guanidinium building block D

Cage $[Pd_{12}D_{24}]^{48+}$

Preparation: A Schlenk flask was charged with 21.261 mg (1 equiv, 40 µmol) of building block **D**, and 12.33 mg $[Pd(PF_6)_2(MeCN)_4]$ (0.55 equiv, 22 µmol). The flask was flushed with nitrogen before 4 ml of degassed CD_3CN were added. The resulting mixture was heated under N_2 at 60 °C overnight.

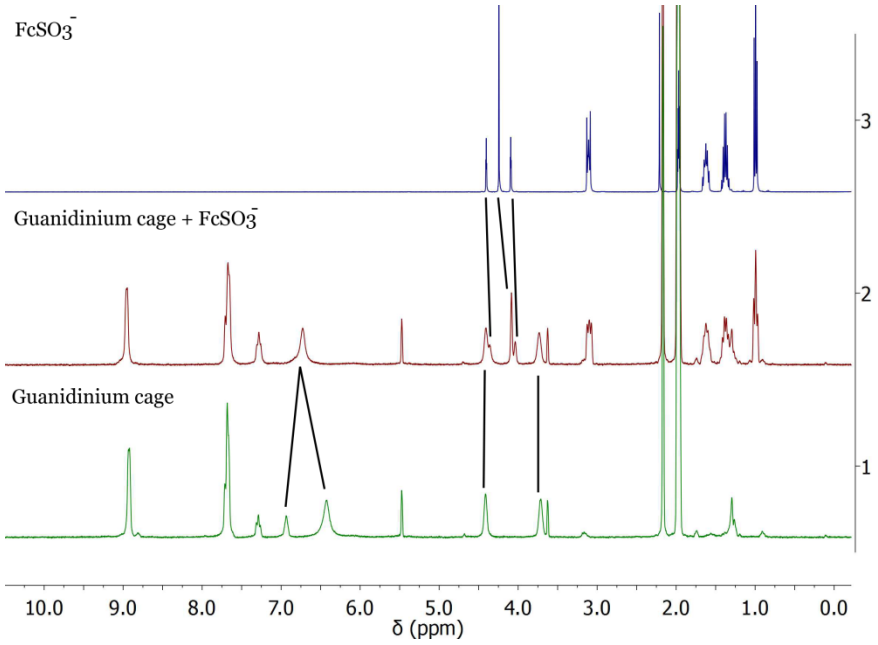

Figure S81. ^{1}H-NMR spectra of a palladium guanidinium cage solution $(Pd_{12}\mathbf{D}_{24})^{48+}$ in a 1:1 ratio of CD_3CN and CD_2Cl_2 (bottom), tetrabutylammonium ferrocenyl sulfonate in CD_3CN (top) and their mixture in 1:8 ratio in a 1:1 ratio of CD_3CN and CD_2Cl_2 (middle).

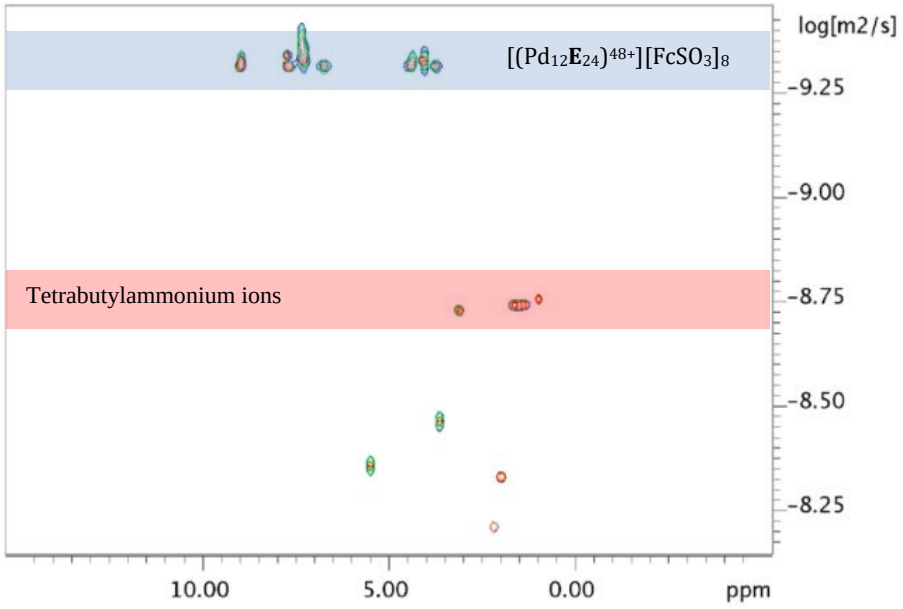

Figure S82. ^{1}H-DOSY NMR of a palladium guanidinium cage containing 8 equivalents of tetrabutylammonium ferrocenyl sulfonate in CD_3CN and CD_2Cl_2 1:1 ratio. The ferrocenyl peaks have the same diffusion coefficient value as the cage peaks, indicating full encapsulation. The set of signals around logD = -8.75 belong to the tetrabutylammonium counter ions that are not encapsulated.

CSI-MS on cage sample $(Pd_{12}\mathbf{D}_{24})(^{-}OTf)_{24}$ with different amounts of guests $[FcSO_3^{-}]$ 3, 8 and 16

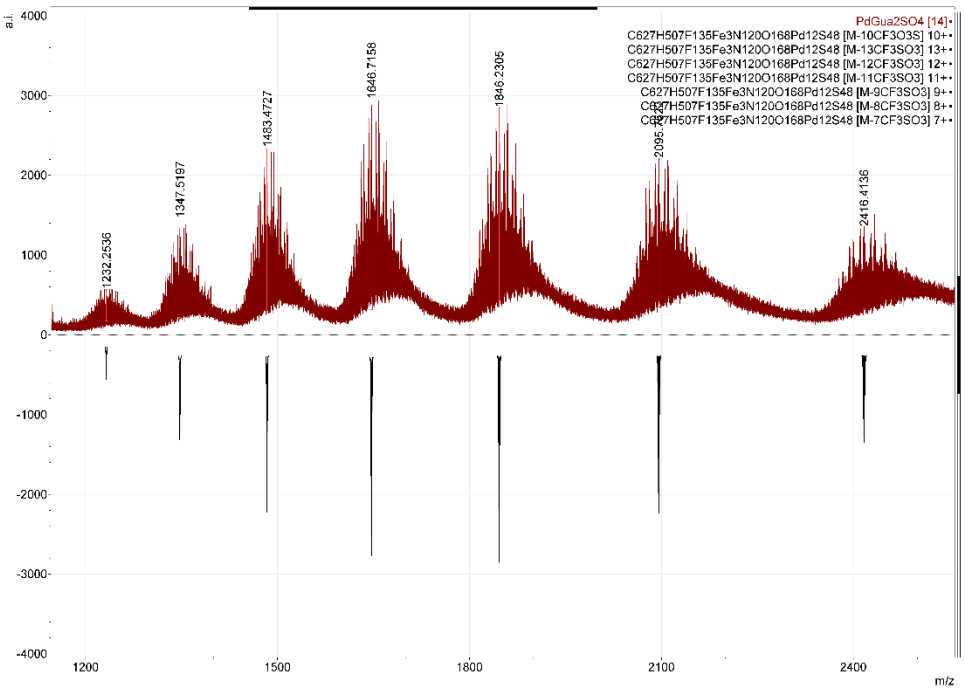

Figure S83. Full CSI-MS spectrum for cage sample $(Pd_{12}\mathbf{D}_{24})(^{-}OTf)_{21}(FcSO_3)_3$ in CD_3CN.

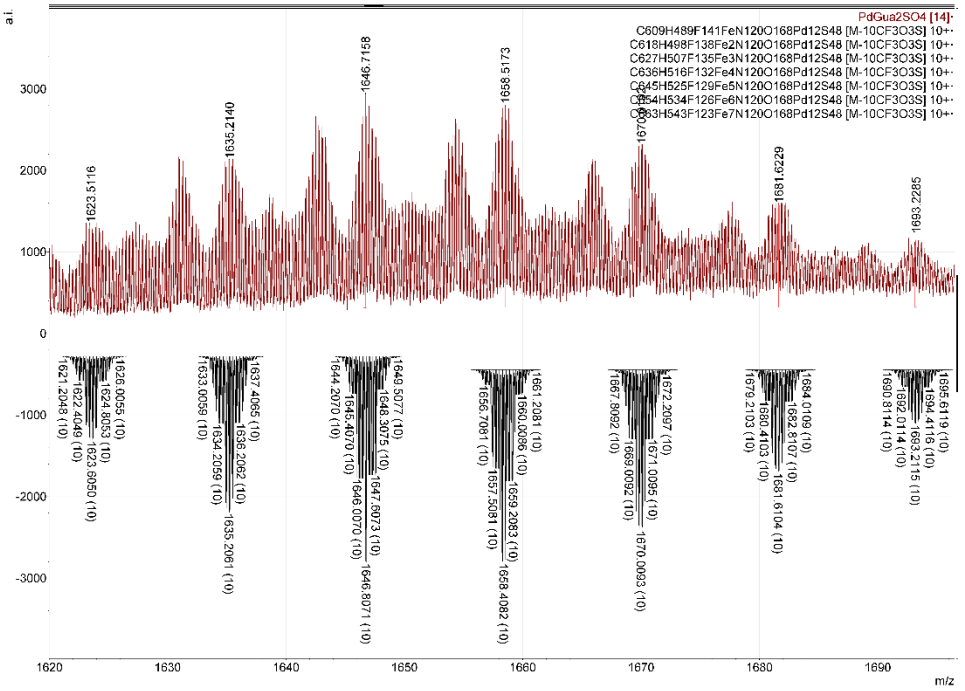

Figure S84. Zoom-in into 10+ species for cage sample $(Pd_{12}\mathbf{D}_{24})(^{-}OTf)_{21}(FcSO_3)_3$ in CD_3CN.

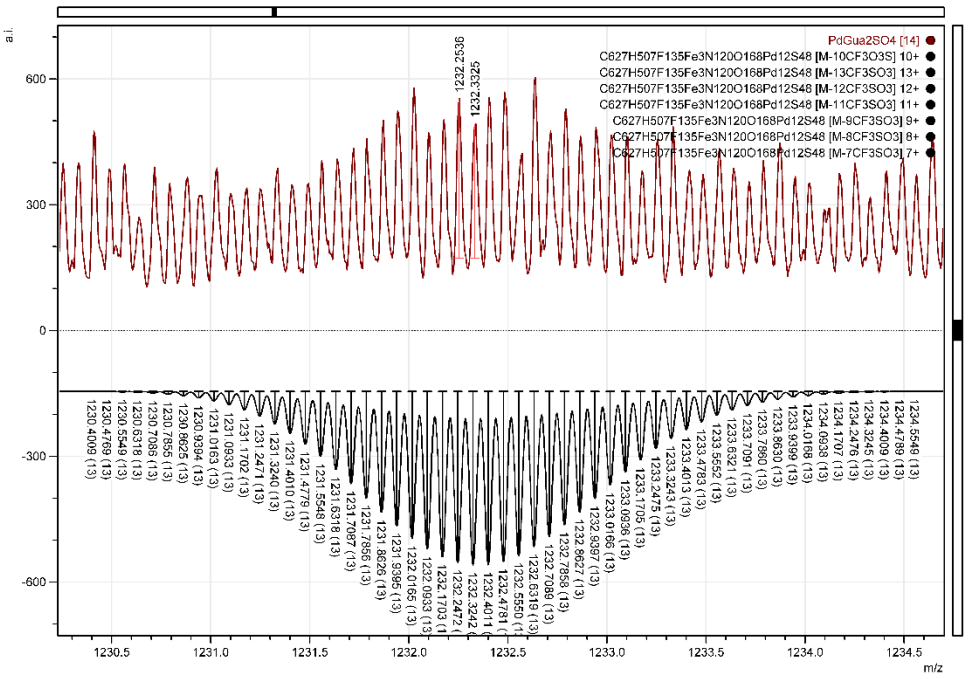

Figure S85. CSI-MS peak for $[(Pd_{12}\mathbf{D}_{24})(^{-}OTf)_8(FcSO_3)_3]^{13+}$ in CD_3CN, *m/z* 1232.3325; calculated *m/z* 1232.3242.

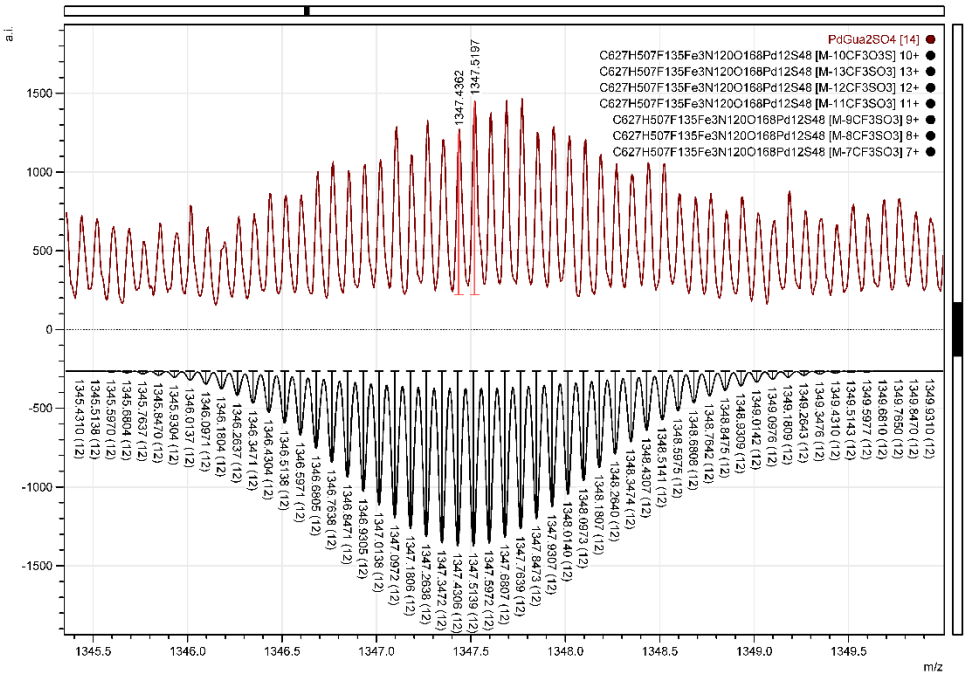

Figure S86. CSI-MS peak for $[(Pd_{12}\mathbf{D}_{24})(^{-}OTf)_9(FcSO_3)_3]^{12+}$ in CD_3CN, *m/z* 1347.5197; calculated *m/z* 1347.5139.

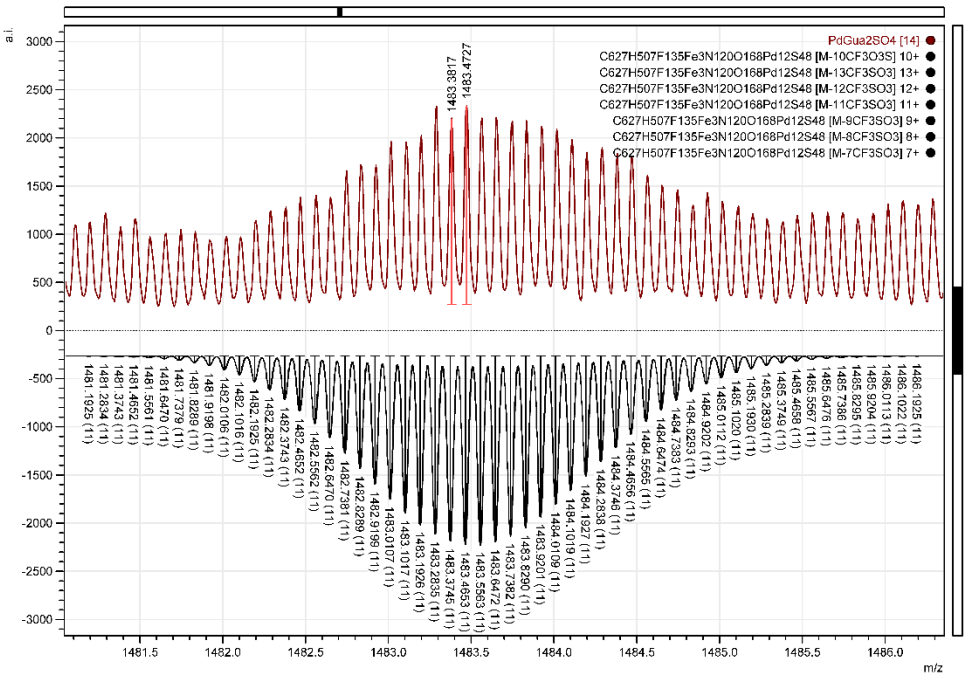

Figure S87. CSI-MS peak for $[(Pd_{12}\mathbf{D}_{24})(^{-}OTf)_{10}(FcSO_3)_3]^{11+}$ in CD_3CN, *m/z* 1483.4727; calculated *m/z* 1483.4653.

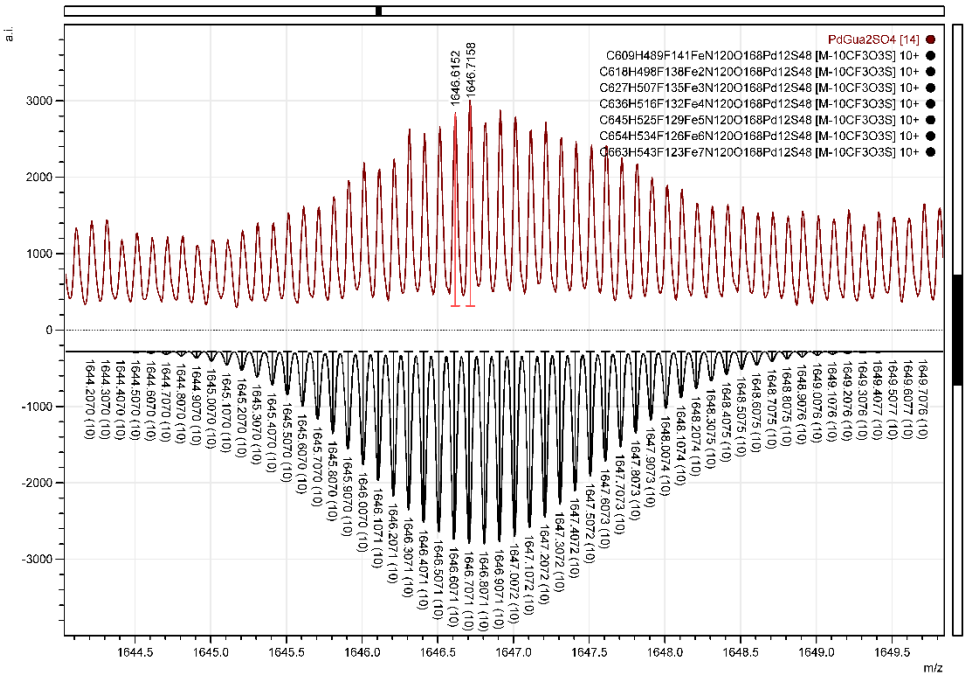

Figure S88. CSI-MS peak for $[(Pd_{12}\mathbf{D}_{24})(^{-}OTf)_{11}(FcSO_3)_3]^{10+}$ in CD_3CN, *m/z* 1646.7158; calculated *m/z* 1646.7071.

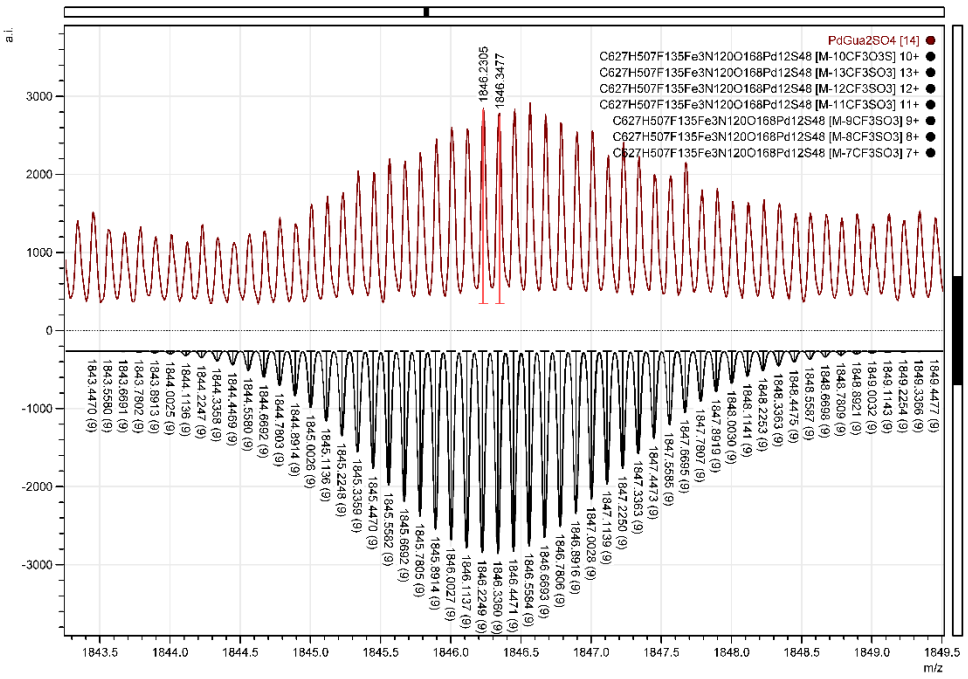

Figure S89. CSI-MS peak for $[(Pd_{12}\mathbf{D}_{24})(^{-}OTf)_{12}(FcSO_3)_3]^{9+}$ in CD_3CN, *m/z* 1846.3477; calculated *m/z* 1846.3380.

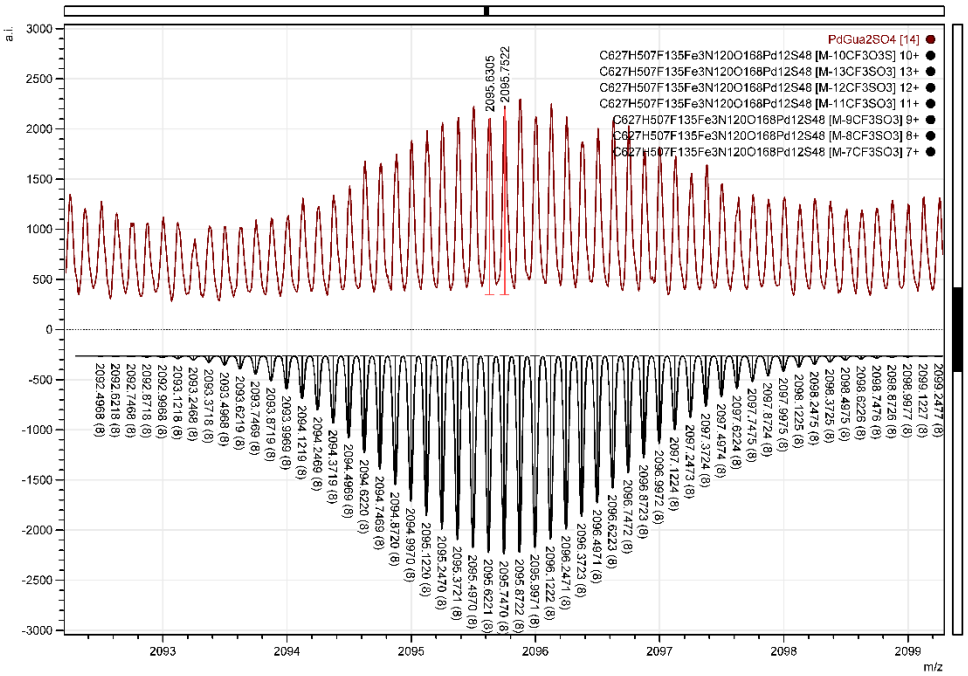

Figure S90. CSI-MS peak for $[(Pd_{12}\mathbf{D}_{24})(^{-}OTf)_{13}(FcSO_3)_3]^{8+}$ in CD_3CN, *m/z* 2095.7522; calculated *m/z* 2095.7470.

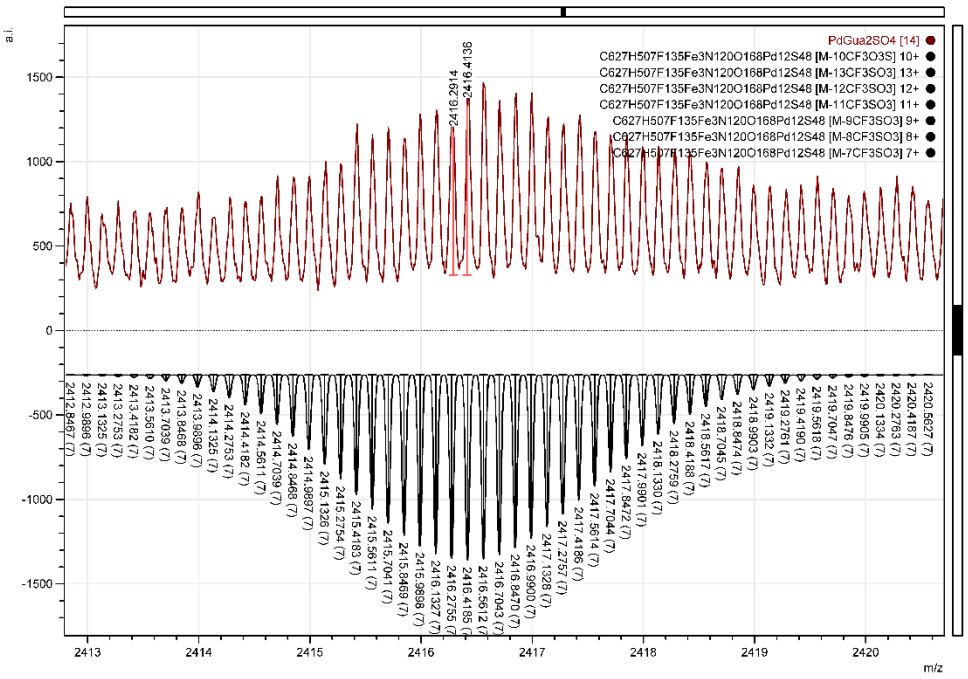

Figure S91. CSI-MS peak for $[(Pd_{12}\mathbf{D}_{24})(^{-}OTf)_{14}(FcSO_3)_3]^{7+}$ in CD_3CN, *m/z* 2416.4136; calculated *m/z* 2416.4185.

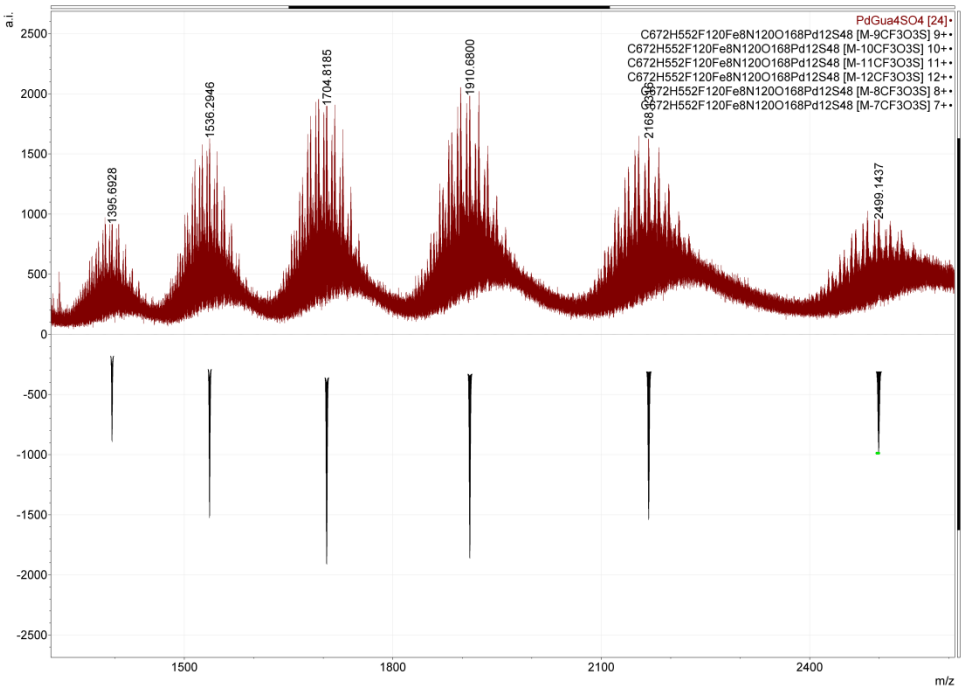

Figure S92. Full CSI-MS spectrum for cage sample $(Pd_{12}\mathbf{D}_{24})(^{-}OTf)_{16}(FcSO_3)_8$ in CD_3CN.

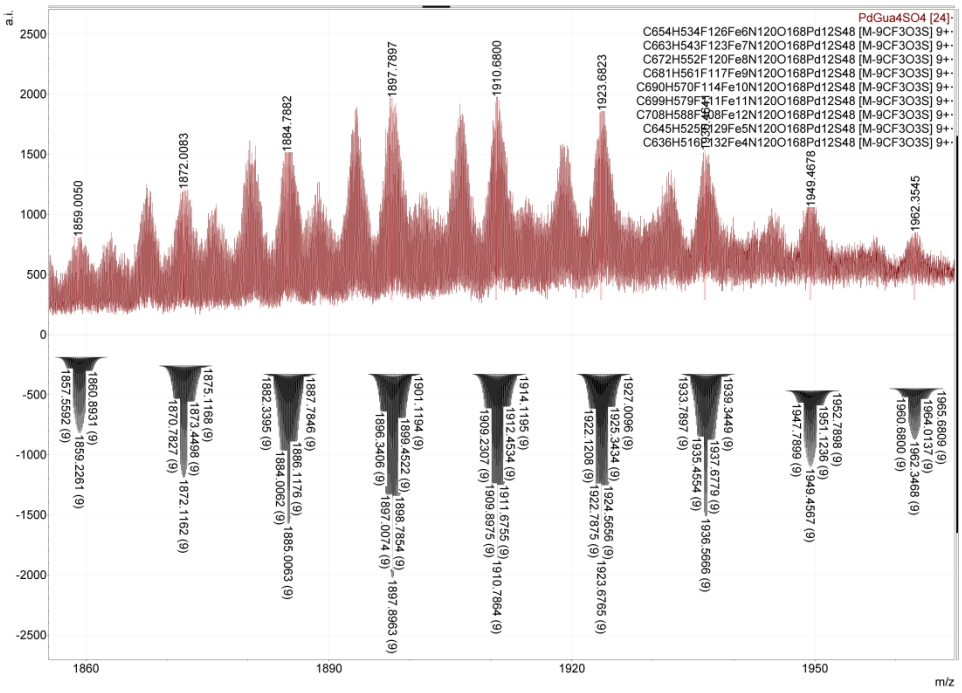

Figure S93. Zoom-in into 9+ species for cage sample $(Pd_{12}\mathbf{D}_{24})(^{-}OTf)_{16}(FcSO_3)_8$ in CD_3CN.

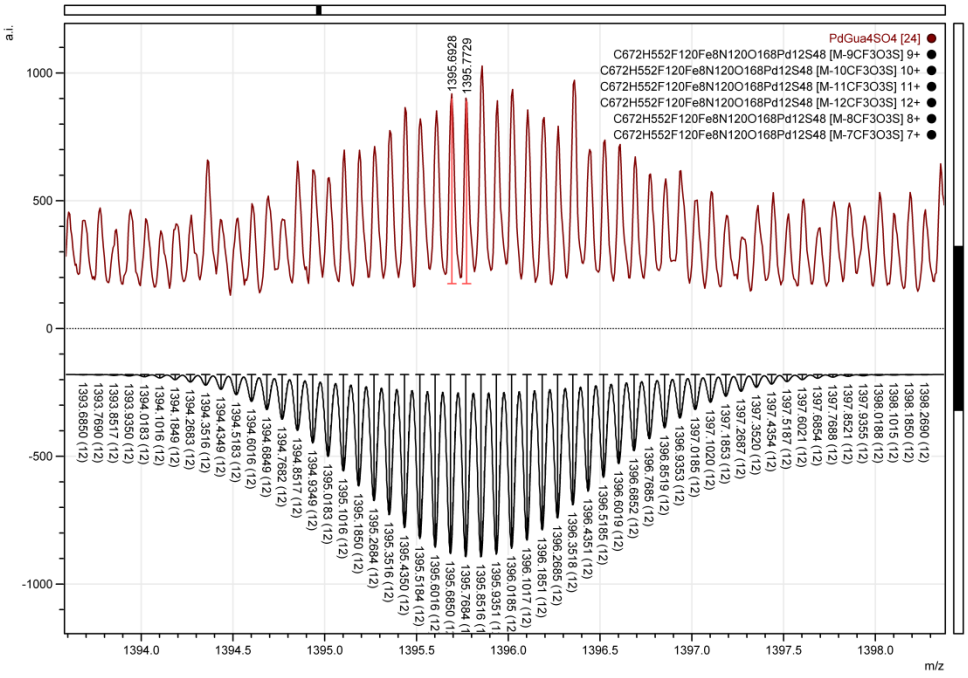

Figure S94. CSI-MS peak for $[(Pd_{12}\mathbf{D}_{24})(^{-}OTf)_4(FcSO_3)_8]^{12+}$ in CD_3CN, *m/z* 1395.7729; calculated *m/z* 1395.6784.

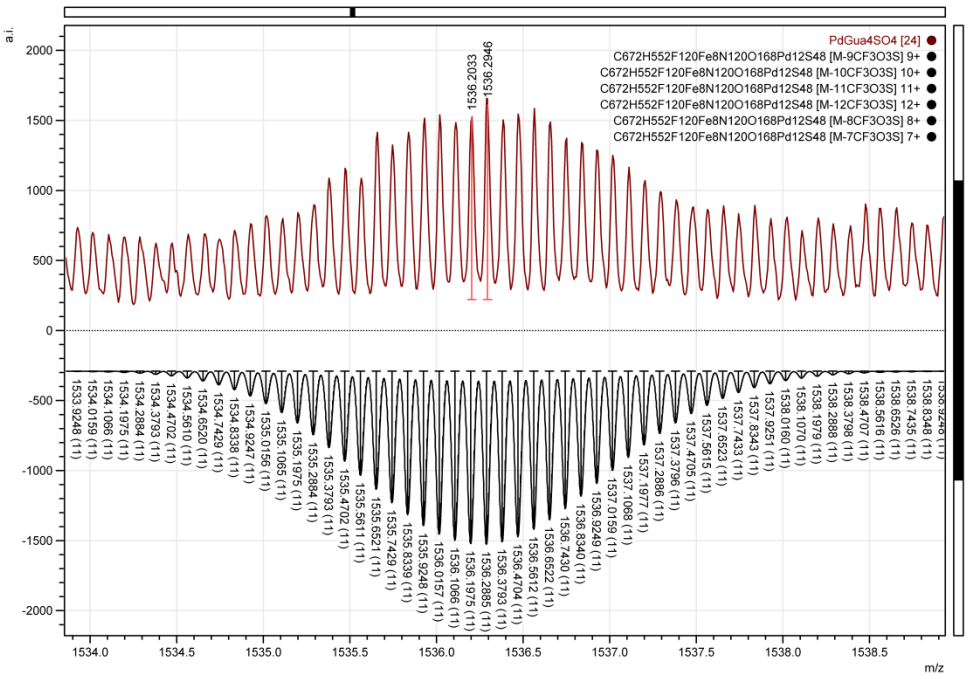

Figure S95. CSI-MS peak for $[(Pd_{12}\mathbf{D}_{24})(^{-}OTf)_5(FcSO_3)_8]^{11+}$ in CD_3CN, *m/z* 1536.2946; calculated *m/z* 1536.2885.

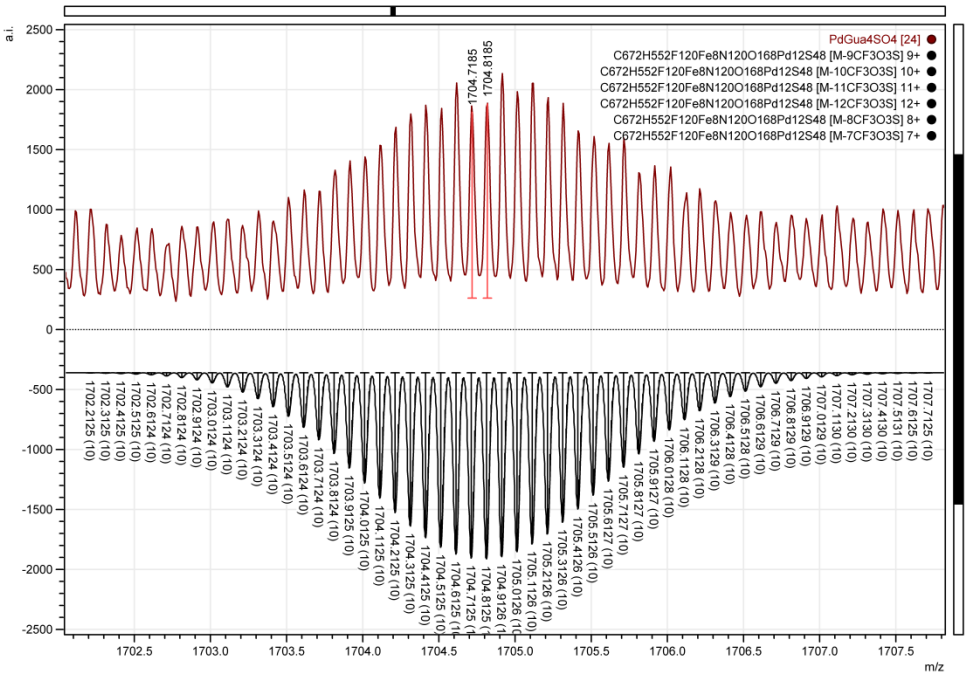

Figure S96. CSI-MS peak for $[(Pd_{12}\mathbf{D}_{24})(^{-}OTf)_6(FcSO_3)_8]^{10+}$ in CD_3CN, *m/z* 1704.8185; calculated *m/z* 1704.8125.

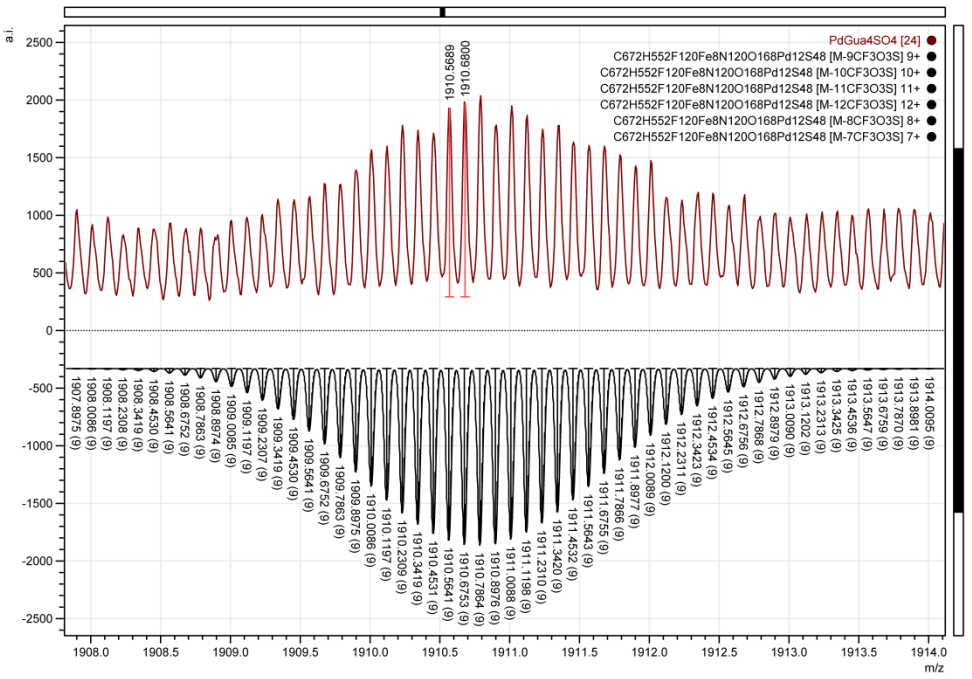

Figure S97. CSI-MS peak for $[(Pd_{12}\mathbf{D}_{24})(^{-}OTf)_7(FcSO_3)_8]^{9+}$ in CD_3CN, *m/z* 1910.6800; calculated *m/z* 1910.6753.

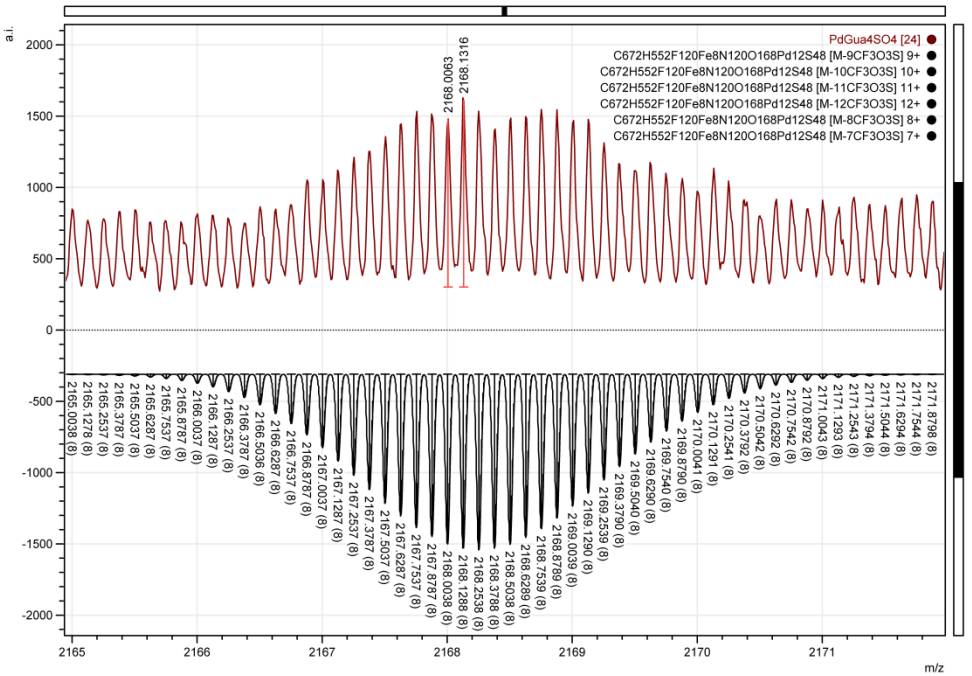

Figure S98. CSI-MS peak for $[(Pd_{12}\mathbf{D}_{24})(^{-}OTf)_8(FcSO_3)_8]^{8+}$ in CD_3CN, *m/z* 2168.1216; calculated *m/z* 2168.1288.

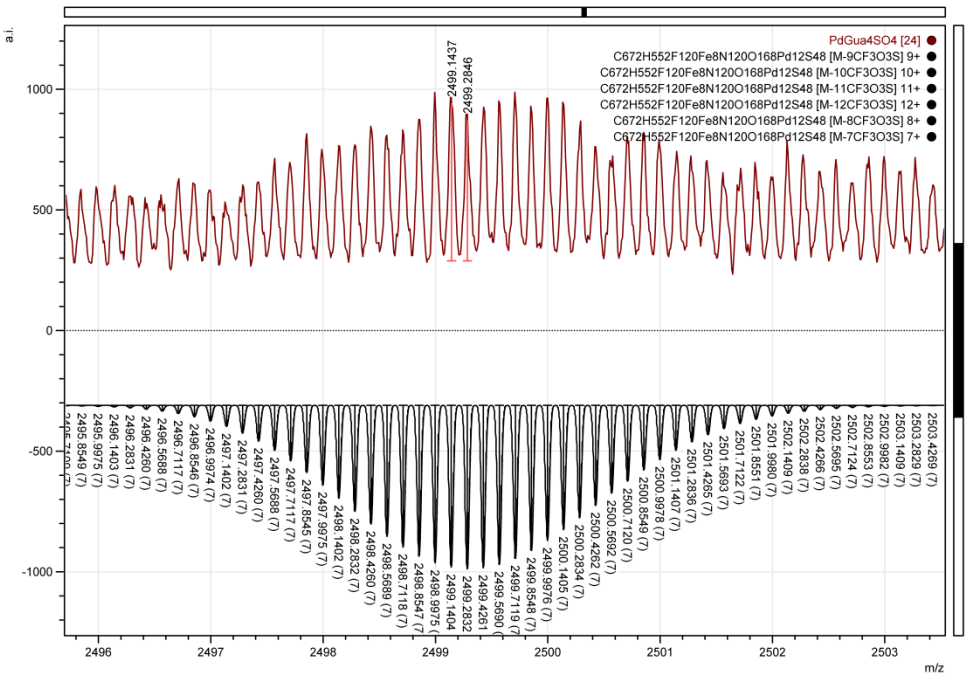

Figure S99. CSI-MS peak for $[(Pd_{12}\mathbf{D}_{24})(^{-}OTf)_9(FcSO_3)_8]^{7+}$ in CD_3CN, *m/z* 2499.2846; calculated *m/z* 2499.2832.

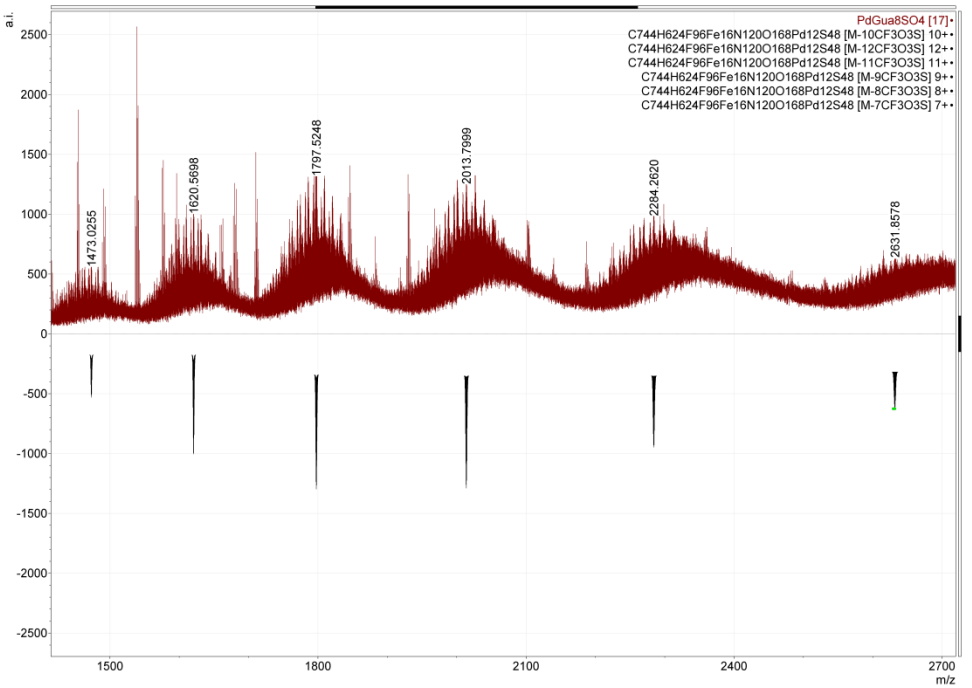

Figure S100. Full CSI-MS spectrum for cage sample $(Pd_{12}\mathbf{D}_{24})(^{-}OTf)_8(FcSO_3)_{16}$ in CD_3CN.

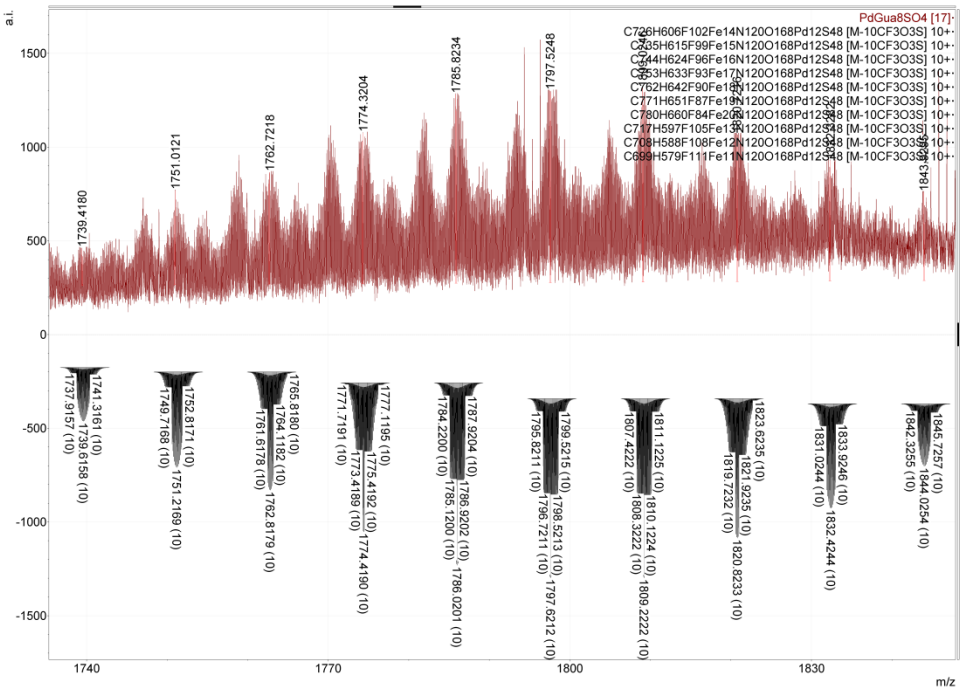

Figure S101. Zoom-in into 10+ species for cage sample $(Pd_{12}\mathbf{D}_{24})(^{-}OTf)_8(FcSO_3)_{16}$ in CD_3CN.

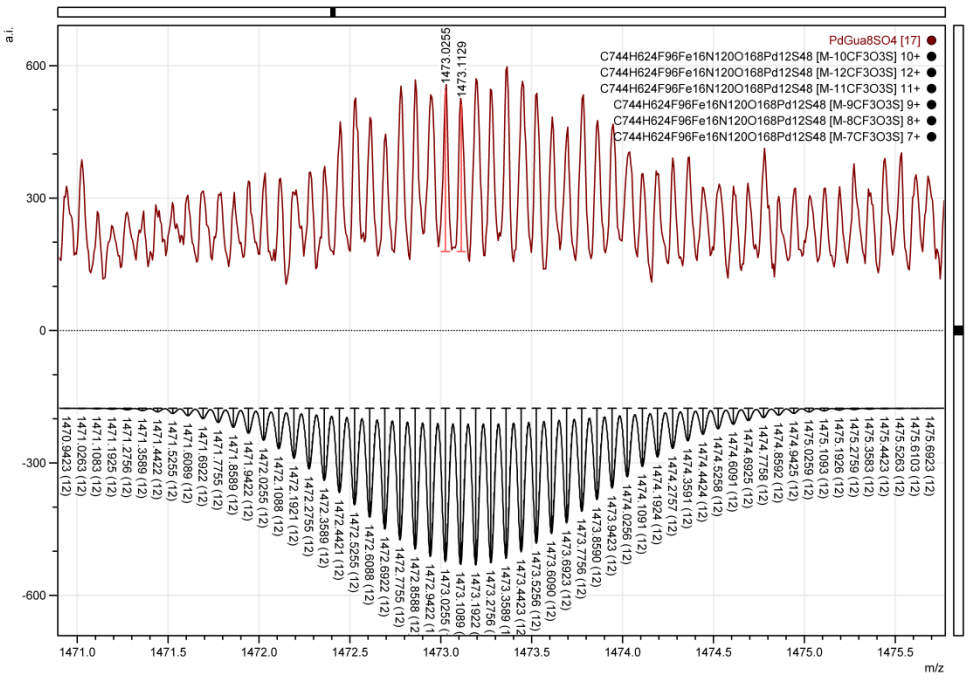

Figure S102. CSI-MS peak for $[(Pd_{12}\mathbf{D}_{24})(FcSO_3)_{16}]^{12+}$ in CD_3CN, *m/z* 1473.1129; calculated *m/z* 1473.1089.

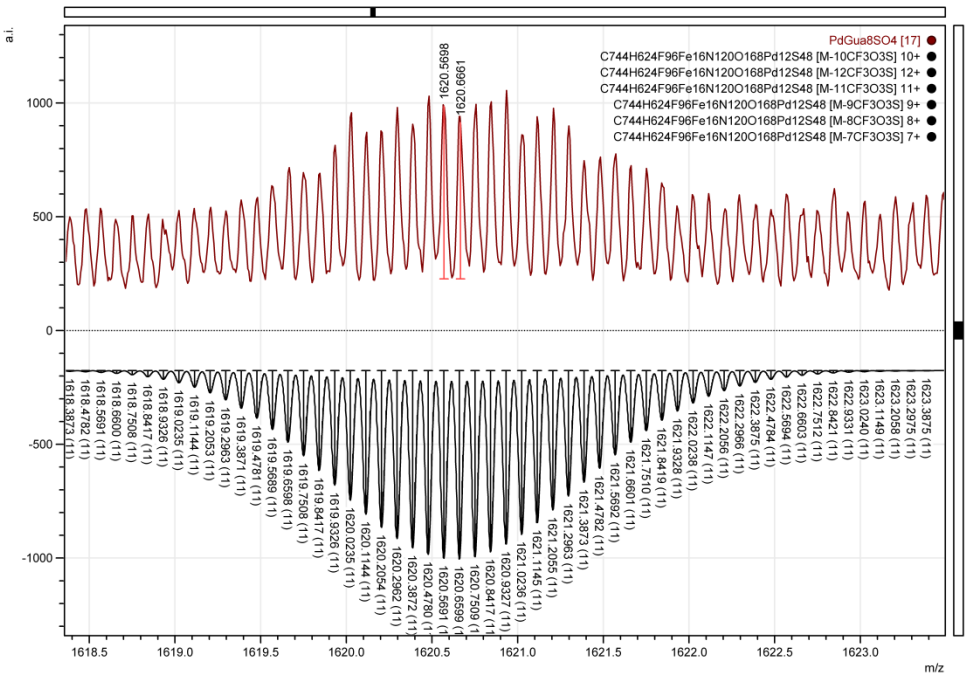

Figure S103. CSI-MS peak for $[(Pd_{12}\mathbf{D}_{24})(FcSO_3)_{16}]^{11+}$ in CD_3CN, *m/z* 1620.6661; calculated *m/z* 1620.6559.

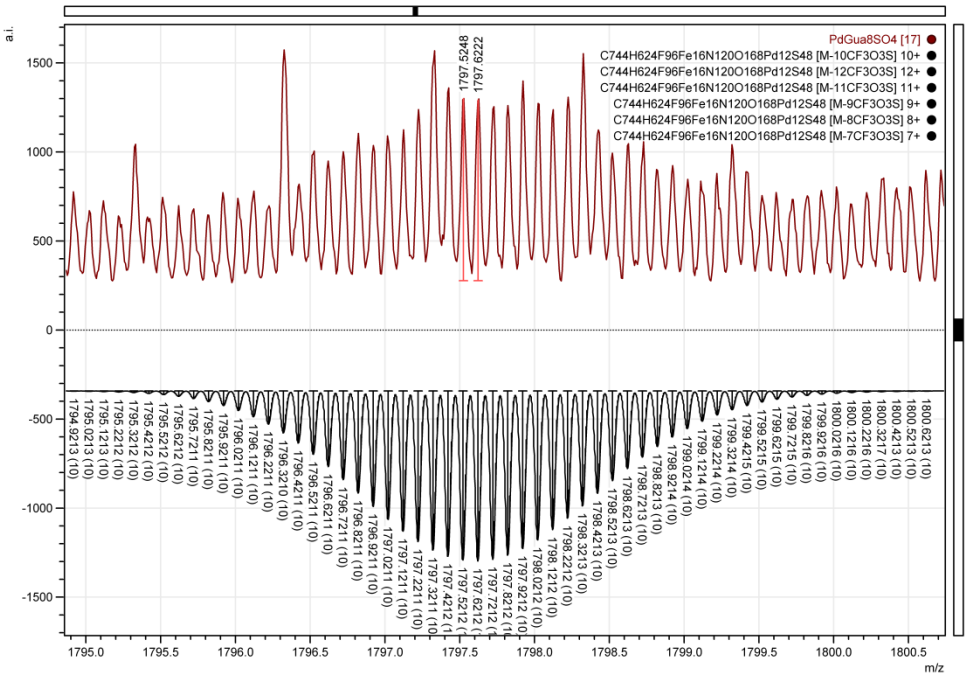

Figure S104. CSI-MS peak for $[(Pd_{12}\mathbf{D}_{24})(FcSO_3)_{16}]^{10+}$ in CD_3CN, *m/z* 1797.6222; calculated *m/z* 1797.6212.

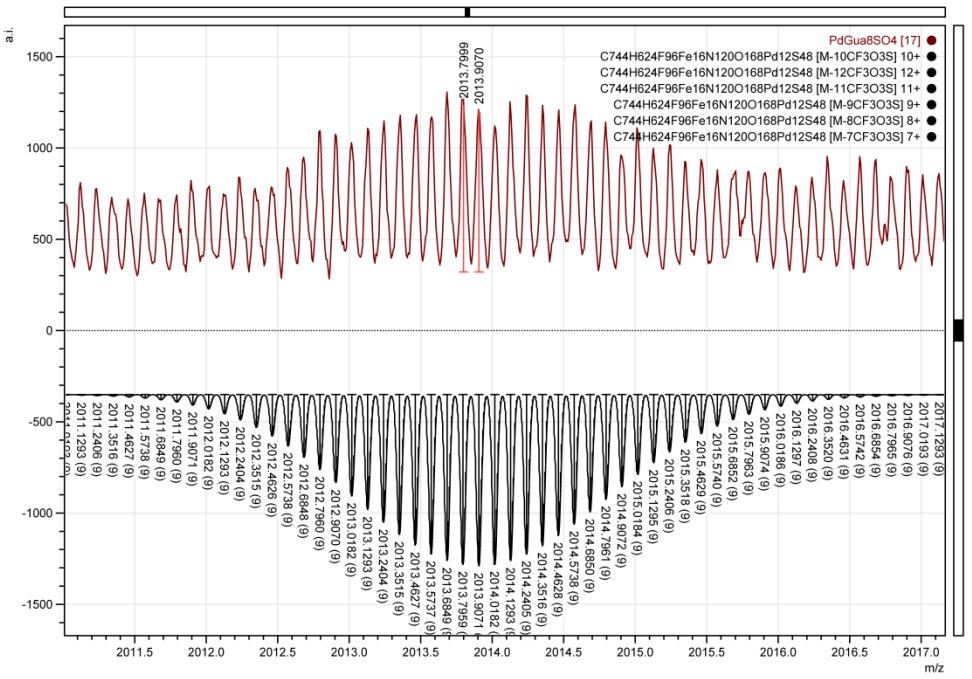

Figure S105. CSI-MS peak for $[(Pd_{12}\mathbf{D}_{24})(FcSO_3)_{16}]^{9+}$ in CD_3CN, *m/z* 2013.9070; calculated *m/z* 2013.9071.

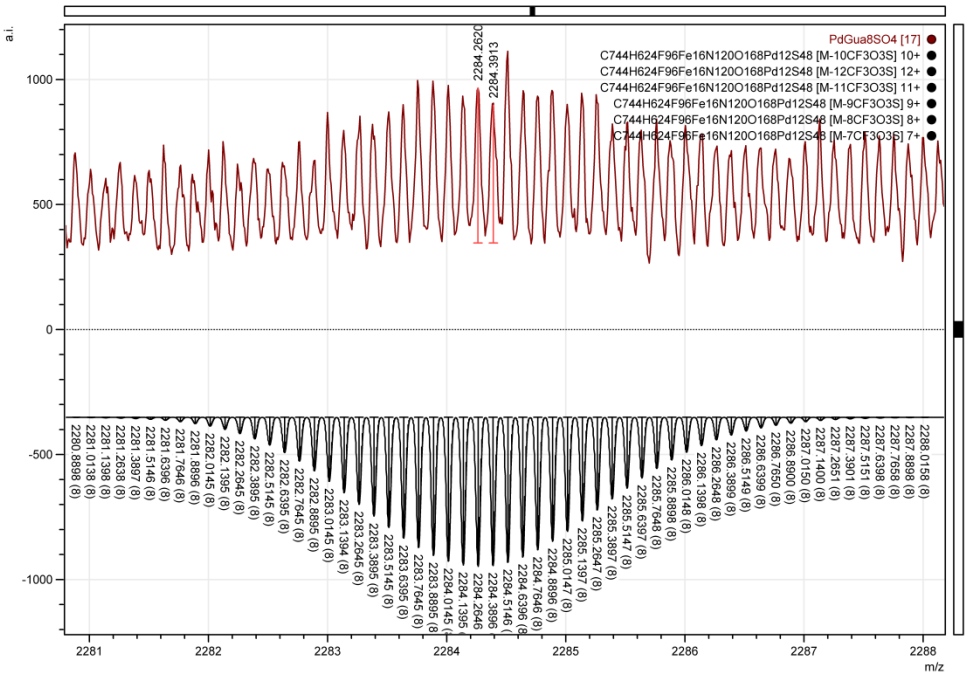

Figure S106. CSI-MS peak for $[(Pd_{12}\mathbf{D}_{24})(FcSO_3)_{16}]^{8+}$ in CD_3CN, *m/z* 2284.3913; calculated *m/z* 2284.3896.

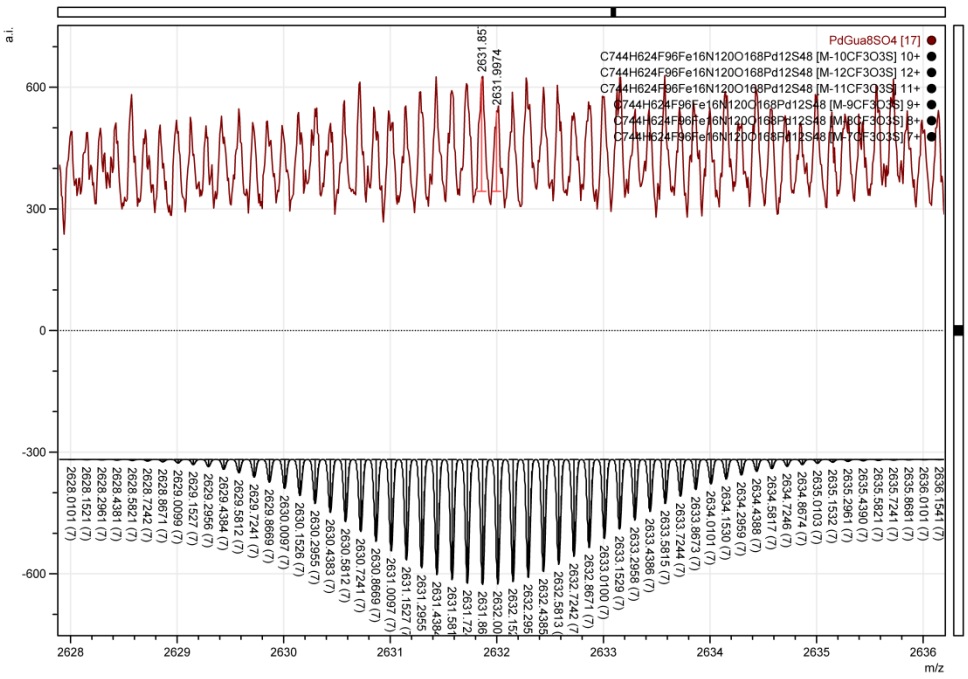

Figure S107. CSI-MS peak for $[(Pd_{12}\mathbf{D}_{24})(FcSO_3)_{16}]^{7+}$ in CD_3CN, *m/z* 2631.9974; calculated *m/z* 2632.0012.

Electrochemistry

FcBB A and FcBB A containing cages

FcBB A

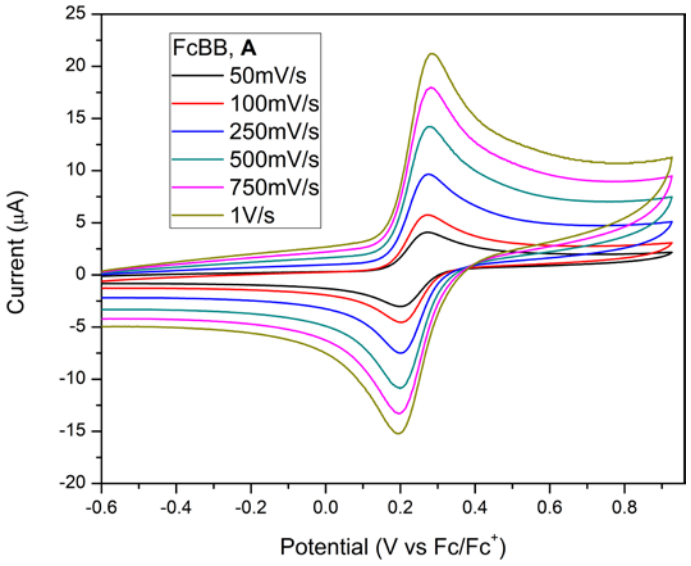

Figure S108. Cyclic voltammograms recorded at different scan speeds for a solution of FcBB **A** in a 1:1 mixture of DCM and MeCN.

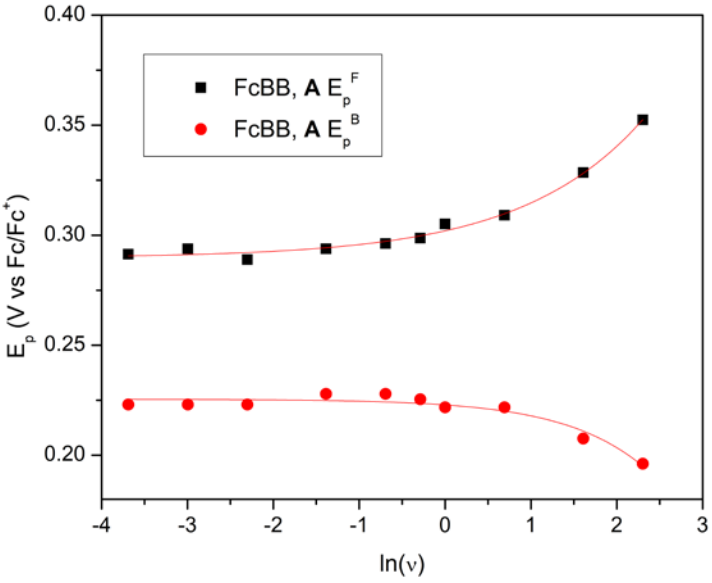

Figure S109. Plot of peak potential vs. natural logarithm of the scan speed for the FcBB **A** in a 1:1 mixture of DCM and MeCN.

Cage ($Pd_{12}A_{24}$)$^{24+}$

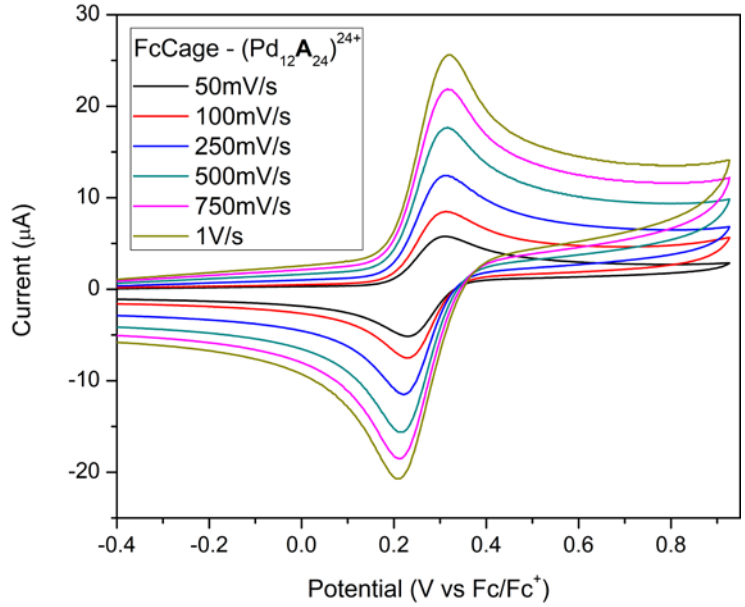

Figure S110. Cyclic voltammograms recorded at different scan speeds for a sample of the ferrocene cage, $(Pd_{12}\mathbf{A}_{24})^{24+}$ in a 1:1 mixture of DCM and MeCN, showing a single oxidation wave for the 24 ferrocene units present at its cavity.

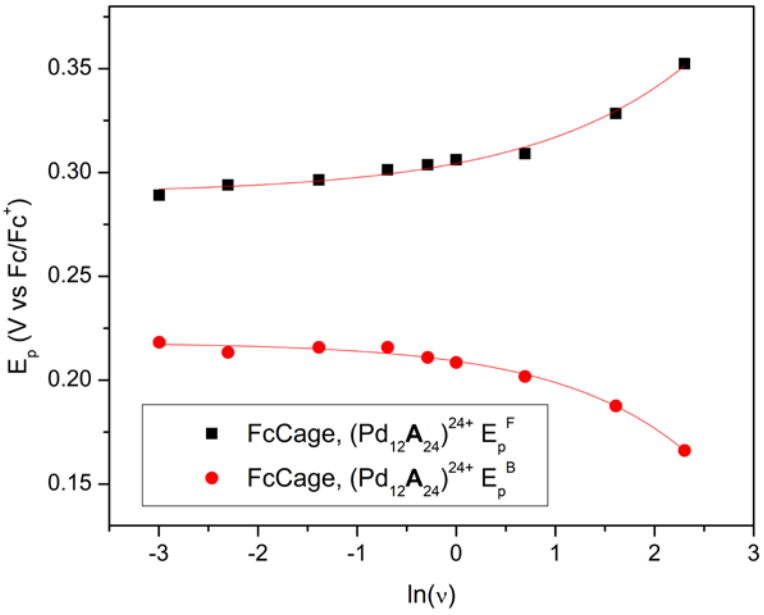

Figure S111. Plot of peak potential vs. natural logarithm of the scan speed for a cage sample $(Pd_{12}\mathbf{A}_{24})^{24+}$ in a 1:1 mixture of DCM and MeCN.

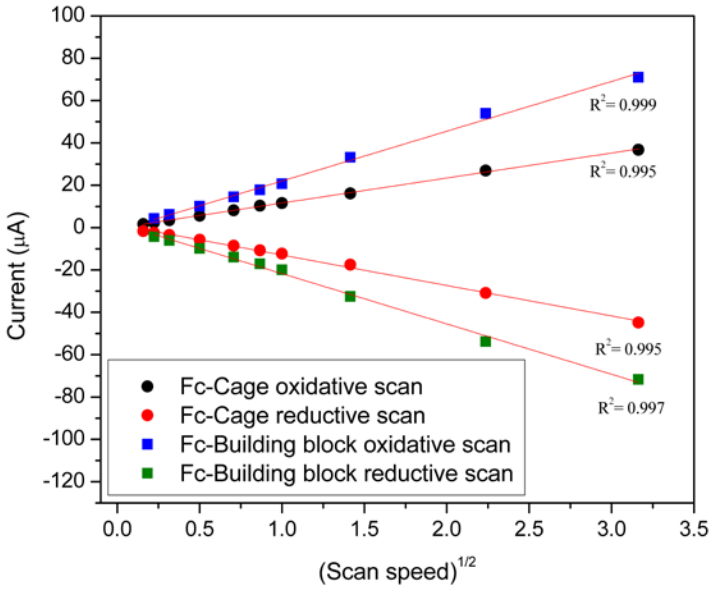

Figure S112. Plots of peak current vs. square root of the scan speed for a cage solution $(Pd_{12}\mathbf{A}_{24})^{24+}$ (black and red circles) and its free building block FcBB, **A** (blue and green squares) in a 1:1 mixture of DCM and MeCN.

Cage $(Pd_{12}E_{23}A_1)^{24+}$

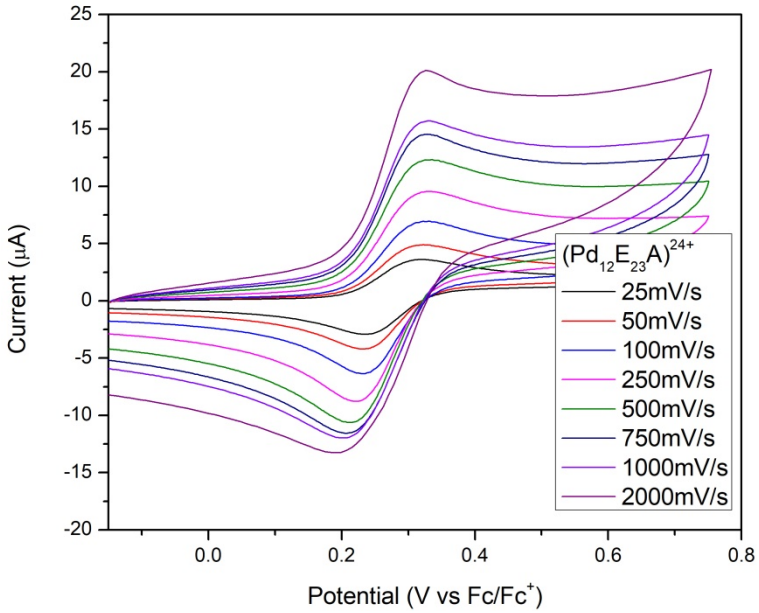

Figure S113. Cyclic voltammograms recorded at different scan speeds for a sample of the ferrocene cage, $(Pd_{12}\mathbf{E}_{23}\mathbf{A}_1)^{24+}$ in a 1:1 mixture of DCM and MeCN.

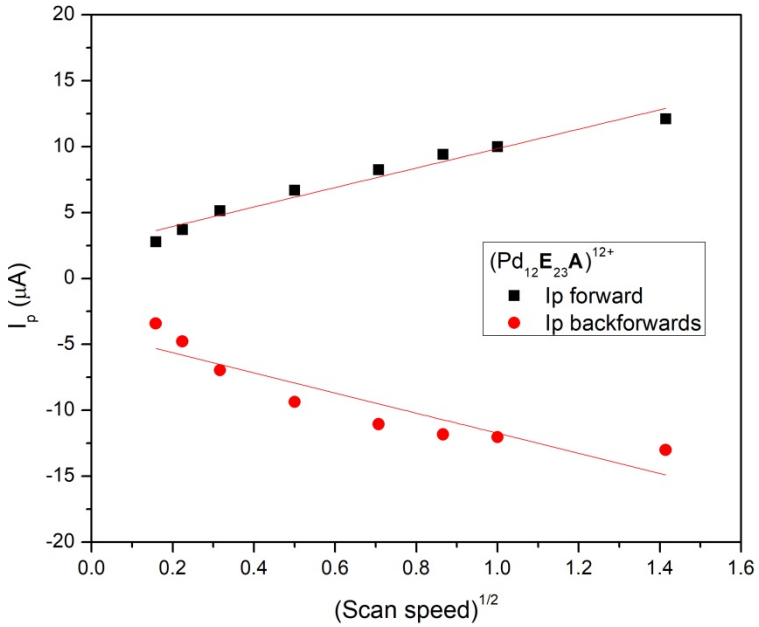

Figure S114. Plots of peak current vs. square root of the scan speed for a cage solution $(Pd_{12}\mathbf{E}_{23}\mathbf{A}_1)^{24+}$ in a 1:1 mixture of DCM and MeCN.

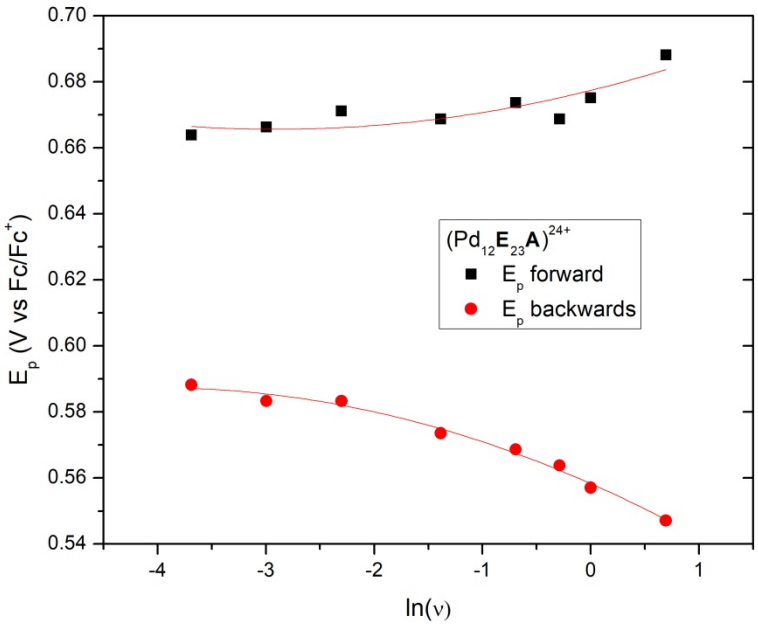

Figure S115. Plot of peak potential vs. natural logarithm of the scan speed for a cage sample $(Pd_{12}\mathbf{E}_{23}\mathbf{A}_1)^{24+}$ in a 1:1 mixture of DCM and MeCN.

Cage $(Pt_6A_{12})^{12+}$

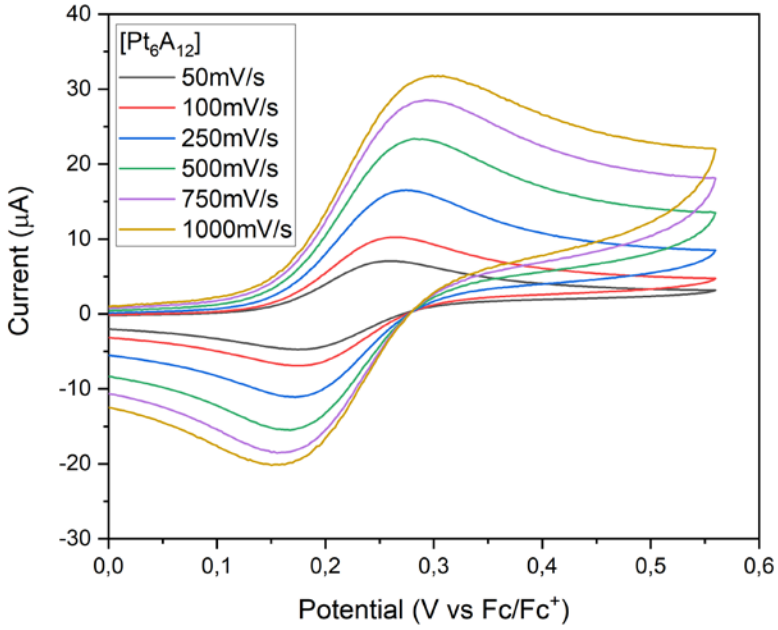

Figure S116. Cyclic voltammograms recorded at different scan speeds for a sample of the ferrocene cage, $(Pt_6\mathbf{A}_{12})^{12+}$ in a 1:1 mixture of DCM and MeCN, showing a single oxidation wave for the 12 ferrocene units present at its cavity.

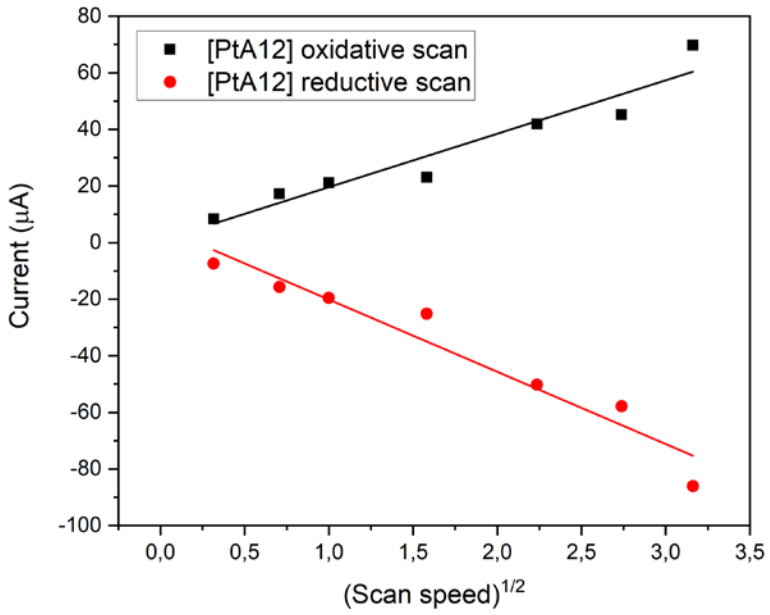

Figure S117. Plot of peak current vs. square root of the scan speed for a cage solution $(Pt_6\mathbf{A}_{12})^{12+}$ in a 1:1 mixture of DCM and MeCN.

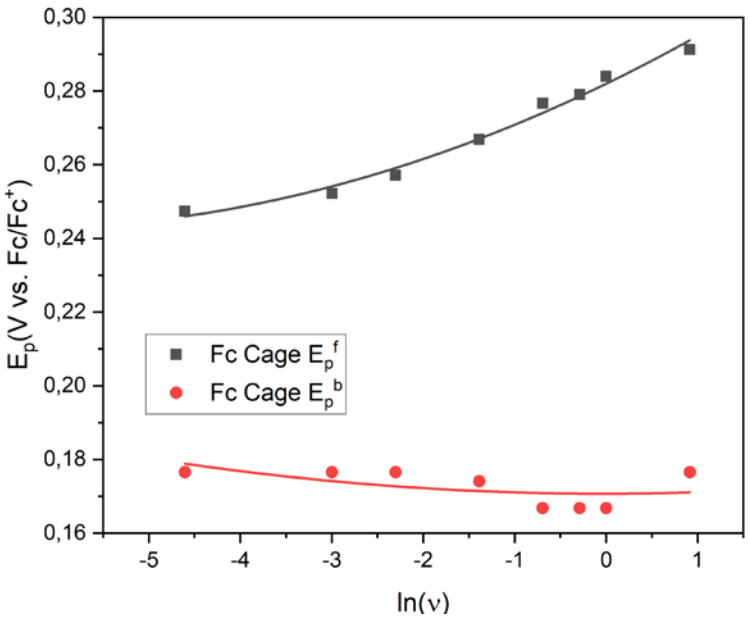

Figure S118. Plot of peak potential vs. natural logarithm of the scan speed for a cage sample $(Pt_6\mathbf{A}_{12})^{12+}$ in a 1:1 mixture of DCM and MeCN.

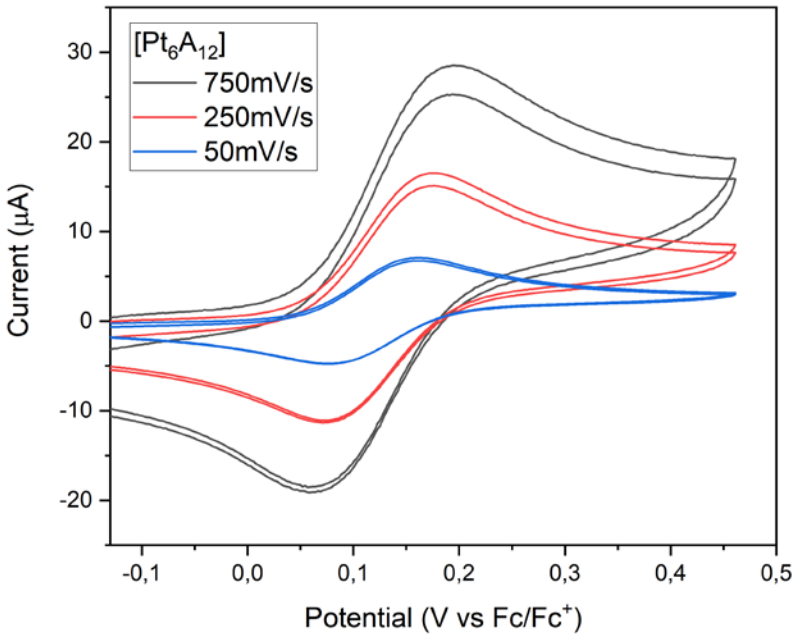

Figure S119. Consecutive cyclic voltammograms recorded at different scan speeds for a sample of the ferrocene cage, $(Pt_6\mathbf{A}_{12})^{12+}$ in a 1:1 mixture of DCM and MeCN.

Cage $(Pt_6E_{11}A_1)^{12+}$

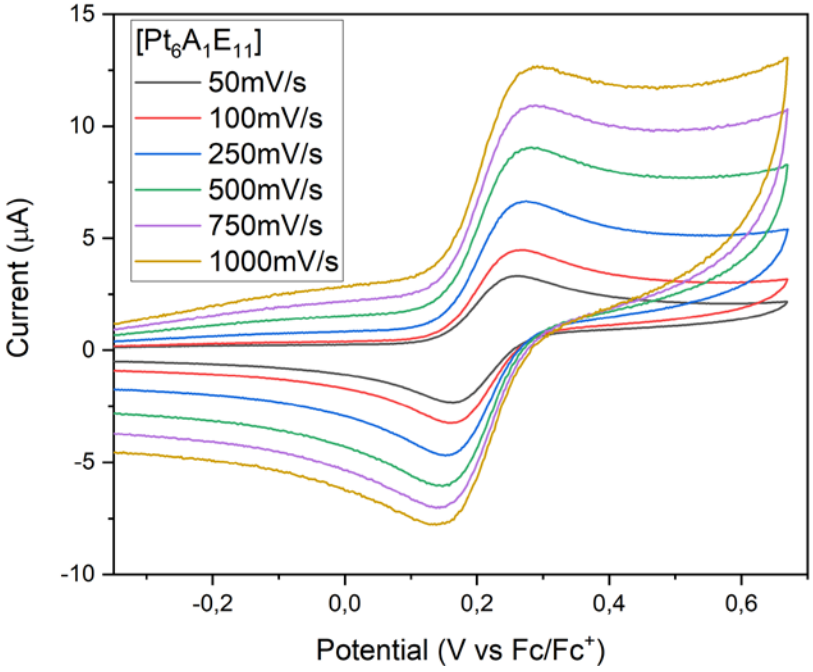

Figure S120. Cyclic voltammograms recorded at different scan speeds for a sample of the ferrocene cage, $(Pt_6\mathbf{E}_{11}\mathbf{A}_1)^{12+}$ in a 1:1 mixture of DCM and MeCN.

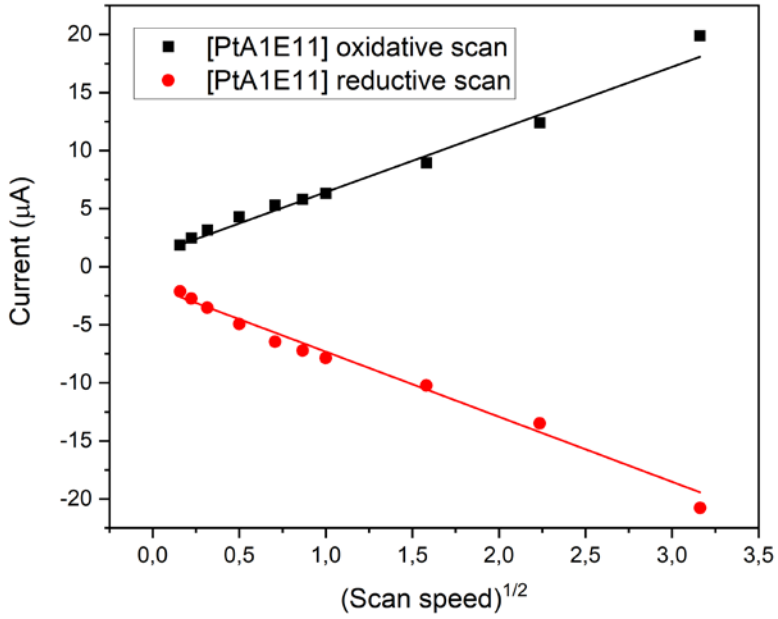

Figure S121. Plot of peak current vs. square root of the scan speed for a cage solution $(Pt_6\mathbf{E}_{11}\mathbf{A}_1)^{12+}$ in a 1:1 mixture of DCM and MeCN.

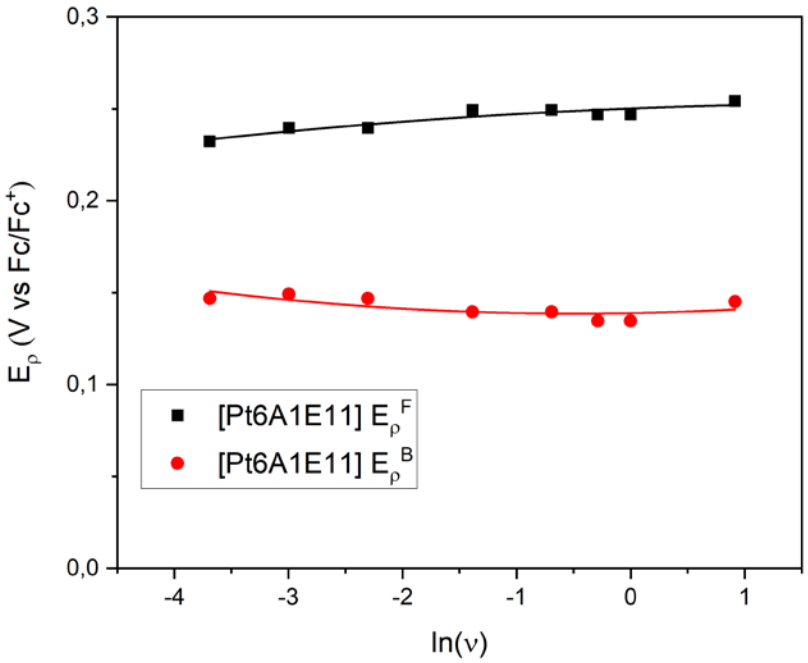

Figure S122. Plot of peak potential vs. natural logarithm of the scan speed for a cage sample $(Pt_6\mathbf{E}_{11}\mathbf{A}_1)^{12+}$ in a 1:1 mixture of DCM and MeCN.

TTFBB B and TTFBB B containing cages

TTFBB B

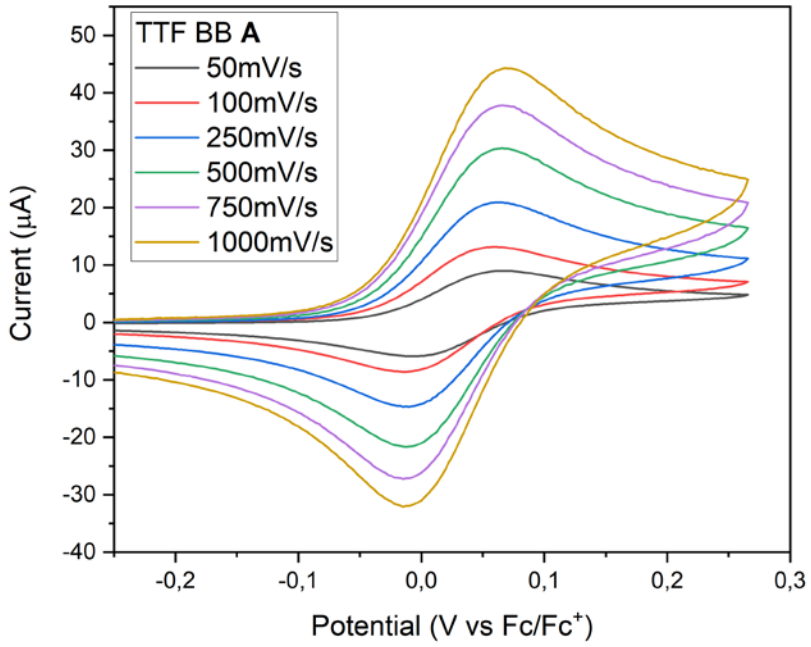

Figure S123. Cyclic voltammograms recorded at different scan speeds for the first oxidation of a solution of TTFBB, **B** in MeCN.

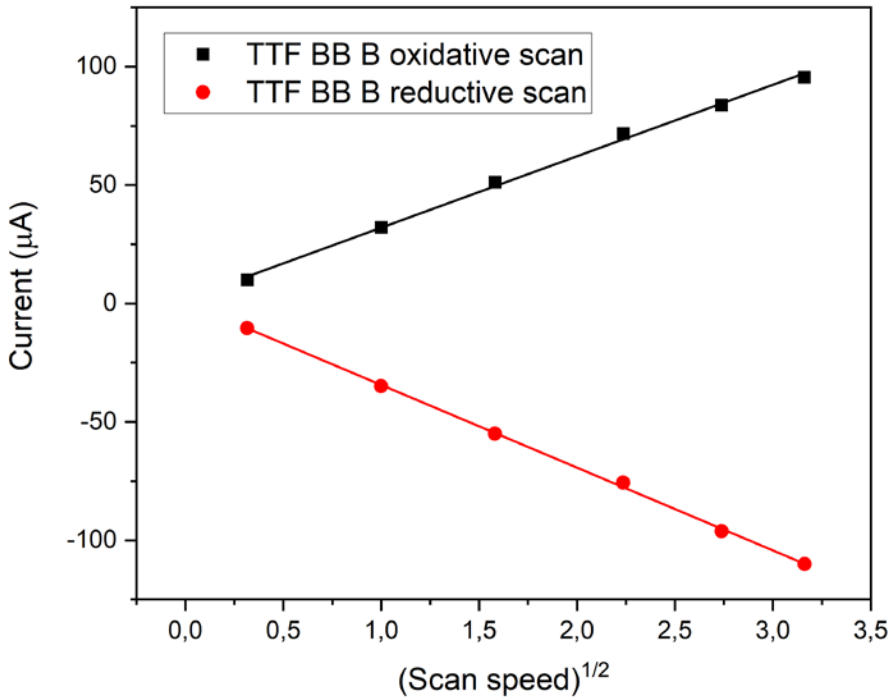

Figure S124. Plots of peak current vs. square root of the scan speed for the first oxidation of free TTFBB, **B** in MeCN.

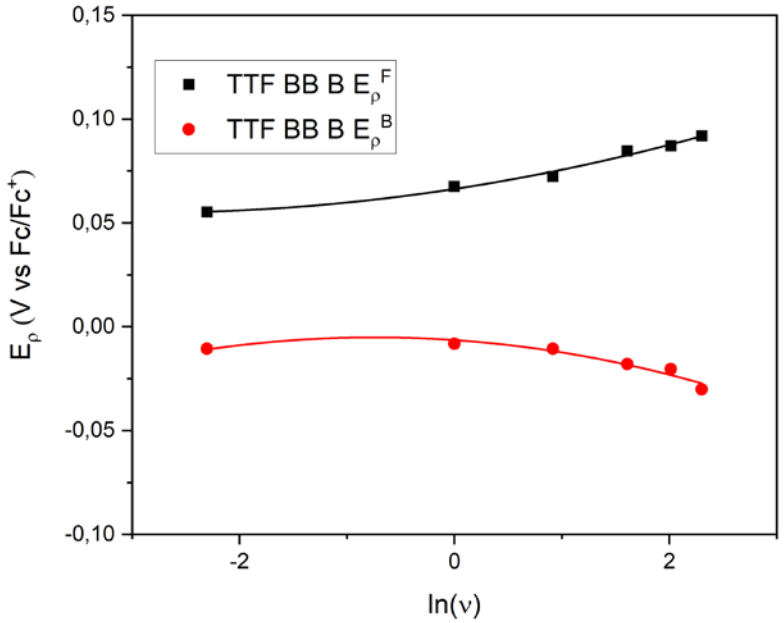

Figure S125. Plot of peak potential vs. natural logarithm of the scan speed for first oxidation of the free TTFBB **B** in MeCN.

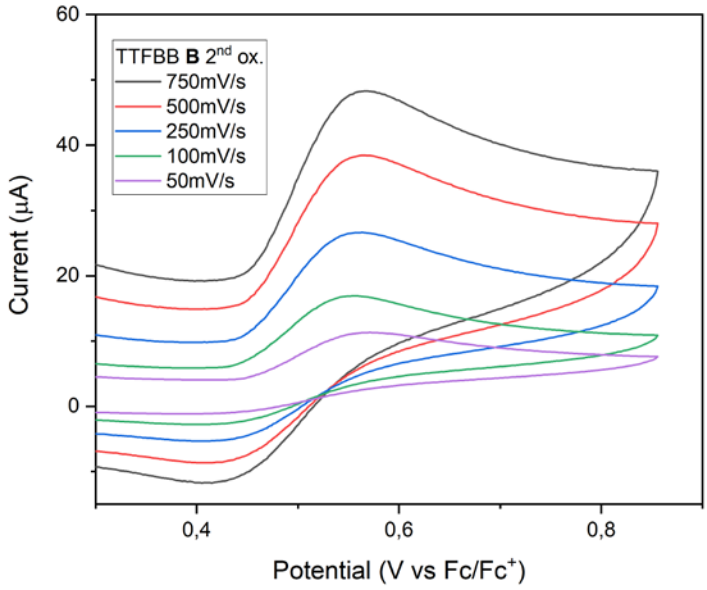

Figure S126. Cyclic voltammograms recorded at different scan speeds for the second oxidation of a solution of TTFBB, **B** in MeCN.

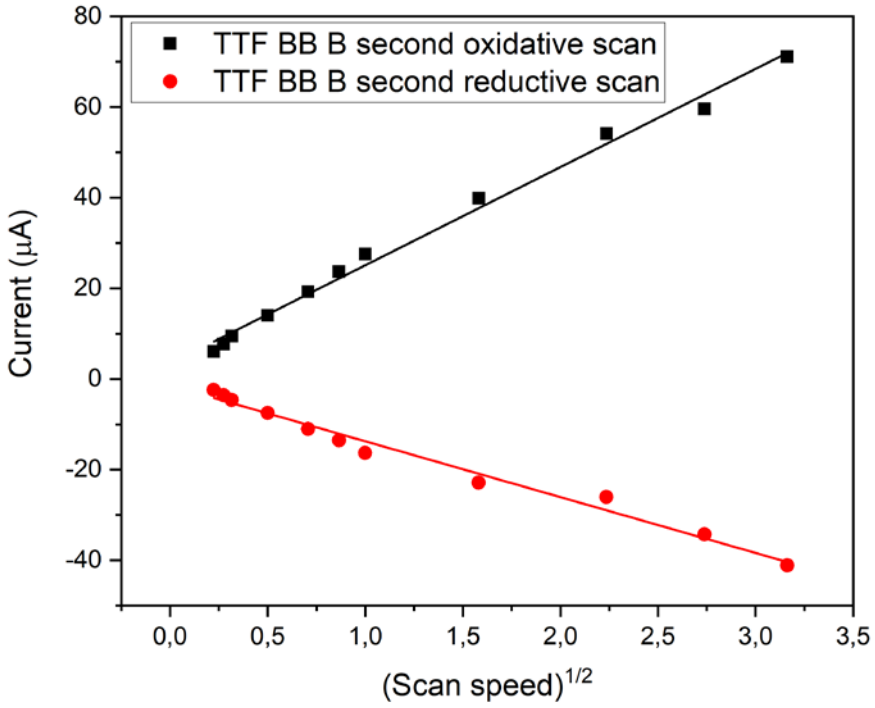

Figure S127. Plot of peak current vs. square root of the scan speed for the second oxidation of TTFBB **B** in MeCN.

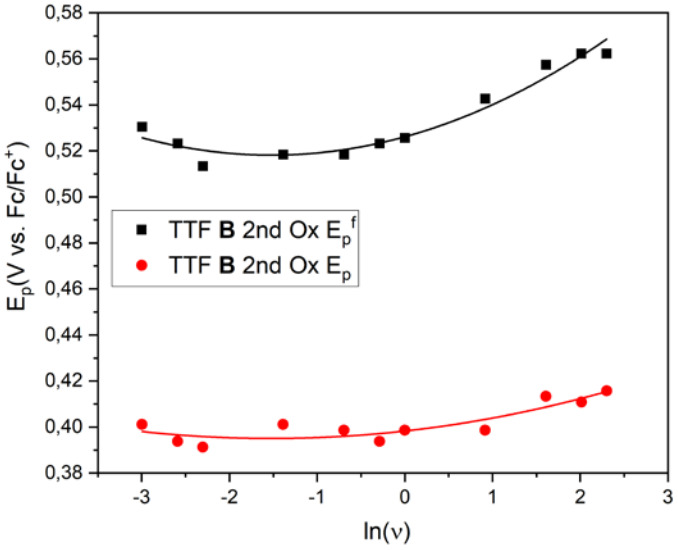

Figure S128. Plot of peak potential vs. natural logarithm of the scan speed for second oxidation of the free TTFBB **B** in MeCN.

Cage $(Pt_6E_{11}B_1)^{12+}$

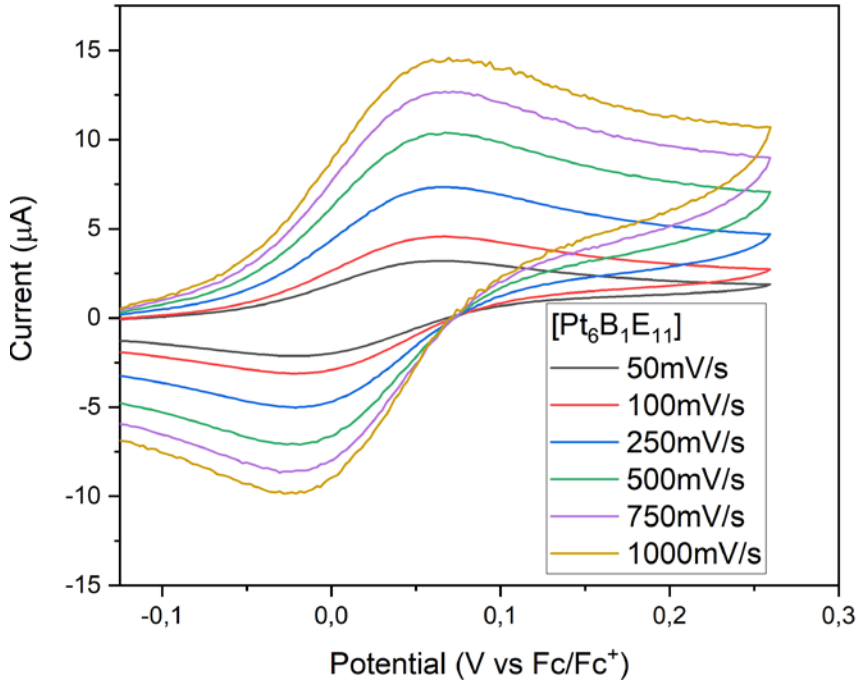

Figure S129. Cyclic voltammograms recorded at different scan speeds for a cage solution $(Pt_6E_{11}B_1)^{12+}$ at first oxidation wave in MeCN.

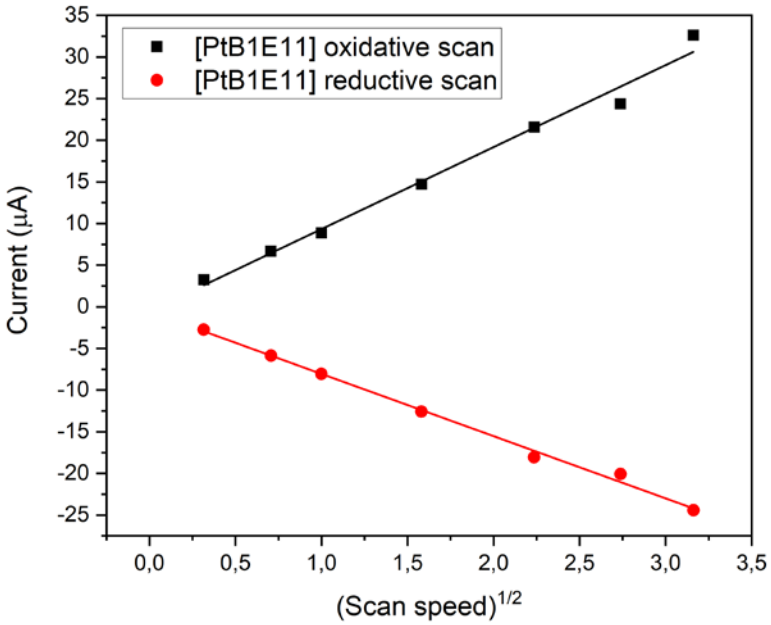

Figure S130. Plot of peak current vs. square root of the scan speed for a cage solution $(Pt_6E_{11}B_1)^{12+}$ in MeCN at first oxidation wave.

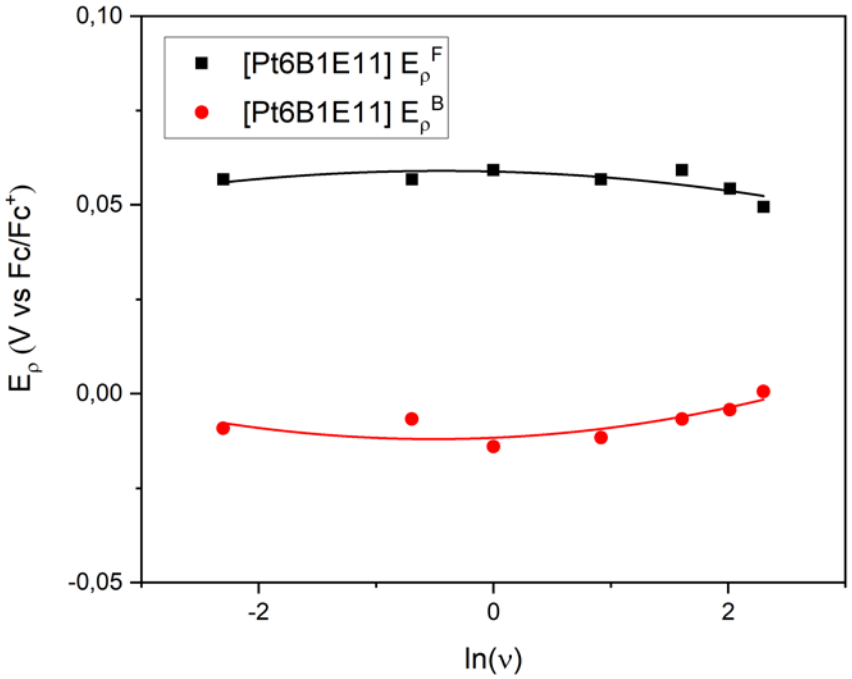

Figure S131. Plot of peak potential vs. natural logarithm of the scan speed for a cage solution $(Pt_6\mathbf{E}_{11}\mathbf{B}_1)^{12+}$ in MeCN at first oxidation wave.

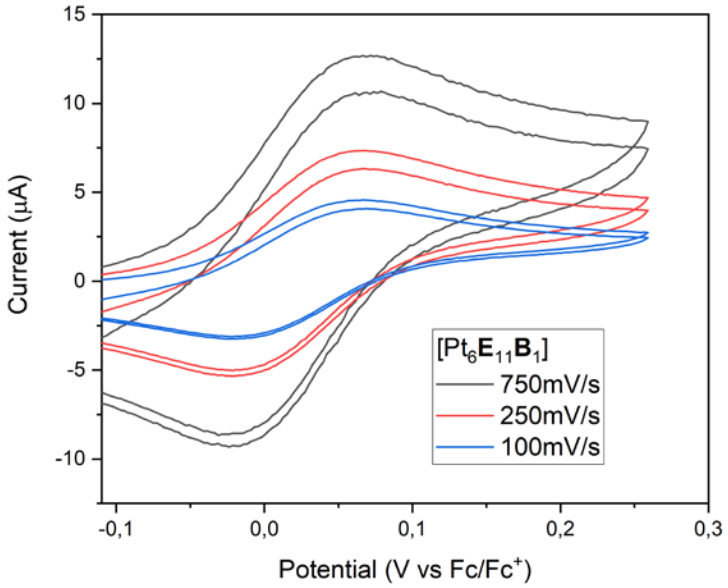

Figure S132. Consecutive cyclic voltammograms recorded at different scan speeds for a sample of the TTF cage, $(Pt_6\mathbf{E}_{11}\mathbf{B}_1)^{12+}$ at first oxidation wave in MeCN.

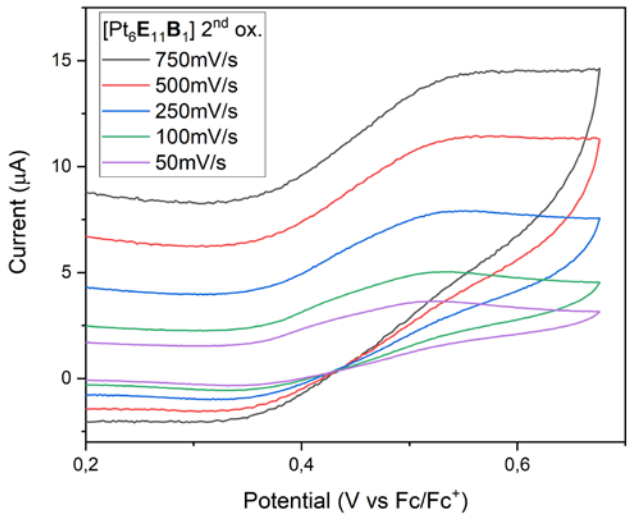

Figure S133. Cyclic voltammograms recorded at different scan speeds for a cage solution $(Pt_6\mathbf{E}_{11}\mathbf{B}_1)^{12+}$ in MeCN at second oxidation wave.

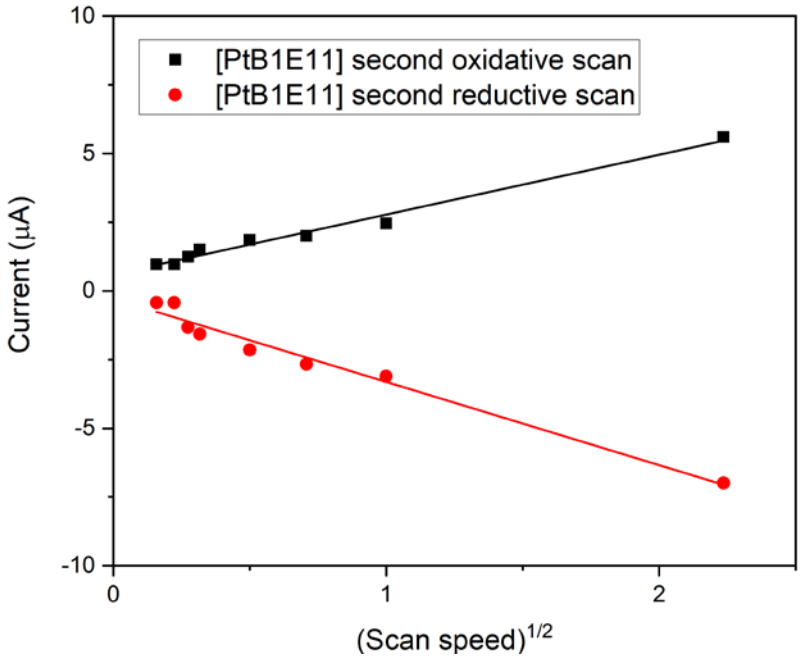

Figure S134. Plot of peak current vs. square root of the scan speed for a cage solution $(Pt_6\mathbf{E}_{11}\mathbf{B})^{12+}$ in MeCN at second oxidation wave.

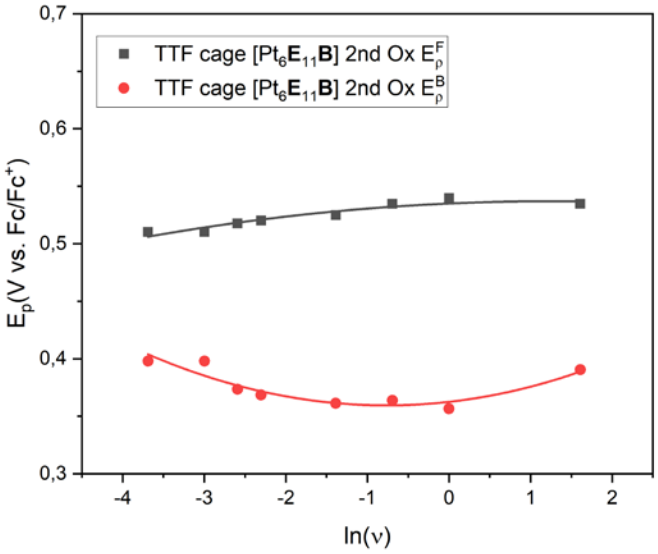

Figure S135. Plot of peak potential vs. natural logarithm of the scan speed for a cage solution $(Pt_6\mathbf{E}_{11}\mathbf{B})^{12+}$ in MeCN at second oxidation wave.

Cage $(Pt_6E_{10}B_2)^{12+}$

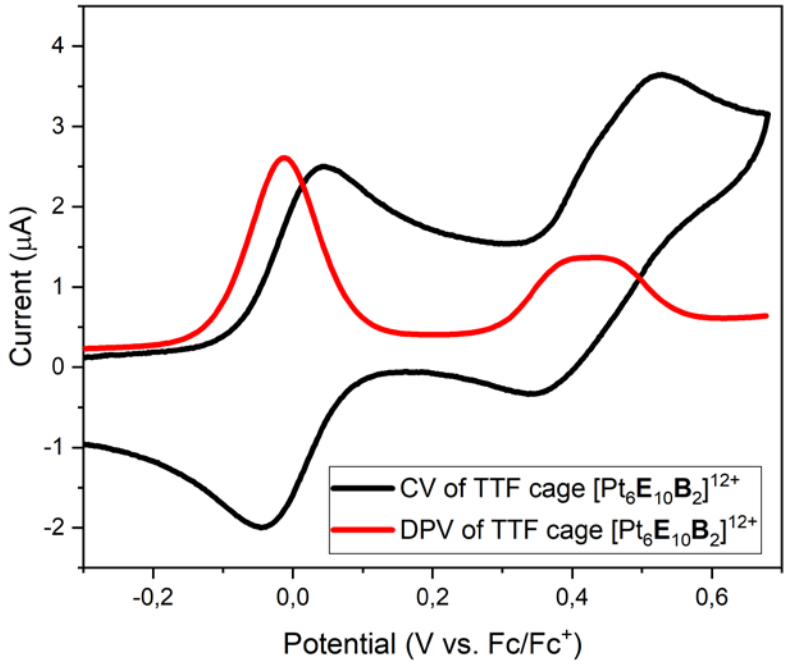

Figure S136. Oxidation behavior of TTF cage $(Pt_{12}E_{10}B_2)^{12+}$ in MeCN, containing on average 2 equivalents of TTFBB **B**. by cyclic voltammetry (black) and by differential pulse voltammetry (red).

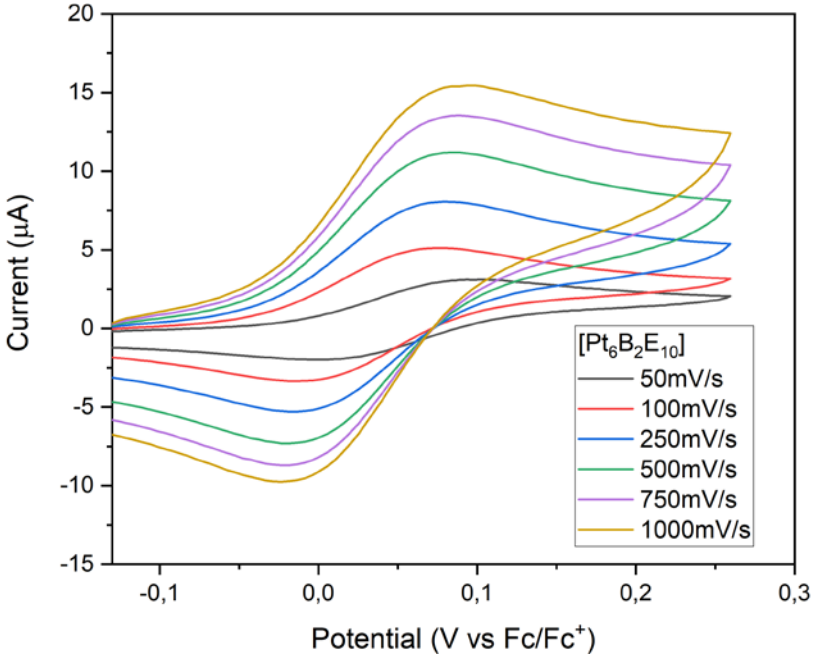

Figure S137. Cyclic voltammograms recorded at different scan speeds for a cage solution $(Pt_6E_{10}B_2)^{12+}$ in MeCN at first oxidation wave.

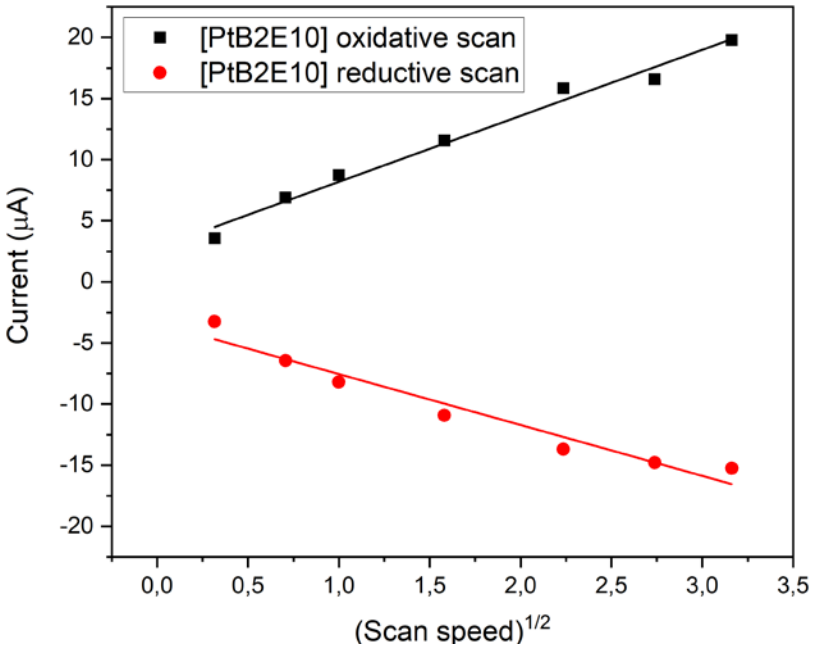

Figure S138. Plot of peak current vs. square root of the scan speed for a cage solution $(Pt_6\mathbf{E}_{10}\mathbf{B}_2)^{12+}$ in MeCN at first oxidation wave.

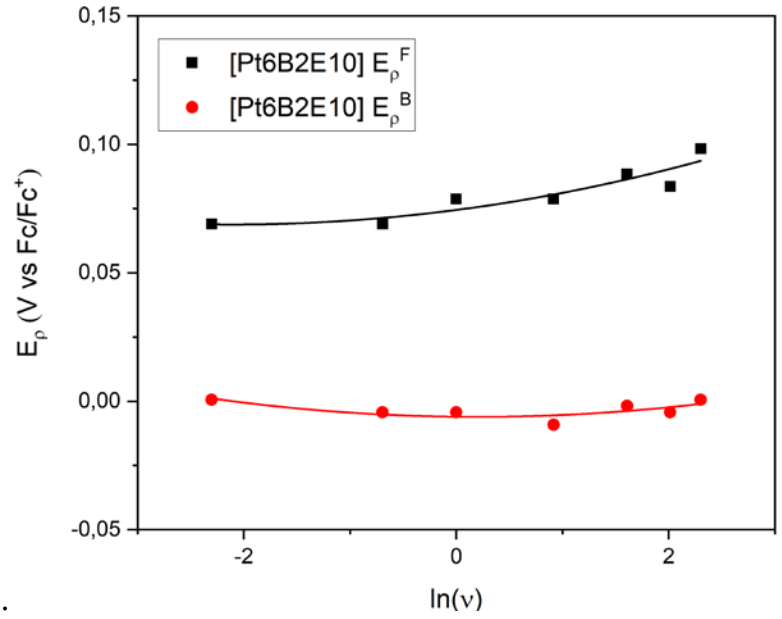

.

Figure S139. Plot of peak potential vs. natural logarithm of the scan speed for a cage solution $(Pt_6\mathbf{E}_{10}\mathbf{B}_2)^{12+}$ in MeCN at first oxidation wave.

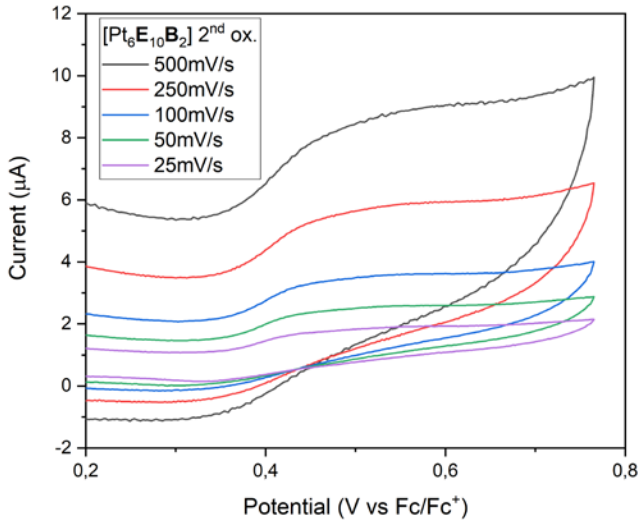

Figure S140. Cyclic voltammograms recorded at different scan speeds for a cage solution $(Pt_6\mathbf{E}_{10}\mathbf{B}_2)^{12+}$ in MeCN at second oxidation wave.

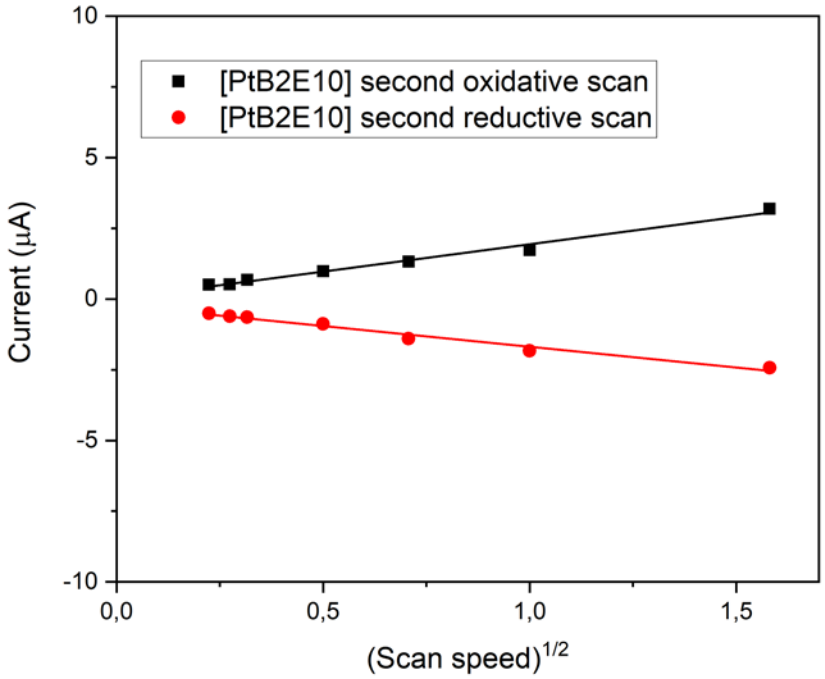

Figure S141. Plot of peak current vs. square root of the scan speed for a cage solution $(Pt_6\mathbf{E}_{10}\mathbf{B}_2)^{12+}$ in MeCN at second oxidation wave.

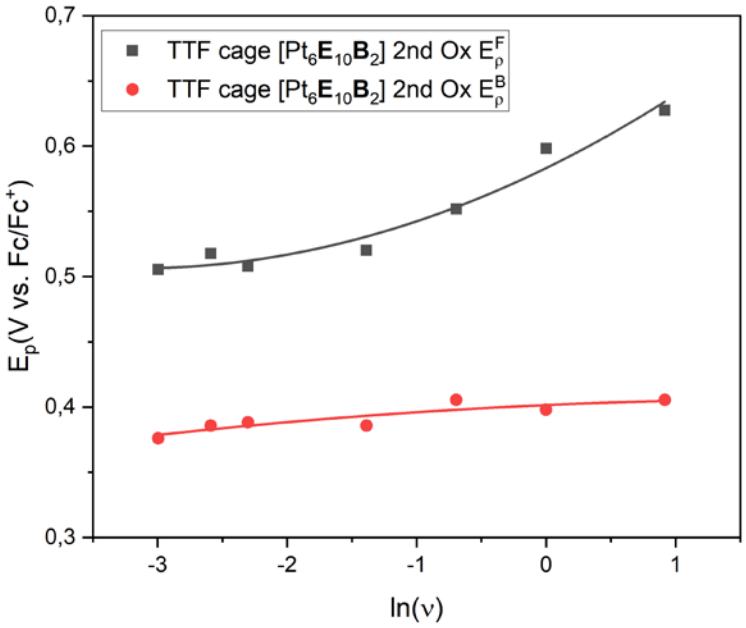

Figure S142. Plot of peak potential vs. natural logarithm of the scan speed for a cage solution $(Pt_6\mathbf{E}_{10}\mathbf{B}_2)^{12+}$ in MeCN at second oxidation wave.

twistedTTFBB C and TTFBB C containing cage

twistedTTFBB C

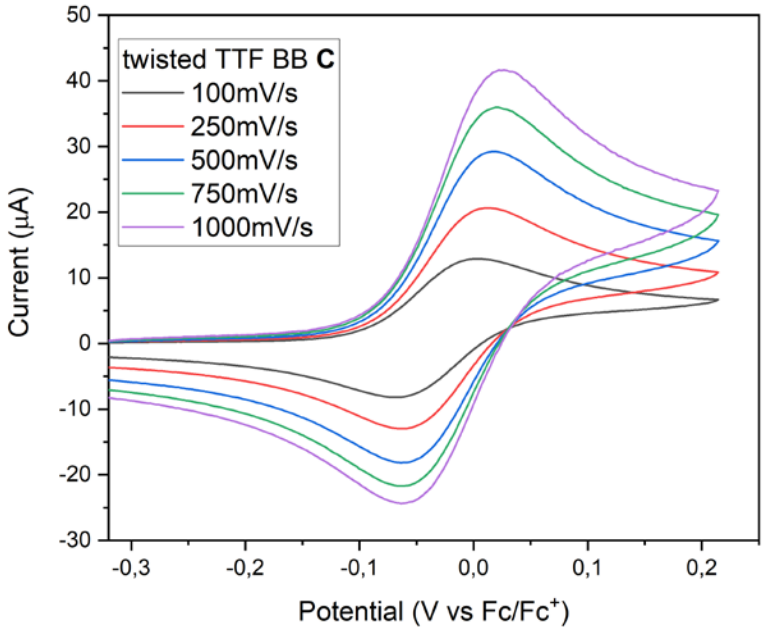

Figure S143. Cyclic voltammograms recorded at different scan speeds for a twistedTTFBB **C** solution in MeCN at first oxidation wave.

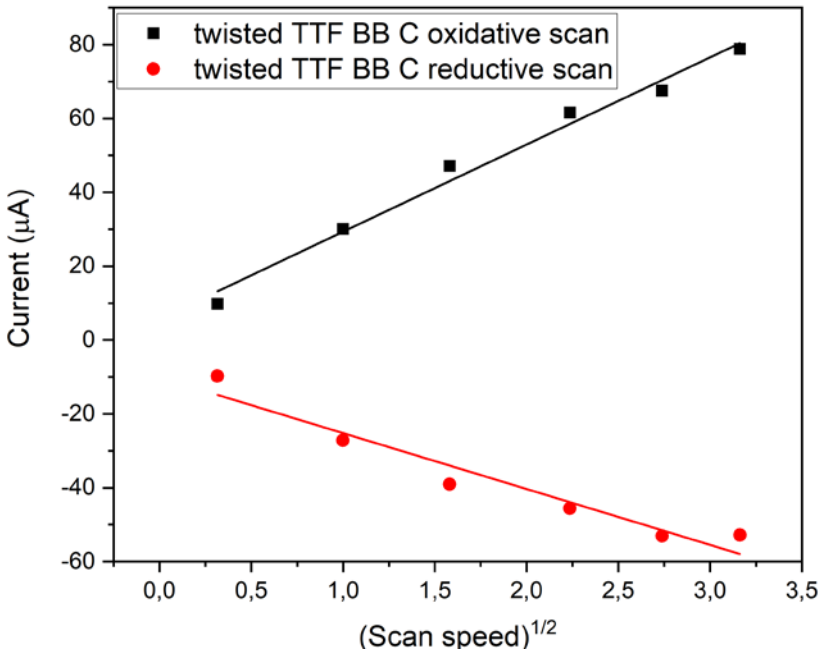

Figure S144. Plot of peak current vs. square root of the scan speed for a twistedTTFBB **C** solution in MeCN at first oxidation wave.

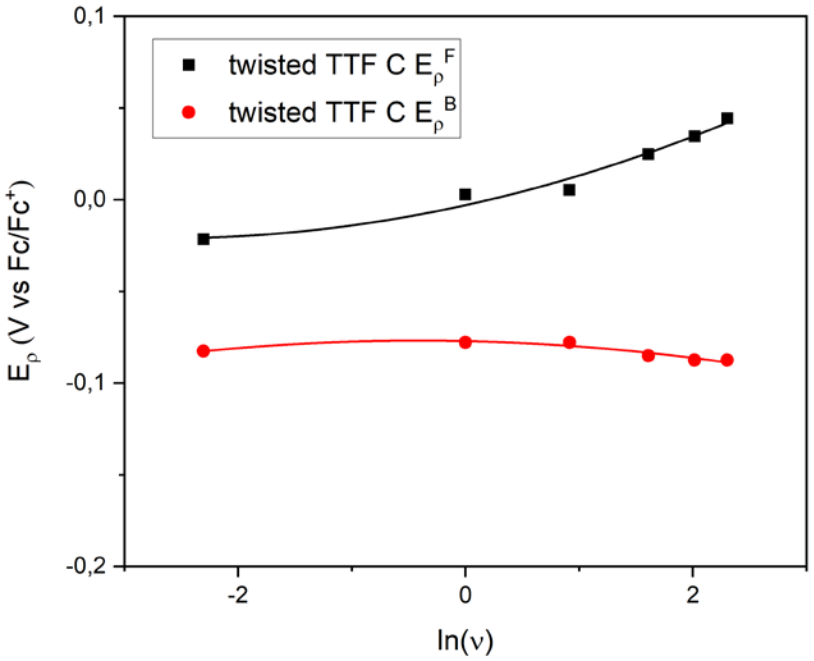

Figure S145. Plot of peak potential vs. natural logarithm of the scan speed for a twistedTTFBB **C** solution in MeCN at first oxidation wave.

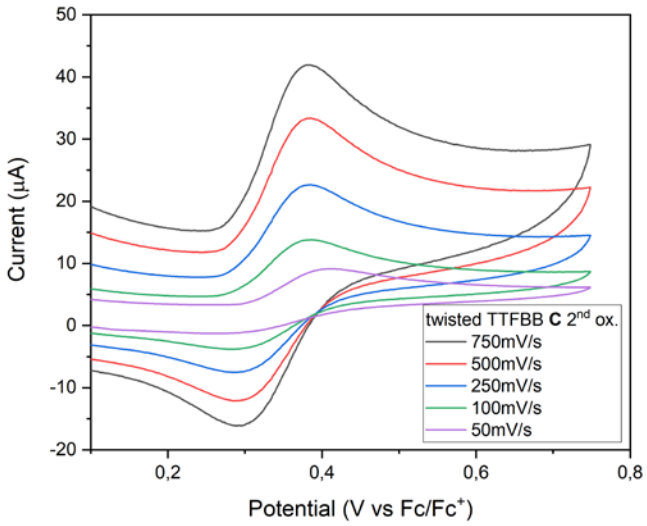

Figure S146. Cyclic voltammograms recorded at different scan speeds for a twistedTTFBB **C** solution in MeCN at second oxidation wave.

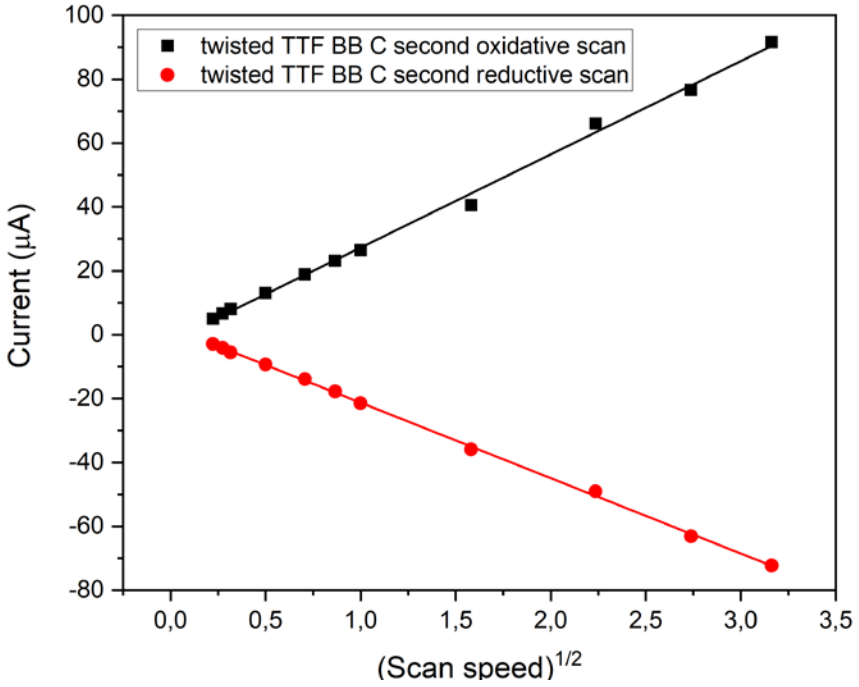

Figure S147. Plot of peak current vs. square root of the scan speed for a twistedTTFBB **C** solution in MeCN at second oxidation wave.

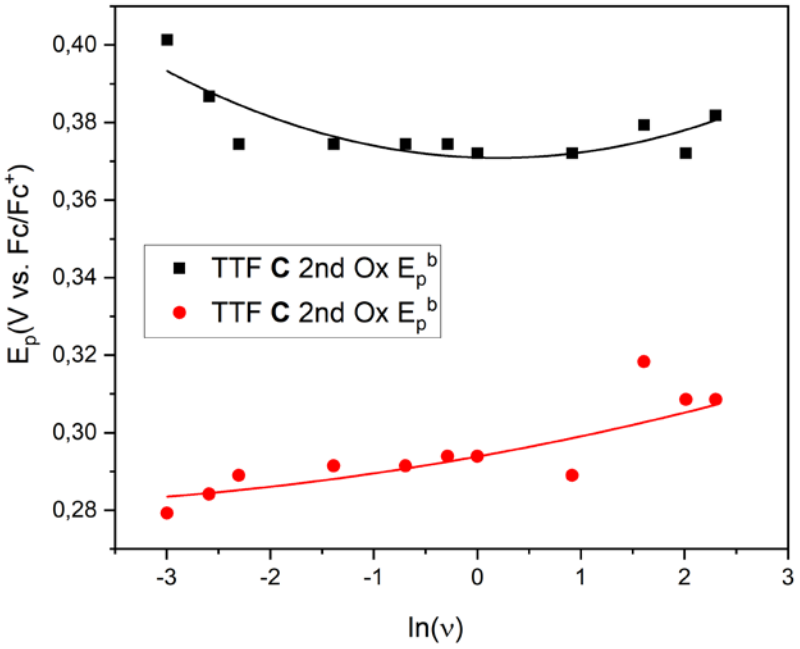

Figure S148. Plot of peak potential vs. natural logarithm of the scan speed for a twistedTTFBB **C** solution in MeCN at second oxidation wave.

Cage $(Pt_6E_{11}C_1)^{12+}$

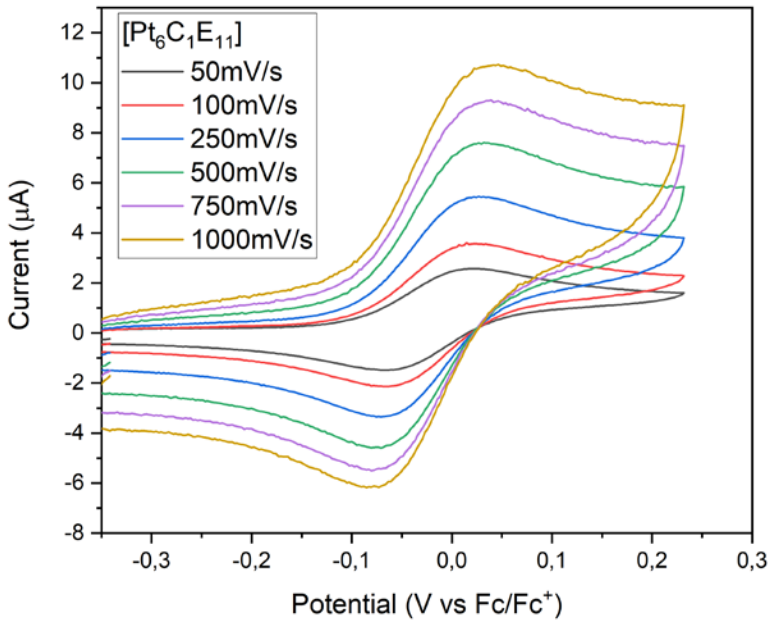

Figure S149. Cyclic voltammograms recorded at different scan speeds for a cage solution $(Pt_6E_{11}C)^{12+}$ in MeCN at first oxidation wave.

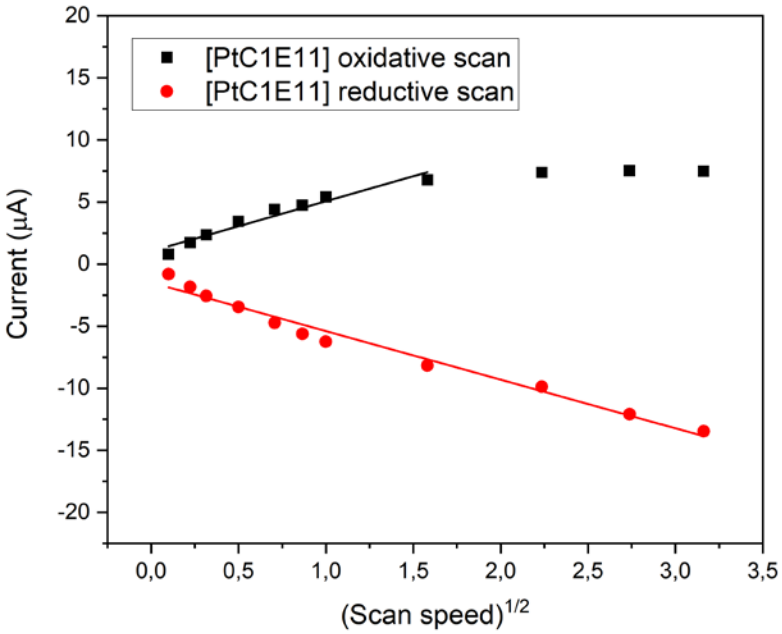

Figure S150. Plot of peak current vs. square root of the scan speed for a cage solution $(Pt_6E_{11}C)^{12+}$ in MeCN at first oxidation wave.

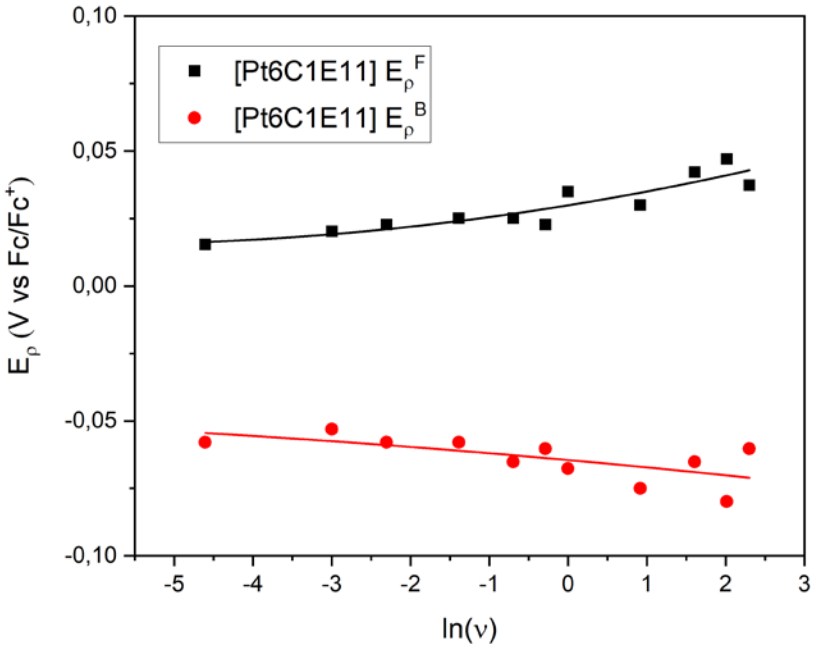

Figure S151. Plot of peak potential vs. natural logarithm of the scan speed for a cage solution $(Pt_6\mathbf{E}_{11}\mathbf{C})^{12+}$ in MeCN at first oxidation wave.

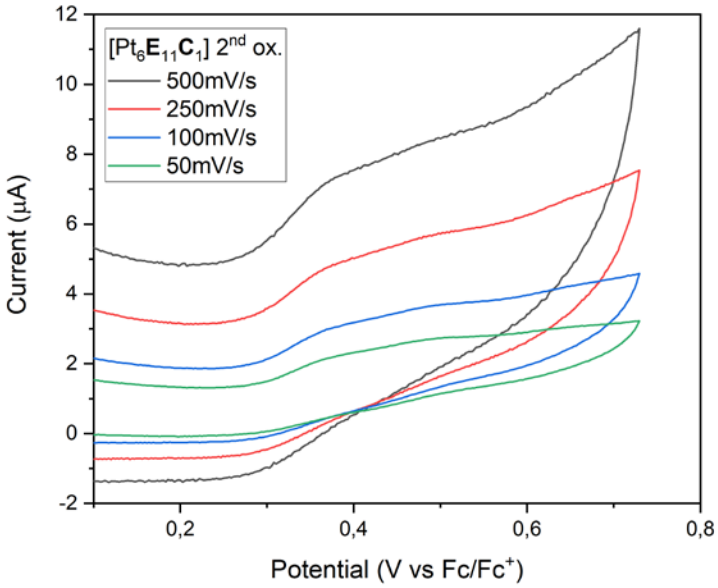

Figure S152. Cyclic voltammograms recorded at different scan speeds for a cage solution $(Pt_6\mathbf{E}_{11}\mathbf{C})^{12+}$ in MeCN at second oxidation wave.

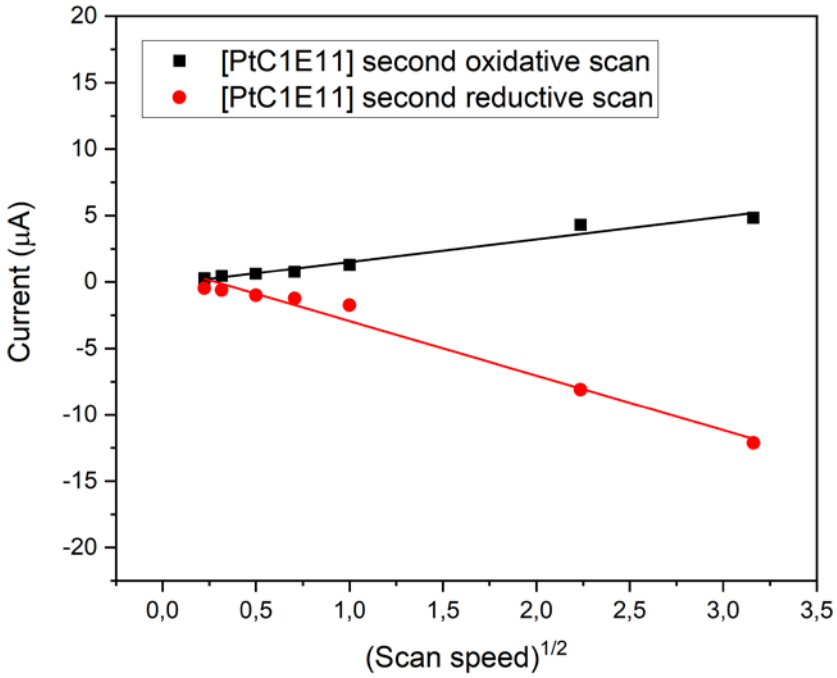

Figure S153. Plot of peak current vs. square root of the scan speed for for a cage solution $(Pt_6\mathbf{E}_{11}\mathbf{C})^{12+}$ in MeCN at second oxidation wave.

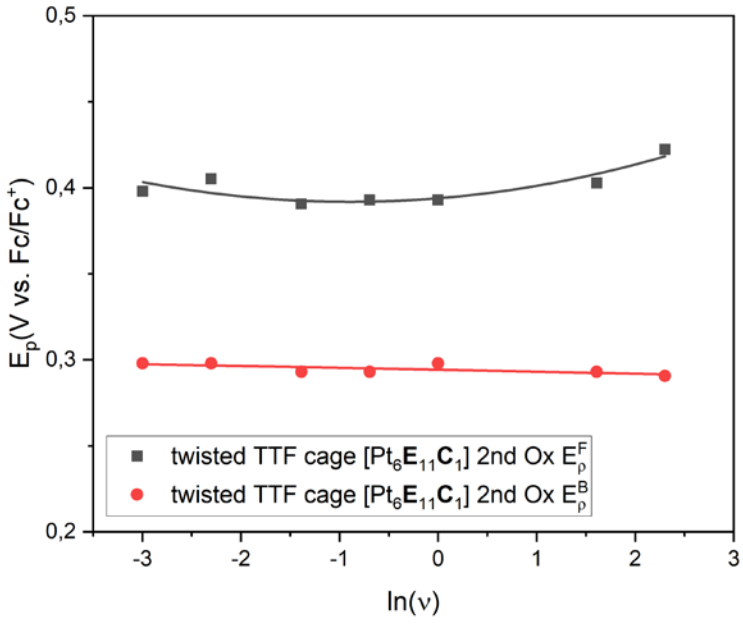

Figure S154. Plot of peak potential vs. natural logarithm of the scan speed for a cage solution $(Pt_6\mathbf{E}_{11}\mathbf{C})^{12+}$ in MeCN at second oxidation wave.

Guanidinium building block D containing cage

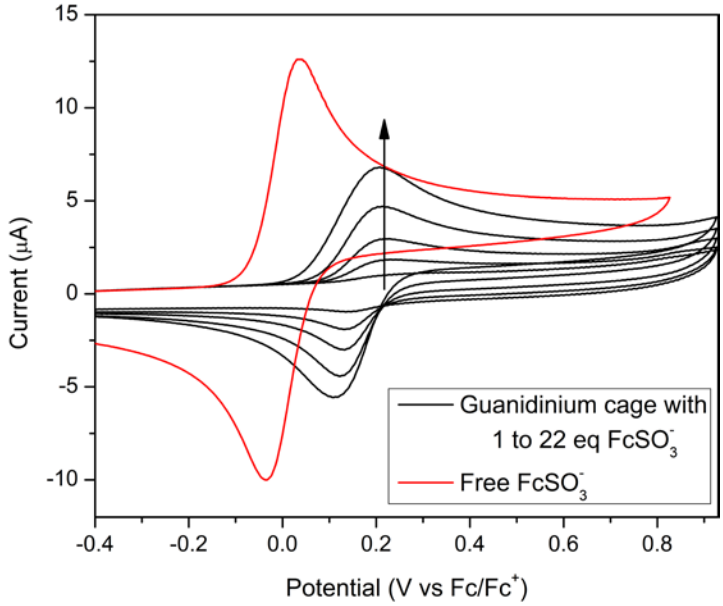

Figure S155. Cyclic voltammogram of free tetrabutylammonium ferrocenyl sulfonate (red) and titration of different equivalents of this compound into a guanidinium cage solution in MeCN, showing increasingly higher currents while the peak potential remains constant.

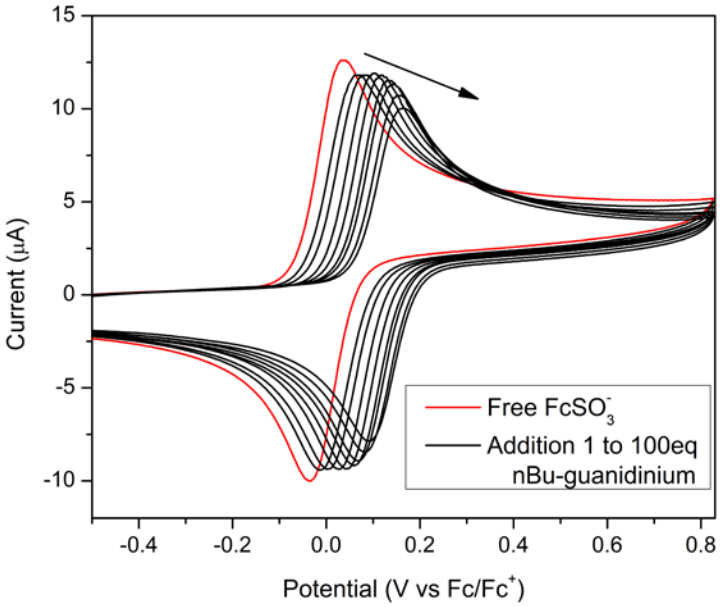

Figure S156. Voltammetric titration of free tetrabutylammonium ferrocenyl sulfonate (red) and subsequent addition of different equivalents of *n*-butylguanidinium hexafluorophosphate (black) in MeCN showing a progressive peak potential shift caused by hydrogen bonding of the complementary functional groups.

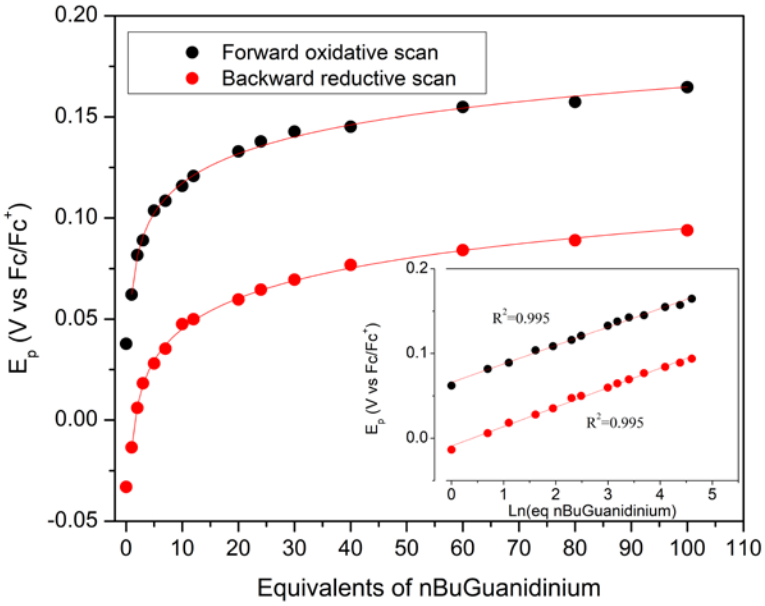

Figure S157. Plot of peak potentials vs. number of equivalents of n-butylguanidinium hexafluorophosphate added. The insert shows the same dataset on a natural logarithmic scale.

UV-VIS and Spectroelectrochemistry

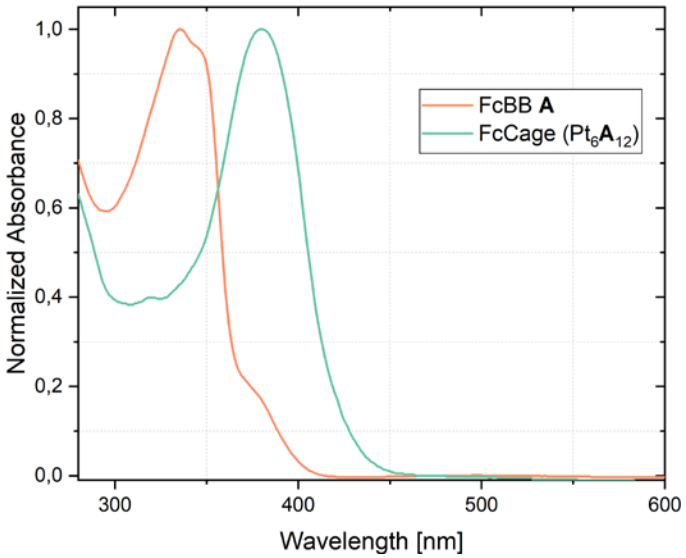

Figure S158. Normalized UV-VIS absorption of free FcBB **A** and its cage of the type $(Pt_6\mathbf{A}_{12})^{12+}$ in a 1:1 mixture of DCM and MeCN

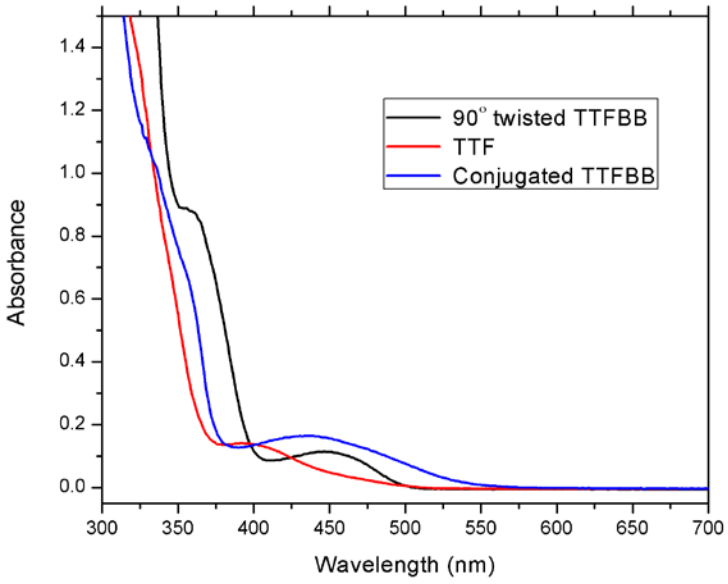

Figure S159. Uv-vis spectrum in acetonitrile of TTF building block **B** (blue) and twistedTTFBB **C** (black) and comparison with bulk TTF (red) showing increasing HOMO-LUMO gap corresponding to increased π delocalization of the orbitals.

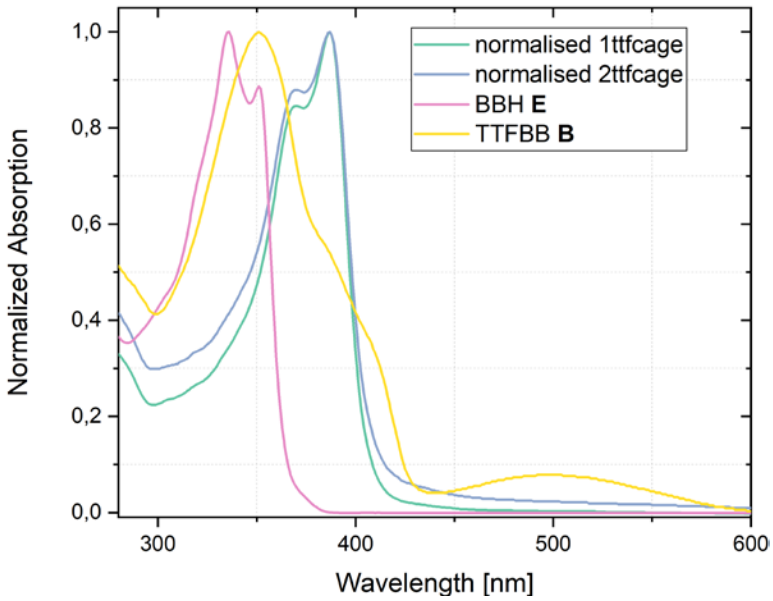

Figure S160. Normalized UV-VIS absorption of free TTFBB **B** (yellow) and free BBH **E** (pink) and cages of the type $(Pt_6\mathbf{E}_{11}\mathbf{B}_1)^{12+}$ (green) and $(Pt_6\mathbf{E}_{10}\mathbf{B}_2)^{12+}$ (blue) in MeCN

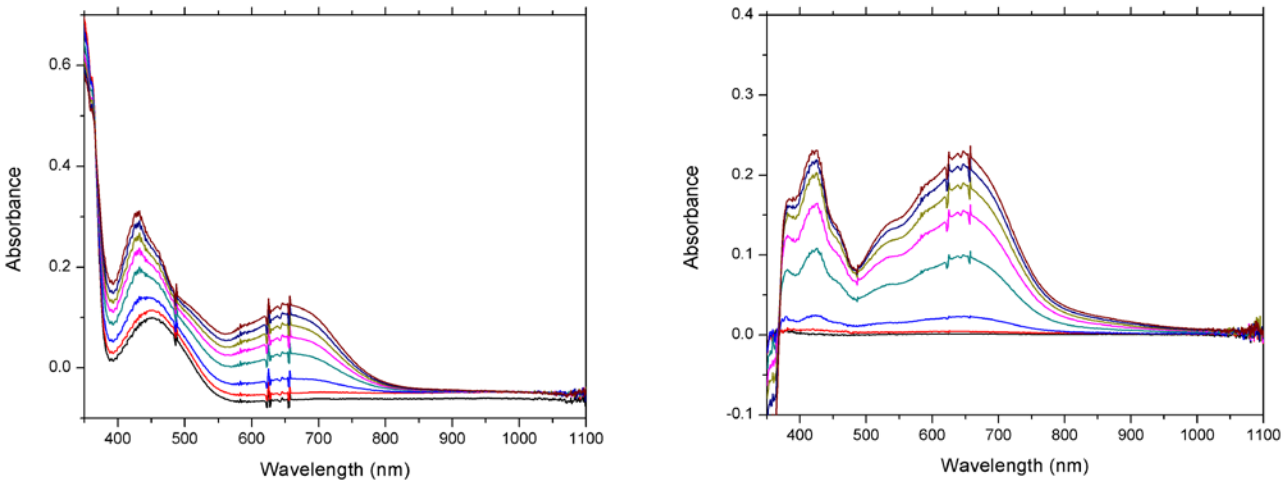

Figure S161. Spectroelectrochemistry of TTFBB **B** in MeCN; normal spectra (left), difference spectra (right).

Molecular mechanics modeling

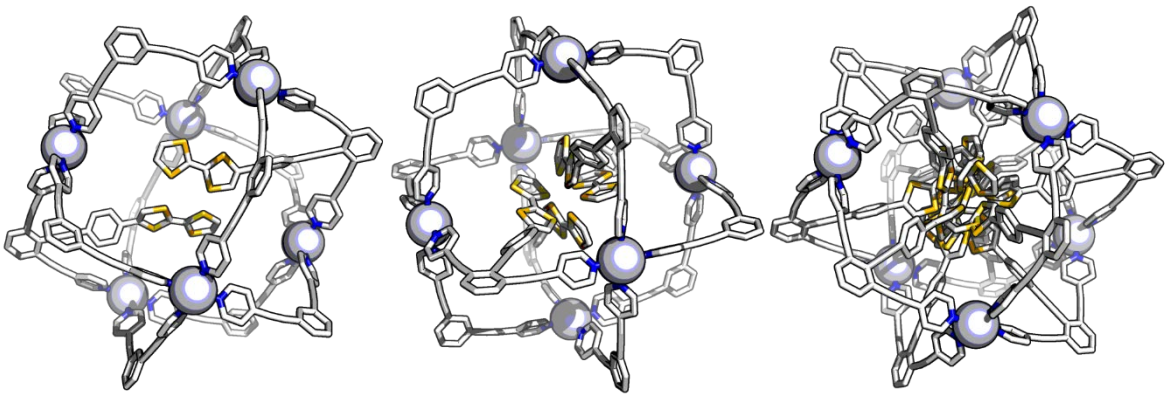

Figure S162. Rudimentary molecular mechanics modeling of the cages $(Pt_6\mathbf{E}_{12-n}\mathbf{B}_n)^{12+}$ with n=2 (left) n=4 (center) and n=12 (right) to visually show steric congestion of the cage cavity when four or more TTF units are present. The ^{t}Bu groups on building block frame were removed for better visualization The cage structures are optimized at molecular mechanics level (MMFF) and shown in wire-style; carbon in white, nitrogen in blue, sulfur in yellow and metallic Pt corners as grey spheres

DFT orbital computations

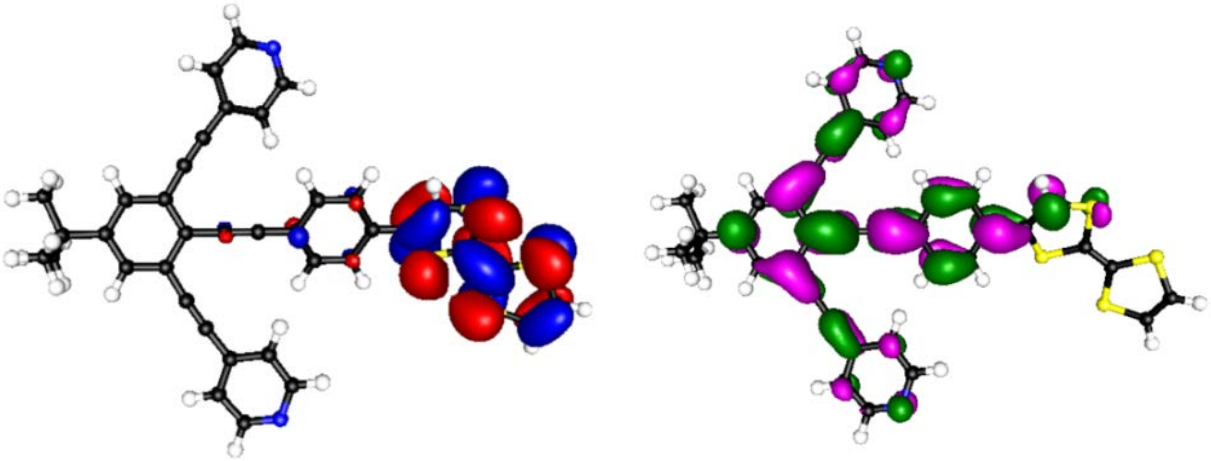

HOMO (-4.80 eV) LUMO (-2.50 eV)

Figure S163. Computed HOMO and LUMO orbitals of TTFBB **B**.

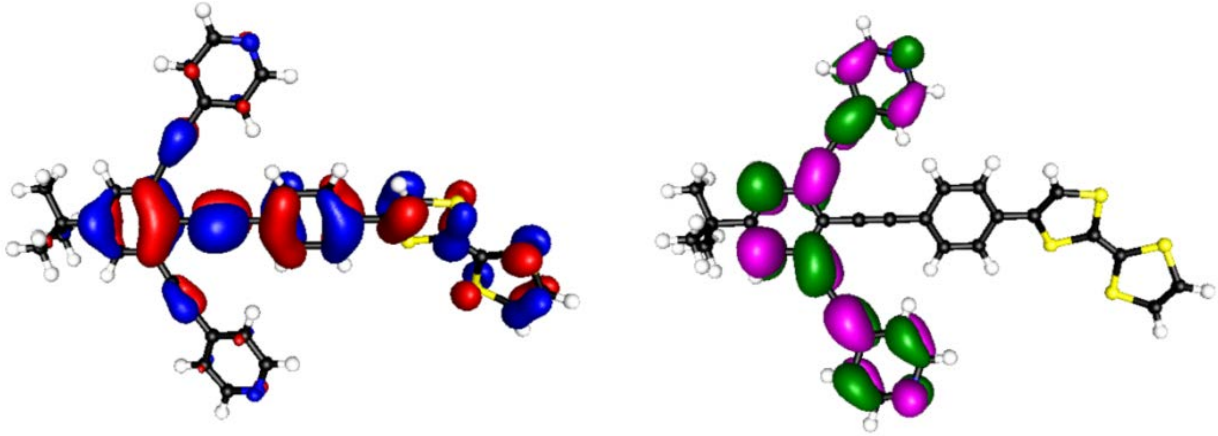

HOMO-1 (-5.89 eV) LUMO+1 (-2.26 eV)

Figure S164. Computed HOMO-1 and LUMO+1 orbitals of TTFBB **B**.

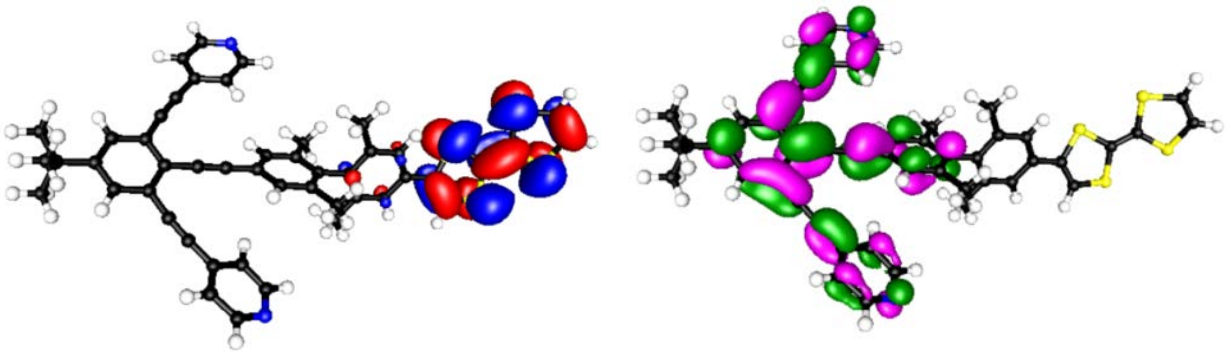

Figure S165. Computed HOMO and LUMO orbitals of twistedTTF building block **C**.

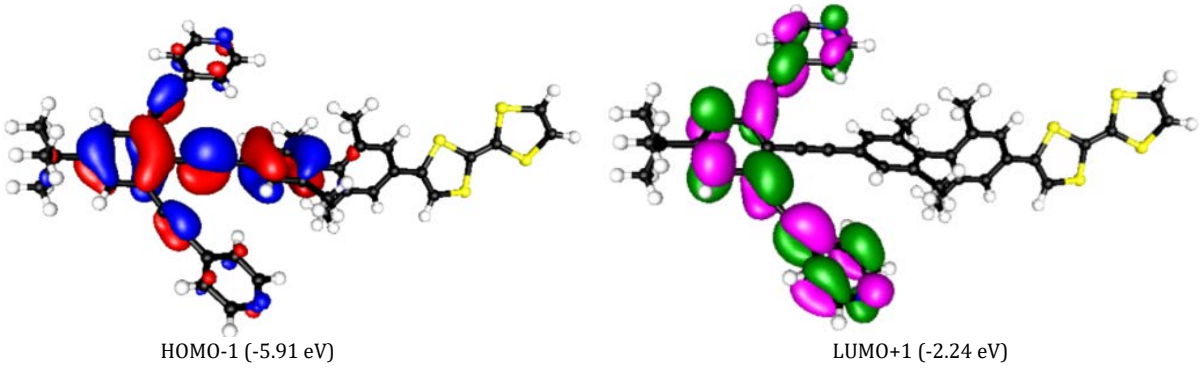

Figure S166. Computed HOMO-1 and LUMO+1 of TTF building block **C**.

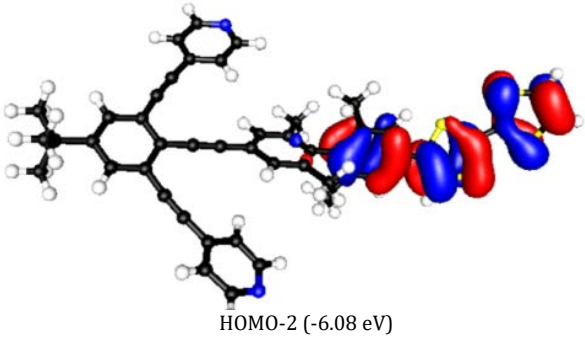

Figure S167. Computed HOMO-2 orbital of TTF building block **C**.

EPR

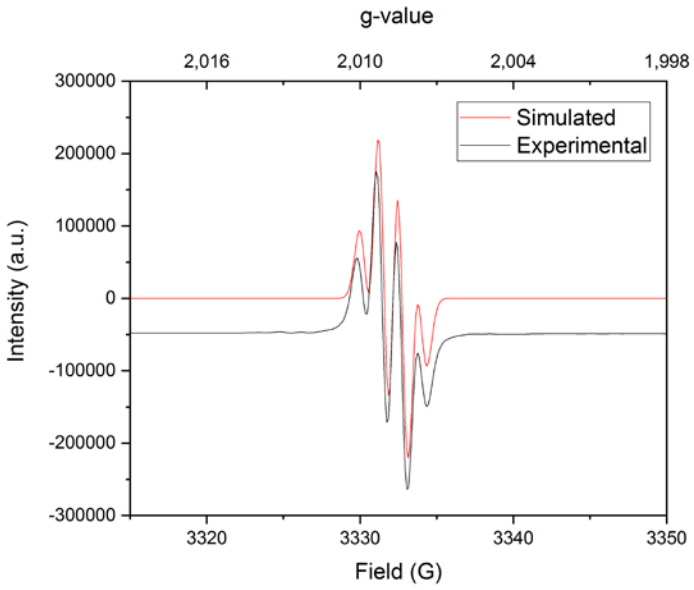

Figure S168. Experimental (black) and simulated (red) X-band EPR spectrum of TTFBB **B** at room temperature in acetonitrile. Microwave freq. 9.367668 GHz, mod. amp. 1 G, power 6.325 mW. Simulated parameters, using an AB_2-pattern: g_{iso} = 2.00856, A^{A}_{iso} = 3.598 MHz, A^{B}_{iso} = 3.2 MHz and W = 0.5 MHz.

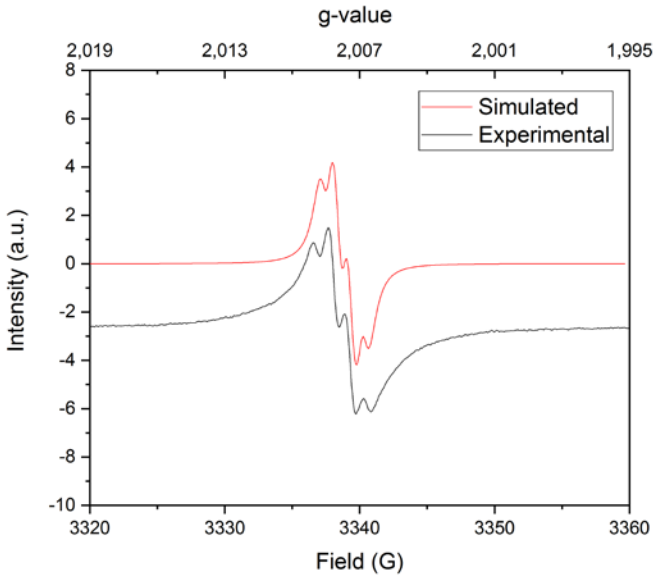

Figure S169. Experimental (black) and simulated (red) X-band EPR spectrum of 2 TTF in a cage $[Pt_6\mathbf{E}_{10}\mathbf{B}_2]^{12+}$ at room temperature in acetonitrile. Microwave freq. 9.383726 GHz, mod. amp. 0.2 G, power 6.325 mW. Simulated parameters, using an AB_2-pattern: g_{iso} = 2.00436, A^{A}_{iso} = 2.2455 MHz, A^{B}_{iso} = 3.1573 MHz and W = 0.76 MHz.

References

1. Bruker, APEX2 software, Madison WI, USA, 2014.
2. G. M. Sheldrick, S., Universität Göttingen, Germany, 2008.
3. G. M. Sheldrick, SHELXL2013, University of Göttingen, Germany, 2013.
4. Li, X.; Zhao, X.; Gao, S.; Marqués-González, S.; Yufit, D. S.; Howard, J. A. K.; Low, P. J.; Zhao, Y.; Gan, N.; Guo, Z., The structure and coordinative self-assembly of films based on a palladium compound of pyridyl-acetylene platinum and its application in Suzuki and Heck coupling reactions. *J. Mater. Chem. A* **2013,** *1* (32), 9164-9172.
5. Pop, F.; Seifert, S.; Hankache, J.; Ding, J.; Hauser, A.; Avarvari, N., Modulation of the charge transfer and photophysical properties in non-fused tetrathiafulvalene-benzothiadiazole derivatives. *Org. Biomol. Chem.* **2015,** *13* (4), 1040-1047.
6. Vonlanthen, D.; Rotzler, J.; Neuburger, M.; Mayor, M., Synthesis of Rotationally Restricted and Modular Biphenyl Building Blocks. *Eur. J. Org. Chem.* **2010,** (1), 120-133.
7. Suzuki, S.; Sugimura, R.; Kozaki, M.; Keyaki, K.; Nozaki, K.; Ikeda, N.; Akiyama, K.; Okada, K., Highly Efficient Photoproduction of Charge-Separated States in Donor−Acceptor-Linked Bis(acetylide) Platinum Complexes. *J. Am. Chem. Soc.* **2009,** *131* (30), 10374-10375.